



3 1176 00156 6026 •

*NASA CR-159,579*

**NASA CR-159579**

**TRW ER-8019-1**

NASA-CR-159579

19790021211

# **AUTOMATED PLASMA SPRAY (APS) PROCESS FEASIBILITY STUDY**

**INTERIM REPORT**

**PLASMA SPRAY PROCESS DEVELOPMENT & EVALUATION**

By

**C.W. FETHEROFF**

**T. DERKACS**

**I.M. MATAY**

**TRW**  
EQUIPMENT

**LIBRARY COPY**

**AUG 29 1979**

LANGLEY RESEARCH CENTER  
LIBRARY, NASA  
HAMPTON, VIRGINIA

**Prepared For**

**NATIONAL AERONAUTICS and SPACE ADMINISTRATION  
NASA LEWIS RESEARCH CENTER**

**Contract NAS3-20112**

1. Report No. NASA CR-159579		2. Government Accession No.		3. Recipient's Catalog No.	
4. Title and Subtitle AUTOMATED PLASMA SPRAY (APS) PROCESS FEASIBILITY STUDY INTERIM REPORT - Plasma Spray Process Development & Evaluation				5. Report Date May 1979	
				6. Performing Organization Code	
7. Author(s) C. W. Fetheroff, T. Derkacs and I. M. Matay				8. Performing Organization Report No. TRW ER-8019-1	
9. Performing Organization Name and Address TRW Materials Technology TRW Inc. 23555 Euclid Avenue Cleveland, OH 44117				10. Work Unit No.	
				11. Contract or Grant No. NAS3-20112	
12. Sponsoring Agency Name and Address National Aeronautics and Space Agency Washington, D.C. 20546				13. Type of Report and Period Covered Interim Contractor Report	
				14. Sponsoring Agency Code	
15. Supplementary Notes Project Manager, John P. Merutka, Materials and Structures Division NASA Lewis Research Center, Cleveland, OH 44135					
16. Abstract  <p>An automated plasma spray (APS) process has been developed to apply two layer (NiCrAlY and <math>ZrO_2-12Y_2O_3</math>) thermal-barrier coatings to aircraft gas turbine engine blade airfoils. The APS process hardware consists of four subsystems: a mechanical blade positioner incorporating two interlaced six-degree-of-freedom assemblies (one for coating deposition and one for coating thickness monitoring); a noncoherent optical metrology subsystem (for in-process gaging of the coating thickness buildup at specified points on the specimen); a microprocessor-based adaptive system controller (to achieve the desired overall thickness profile on the specimen); and commercial plasma spray equipment.</p> <p>Over fifty (50) JT9D first stage turbine blade specimens were coated with the APS process in preliminary checkout and evaluation studies. The best of the preliminary specimens achieved an overall coating thickness uniformity of <math>\pm 53 \mu m</math> (2.1 mils), much better than is achievable manually. Factors limiting this performance were identified and process modifications were initiated accordingly. Comparative evaluations of coating thickness uniformity for manually sprayed and APS coated specimens were initiated. One of the preliminary evaluation specimens was subjected to a torch test and metallographic evaluation.</p> <p>The above work covers Task I of five technical tasks under contract NAS3-20112.</p>					
17. Key Words (Suggested by Author(s)) Plasma spray                      Software Bond coat                         Firmware Thermal barrier coat Microprocessor Dimensional Metrology			18. Distribution Statement Unclassified - unlimited		
19. Security Classif. (of this report) Unclassified		20. Security Classif. (of this page) Unclassified		21. No. of Pages 107	
				22. Price*	

\* For sale by the National Technical Information Service, Springfield, Virginia 22161

N79-29382 #

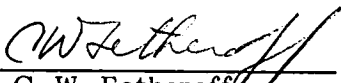
## 1.0 FOREWORD

This Interim Technical Report covers work performed under Task I, Plasma Spray Process Development and Evaluation of Contract NAS3-20112, entitled "Automated Plasma Spray Process Feasibility Study," during the period from June 1976 to November 1978.


The contract with the Materials Development Department, TRW Materials Technology of TRW Inc., Cleveland, Ohio was performed under the technical direction of Mr. John P. Merutka, Program Manager, Materials and Structures Division, NASA Lewis Research Center, Cleveland, Ohio. Mr. I. M. Matay was the Program Manager and Mr. C. W. Fetheroff was the Principal Investigator. Several TRW personnel contributed to the program on many, often overlapping technical disciplines. Key individuals and their most important contributions are as follows: Mr. T. Derkacs, metrology subsystem development and APS System/Process evaluations; Mr. H. A. Steiglitz, design and fabrication of the mechanical subsystem; Mr. P. E. Neal, microprocessor subsystem development/fabrication as well as soft and firmware developments and debug; Mr. J. Touhalisky, plasma spray activities and electronic hardware fabrication and system assembly.

The initial spray deposition process development effort was conducted under subcontract by Plasmadyne, Inc., a Geotel Company at their Santa Ana, California facility. This activity was under the direction of Mr. A. Bernstein, General Manager, and was performed by Mr. J. R. Wiest, Principal Investigator.

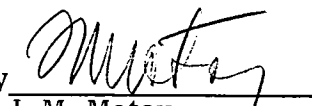
Prepared by

  
C. W. Fetheroff  
Principal Engineer

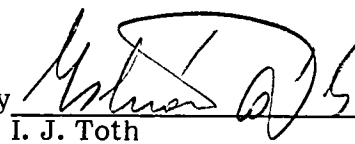
Prepared by

  
T. Derkacs  
NDE Engineer

Reviewed by

  
I. M. Matay  
Section Manager  
NDE Development

Approved by

  
I. J. Toth  
Manager  
Materials Development

## TABLE OF CONTENTS

	<u>Page No.</u>
1.0 FOREWORD . . . . .	iii
2.0 SUMMARY . . . . .	1
3.0 INTRODUCTION . . . . .	3
4.0 PROCESS DEVELOPMENT . . . . .	5
4.1 Initial Spray Deposition Process Development . . . . .	5
Introduction . . . . .	5
Process Parameters . . . . .	8
Evaluations . . . . .	9
APS Process Parameters . . . . .	16
4.2 APS System Development . . . . .	20
Technical Approach . . . . .	20
Mechanical Subsystem . . . . .	23
Blade Handling Device . . . . .	23
Mechanical Design Concept . . . . .	27
Electrical Design Concept . . . . .	27
Blade Holding Fixture . . . . .	28
Gun Positioner . . . . .	28
Optical Detector Positioner . . . . .	30
Metrology Subsystem . . . . .	30
Control Subsystem . . . . .	38
General Discussion . . . . .	38
Hardware Development . . . . .	40
Software Development . . . . .	43
General Executive Program Description . . . . .	43
Software Program Options . . . . .	47
Options Used for JT9D Coatings . . . . .	49
4.3 APS System Operation . . . . .	51



## TABLE OF CONTENTS (cont's)

	<u>Page No.</u>
5.0 EVALUATIONS AND DISCUSSION OF RESULTS . . . . .	56
5.1 Overall APS System Evaluation . . . . .	56
Measurement Subsystem Evaluations. . . . .	56
Plasma Spray Subsystem Evaluation . . . . .	60
Spray Deposition Process Modifications . . . . .	64
Mechanical Subsystem Modifications . . . . .	68
Control Subsystem Modifications . . . . .	70
Evaluation of the Modified System . . . . .	70
5.2 APS Process Evaluation . . . . .	73
General Discussion . . . . .	73
Coating Thickness Evaluation . . . . .	73
Evaluation of Manually Sprayed Blades . . . . .	75
Evaluation of the APS System Sprayed Blades . . . . .	75
Macro Coating Characteristics . . . . .	91
Torch Test Evaluation . . . . .	91
6.0 CONCLUSIONS AND RECOMMENDATIONS . . . . .	101
7.0 APPENDICES. . . . .	103
7.1 List of Abbreviations and Symbols . . . . .	104
7.2 Prefixes . . . . .	105
7.3 APS Mechanism Drawings . . . . .	Published
7.4 APS System Circuit Diagrams . . . . .	in separate
7.5 APS Process Software Flowcharts and Assembly Listings . . . . .	volumes
8.0 REFERENCES . . . . .	106

## LIST OF FIGURES

<u>Figure No.</u>	<u>Title</u>	<u>Page No.</u>
1	Microstructure of Two-Layer Plasma Sprayed Specimen Prepared by Plasmadyne Using Parameters Selected for APS Process . . . . .	13
2	Microstructure of Typical Specimen Prepared by NASA in 1976 . . . . .	13
3	Spray Profile for a Single Scan Line Pass Using $12\%Y_2O_3-ZrO_2$ . . . . .	14
4	Coating Deposition Thickness Profiles (Yttria Stabilized Zirconia, 6 Passes). . . . .	15
5	Computer Calculated Plasma Sprayed Coating Deposition Profile for Single Scan Line First Pass Using NiCrAlY . . . . .	17
6	Computer Calculated Plasma Sprayed Coating Deposition Profile for Passes Other Than First for a Single Scan Line Using NiCrAlY . . . . .	18
7	Coating Deposition Thickness Profiles (NiCrAlY, 4 Passes). . . . .	19
8	APS Function Block Diagram . . . . .	22
9	APS System Concept Defining the Seven Axes of Motion . . . . .	25
10	APS System Controller, Blade Handling Device, Coating Thickness Measurement Device and Spray Gun Scanning Fixture Assemblies as Implemented for APS Process Feasibility Demonstration . . . . .	26
11	Closeup of Blade and Optical Probe During Gage Point Measurement Routine . . . . .	29
12	Concept Diagram of Noncoherent Optical Probe. . . . .	31
13	Typical Optical Detector Response with Bare Fiber Optic Probe. . . . .	32
14	Typical Optical Detector Response With Fiber Optic Probe and Optical Extender . . . . .	34
15	Optical Detector Output Response in the Valley Region . . . . .	35

LIST OF FIGURES (cont'd)

<u>Figure No.</u>	<u>Title</u>	<u>Page No.</u>
16	Example of FIFO Valley Detector Concept . . . . .	37
17	Block Diagram of APS Process Control Subsystem . . . . .	39
18	Functional Block Diagram of APS System Controller . . . . .	41
19	Simplified Flow Chart of APS Process Software Executive Program . . . . .	44
20	Photograph of JT9D First Stage Turbine Blade Used as Master Reference for Establishing the APS Process Firmware . . . . .	52
21	Photograph Taken During the Operation of the APS System.	54
22	Initial Measurement Locations on JT9D First Stage Blade Airfoil Section . . . . .	61
23	Spraying Pattern of Plasma Gun in APS . . . . .	65
24	Average Beam Profile for ZrO <sub>2</sub> Spray . . . . .	66
25	Average Beam Profile for NiCrAlY Spray. . . . .	67
26	First Modified Measurement Location on JT9D First Stage Blade Airfoil Section . . . . .	69
27	Locations of Sections Examined for Manually Sprayed Blades . . . . .	76
28	Photomacrograph Cross-Section of Manually Sprayed JT9D Blade Specimen No. "X" at Surface Location "A" . . . . .	77
29	Photomacrograph Cross-Section of Manually Sprayed JT9D Blade Specimen No. "X" at Surface Location "B" . . . . .	78
30	Photomacrograph Cross-Section of Manually Sprayed JT9D Blade Specimen No. "Y" at Surface Location "A" . . . . .	79
31	Photomacrograph Cross-Section of Manually Sprayed JT9D Blade Specimen No. "Y" at Surface Location "B" . . . . .	80
32	Cross-Section of JT9D Blade Specimen No. 26 from Center to Leading Edge After Coating with APS System . . . . .	84

# LIST OF FIGURES (cont'd)

<u>Figure No.</u>	<u>Title</u>	<u>Page No.</u>
33	Length Section of JT9D Blade Specimen No. 26 from Tip to Section "A" After Coating with APS System and Torch Test. . . . .	85
34	Cross-Section of JT9D Blade Specimen No. 27 After Coating by APS System . . . . .	86
35	Photomicrograph of APS Coated JT9D Blade Specimen No. 27 at Point No. 23 . . . . .	88
36	Photomicrograph of APS Coated Blade Specimen No. 27 at Point No. 1. . . . .	89
37	Comparison of Photomicrograph and Optical Probe Coating Thickness Measurements on Blade No. 27 . . . . .	90
38	Photomicrograph of Manually Coated JT9D Blade No. "X", Surface "A" at Location 14 . . . . .	92
39	Photomicrograph of Manually Coated JT9D Blade No. "X", Surface "A" at Location 12 . . . . .	92
40	Photomicrograph of Manually Coated JT9D Blade No. "X", Surface "A" at Location 13 . . . . .	93
41	Photomicrograph of Manually Coated JT9D Blade No. "X", Surface "B" at Location 5. . . . .	93
42	Photomicrograph of Manually Coated JT9D Blade No. "Y", Surface "A" at Location 20 . . . . .	94
43	Photomicrograph of Manually Coated JT9D Blade No. "Y", Surface "A" at Location 11 . . . . .	94
44	Photomicrograph of Manually Cooled JT9D Blade No. "Y", Surface "A" at Location 21 . . . . .	95
45	Photomicrograph of Manually Coated JT9D Blade No. "Y", Surface "A" at Location 8 . . . . .	95
46	Photomicrograph of the APS System Coated JT9D Blade No. 26, Surface "A" at Location 9 . . . . .	96

LIST OF FIGURES (cont'd)

<u>Figure No.</u>	<u>Title</u>	<u>Page No.</u>
47	Photomicrograph of the APS System Coated JT9D Blade No. 26, Surface "A" at Location 21 . . . . .	96
48	Photomicrograph of the APS System Coated JT9D Blade No. 27, Surface "A" at Location 10 . . . . .	97
49	Photomicrograph of the APS System Coated JT9D Blade No. 27, Surface "A" at Location 20 . . . . .	97
50	APS Coated, NASA Burner Rig tested Airfoil No. 26 After 23 Hour Exposure . . . . .	
51	Photomicrographs of APS Coated Burner Rig tested Airfoil No. 26 After 23 Hour Exposure Showing Localized Thermal Barrier Coat Spalling . . . . .	99
52	Data Printouts from APS System Showing Actual Deposition Thickness of NiCrAlY and Zirconium Oxide Coatings on JT9D Specimen No. 26 as Determined by the Optical Sensor at Each Gage Point . . . . .	100

## LIST OF TABLES

<u>Table No.</u>	<u>Title</u>	<u>Page No.</u>
I	Plasma Spray Parameters for NiCrAlY . . . . .	10
II	Plasma Spray Parameters for 12%Y <sub>2</sub> O <sub>3</sub> -ZrO <sub>2</sub> . . . . .	11
III	Measurement System Repeatability Data at 8 MT/ST . . . . .	59
IV	Coating Thickness Evaluation on Blade No. 5 . . . . .	62
V	Coating Thickness Evaluation on Blade No. 6 . . . . .	63
VI	Evaluation of Modified APS System Using Blades No. 26 & 27 .	71
VII	Effect of Blade/Fixture Thermal Warpage on Coating Thickness . . . . .	74
VIII	Coating Thickness Measurement on Manually Sprayed Blades . . . . .	81
IX	Spread of Optical Probe Data from Ten Best Uniformly Coated JT9D Blades . . . . .	82
X	Coating Thickness Measurements on APS System Sprayed Blades . . . . .	87

## 2.0 SUMMARY

This report covers the interim results of an experimental development effort conducted to study the feasibility of developing an automated plasma spray (APS) process to uniformly and reproducibly apply two layer (NiCrAlY and  $\text{ZrO}_2\text{-12Y}_2\text{O}_3$ ) thermal barrier coatings to aircraft gas turbine engine blade airfoils.<sup>2</sup> Target thicknesses for the metallic bond coat and oxide layers were approximately 4 and 12 mils respectively with a uniformity of  $\pm 38 \mu\text{m}$  (1.5 mils).

During this interim reporting period, an automated process has been developed and demonstrated to be feasible for plasma spraying the two-layer thermal barrier coatings on a JT9D first stage turbine blade airfoil. The hardware fabricated and utilized for feasibility evaluations consisted of a five-degree-of-freedom blade handling fixture, a noncoherent optical instrument for monitoring coating thickness buildup over the specimen surfaces, commercial plasma spray equipment and a microprocessor-based system controller. Both the plasma spray gun and the optical sensor each incorporate a single degree of freedom. This results in two interlaced six-degree-of-freedom subsystems, one for coating application and one for coating thickness monitoring. The process is performed in an ambient environment.

During processing the optical sensor monitors coating deposition buildup at specific points on the airfoil surface and feeds this data to the microprocessor. The microprocessor closes the feedback loop by controlling the spray passes of the plasma gun so as to achieve the specified thickness at each point. The process is thus applicable to deposition of controlled variable thickness coatings as well as uniform coatings, although demonstrations to date have been limited to the latter category.

The feasibility of a totally automated system including integration of the control system with a commercially available plasma spray system was successfully demonstrated. All of the basic concepts involved in the process do work. One of the critical problems solved was to design a control system capable of functioning in the high frequency starter and the electric noise generating arc environments of the plasma spray system.

The noncoherent optical sensor subsystem has successfully demonstrated performance surpassing all design requirements. Repeatability runs on JT9D specimens have consistently demonstrated standard deviations of  $\pm 7.6 \mu\text{m}$  (0.3 mils) in measured values despite the mechanical fixture backlash and wear problems. Repeatability also is independent of specimen surface finish, curvature and reflectance.

APS process system evaluations to date included spraying in excess of 50 JT9D first stage turbine blade specimens. This specimen was selected as representative of the most difficult specimens to coat uniformly because of the small size and the small radii of curvature.

Process evaluations have shown that the best specimen achieved an overall thickness uniformity of  $+53 \mu\text{m}$  ( $+2.1$  mils), but was within the required tolerance range of  $+38 \mu\text{m}$  ( $+1.5$  mils) if the leading and trailing edge thickness measurements were ignored. The best coating uniformity measurements were achieved by halting the automatic coating process and measuring coating thickness after allowing the blade to cool down to room temperature to eliminate erroneous measurements resulting from thermal warpage of the blade. Modifications were made to the process hardware to overcome this problem. At the cooling passage exit holes on the trailing edge, the deposited coating was well contoured to the edge. There was no need for masking the cooling holes and no plugging of the cooling holes occurred.

Because of problems associated with the mechanical hardware development, a coating of  $+76 \mu\text{m}$  ( $+3$  mils) is more representative of the system's performance at this time. This coating thickness tolerance is superior to that typically achieved by manual coating  $+160 \mu\text{m}$  (6.3 mils). A number of areas have been identified where design improvements should be made in the standard commercial hardware items for a preproduction prototype system.

One of the coated blades was submitted to a torch test at NASA for a preliminary exposure evaluation of coating integrity. There was localized spalling at the hottest area on the leading edge after 23 hours of exposure. This was not unexpected since the coating parameters developed were not to optimize the coating structure, but were developed to put down a uniform two layered coating selected.



### 3.0 INTRODUCTION

Gas turbines which operate at higher temperatures have shown increased performance and improved fuel economy. Higher operating temperatures in such advanced gas turbines have been achieved through a combination of higher operating temperature materials and advanced cooling. Advanced cast alloys and directionally solidified alloys are reaching their limit of compositional improvements. Advanced cooling concepts are approaching their limitations due to complexity of component geometry, and limitations on engine performance gains due to the amount of compressor bleeding air needed. For these reasons, an alternate approach involving the use of thermal barrier coatings to insulate the airfoil surfaces from the hot gases has been pursued by NASA Lewis Research Center and others.

The NASA developed thermal barrier coatings, which consist of a NiCrAlY type alloy bond coat, approximately 4 mils thick, and yttria stabilized zirconia overcoat, approximately 12 mils thick, have been used to lower air-cooled turbine blade temperatures by about 149°C (300°F) in ground base research engine tests. In addition, these coatings have survived over 500 engine cycles to full power. In burner rig tests, the coatings survived surface temperatures near 1371°C (2500°F) (Ref. No. 1).

These coatings are applied by hand plasma spray methods. As part of the continuing development effort, involving the determination of the applicability of thermal barrier coatings to various advanced aircraft gas turbines and utility gas turbines, a number of factors were considered. One such factor was the ability to uniformly and reproducibly apply and document the thicknesses of the bond coating and thermal barrier coating on turbine blades beyond manual spray capabilities.

The objective of this program, therefore, is to conduct an automated plasma spray (APS) process feasibility study. The concept of the APS process developed in this effort is based on an advanced processing approach, including the use of non-contact optical metrology and data processing systems that automatically control the plasma spray coating process to uniformly and reproducibly coat gas turbine blade airfoils. The APS process developed integrates a multi-degree-of-freedom blade handling fixture, a non-coherent optical instrument for coating thickness monitoring, conventional plasma spray equipment operating in an ambient environment and a microprocessor-based system controller. The process developed is intended to reduce the coating thickness non-uniformity, but more important, to eliminate the lack of reproducibility associated with the manual plasma spray (MSP) process.

This interim report covers the first task - "Plasma Spray Process Development Evaluation." All efforts were concerned with the spraying of the airfoil section of the JT9D aircraft engine first stage turbine blade. This specimen was selected as representative of the most difficult airfoils which would be encountered due to its small size and small radii of curvature. The material in this report, therefore, is very relevant to the general plasma spray field and to thermal barrier coating of small gas turbine airfoils.

This report contains dimensional measurement data obtained by the APS hardware in the English measurement system (mils). These were converted to the SI system (micrometers,  $\mu\text{m}$ ) without rounding off.

## 4.0 PROCESS DEVELOPMENT

The concept of the Automatic Plasma Spray (APS) process is to apply an advanced processing approach, including the use of modern metrology and data processing systems, that controls the plasma spray coating deposition to uniformly and reproducibly coat gas turbine blades with a two-layered thermal barrier combination of NiCrAlY and yttria stabilized zirconia. Such a process is intended to reduce non-uniformity, particularly the lack of reproducibility involved in the manual plasma spraying (MPS) process.

Development efforts on the APS (Automatic Plasma Spray) process are summarized in these four phases or categories:

- 1) Plasma spray deposition process study
- 2) APS system development
- 3) APS system operation and checkout
- 4) APS process application evaluations

The first two phases were conducted concurrently; the other two were conducted sequentially. This section will summarize the efforts in the first three phases. Efforts in the fourth phase will be summarized in Section 5.

### 4.1 Initial Spray Deposition Process Development

The purpose of the initial spray deposition process development study was to select the specific plasma spray hardware to be incorporated into the APS system and to establish the process and control parameters associated with this hardware. The experimental portion of this study was performed by Plasmadyne, as a sub-contractor. This included selection of the specific process parameters to be used with the plasma spray hardware, preparation and spraying of specimens, and preparation of photomicrographs of selected coated specimens. Additional analysis of this data was done to develop control parameters unique to the APS process.

#### Introduction

The plasma spray technique is a process that produces coatings of a quality unavailable by other spray methods. There are three basic areas that find plasma spraying most useful:

1. Environmental resistant coatings: through the application of specific materials, coatings can be applied to resist abrasion, oxidation, heat (thermal barriers), corrosion, erosion, fretting, friction, galling, etc.

2. Resurface coatings: rebuilding worn areas, salvaging mis-machined parts or improving the characteristics of a finished part, can be accomplished quickly, easily and inexpensively. This often results in a part that will outwear the original by a factor of two, three or more.
3. Special characteristics: coatings can be applied to provide electromagnetic or electrostatic shielding, grip surfaces, thermal conduction, electrical conduction, electrical insulation, etc.

Plasma is often considered the fourth state of matter, after solid, liquid and gas. This extremely hot substance consists of free electrons, positive ions, atoms and molecules. Although it conducts electricity, it is electrically neutral. When a gas passes through an electric arc, the gas loses one of its electrons and becomes extremely hot plasma. Although temperatures can reach 30,000°F most plasma spraying is performed at lower temperatures. As the plasma leaves the spray gun, powdered material is introduced into the stream in precisely controlled amounts. The material is caught up in the plasma stream, becomes molten, and is projected against the surface being coated.

When an individual particle impacts against the surface, thermal and mechanical energy is transferred to the substrate producing forces which favor interatomic bonding. Under these circumstances, plastic deformation of the particle and the local surface area occur. The greater the deformation of the particle upon impact, the greater the probability of interatomic bonding.

Despite the intense heat produced within the gun, the temperature drops rapidly across the intervening gun-to-work distance. This drop is a function of gas enthalpy, energy absorption of the powdered material, and work distance. The composition of the substrate, its mass, relative gun-to-substrate traverse speed, and coating material are factors determining substrate temperature. This temperature can be held to a few hundred degrees by maintaining recommended spray parameters. Auxiliary cooling will reduce substrate heating even further. In laboratory experiments, metals have been sprayed on mylar film without damage to the substrate.

Control of the substrate temperature also leads to a minimization of residual stresses in the coating after deposition. The stress distribution of the coating process results in a tensile stress at the surface which can cause cracking and spalling and a compressive stress at the interface tends to weaken the bond between the coating and substrate and may cause coating breakaway.

Plasma sprayed materials can be sprayed onto virtually any properly prepared surface. Normally this preparation requires no more than grit blasting to slightly roughen the surface and remove any surface contamination. Since the energy of the surface also plays a significant role in the formation of interatomic bonds, this can

explain the success of grit blasting. The work hardening of the grit blasted surface creates a higher energy level at the surface, and serves to promote the formation of interatomic bond.

A wide variety of metallic, ceramic and organic powders have been sprayed by the plasma process. The major criterion for spraying any material is that it has a distinct range of temperature over which it remains in the liquid phase. Material which sublimates cannot be sprayed, and those materials which have a very high viscosity as liquids are difficult to spray.

Once a particular powder chemistry is selected for a coating application several additional variables of the powder must be controlled.

Some of these variables are:

- A. Phases present - materials of identical chemistry may have different crystalline-phases present.
- B. Particle shape, size and density - These characteristics of the powder have a controlling effect on the particle velocity.

It is important to closely control the particle size and size distribution of the powder. The particle size distribution range should be very narrow so that all the particles will require approximately the same thermal treatment for melting. In addition, a powder having a wide particle size distribution range will be subject to a great deal of segregation in the effluent prior to impact and this will result in a non-uniform coating layer.

The use of inert or semi-inert gases such as argon, argon/hydrogen, argon/helium or nitrogen gas mixtures permits the selection of materials which otherwise would oxidize if conventional flame spraying techniques were used. The use of hydrogen gas mixtures provides reducing conditions, increases the arc voltage and increases the heat transfer to the powdered particles.

For any specific arc gas, the effluent pressure, velocity and enthalpy are controlled by the combined effects of arc gas flow rate and input power to the torch. Within the envelope of stable operation these two variables are jointly regulated to accommodate different thermal properties of the various spray materials.

Other parameters which must be regulated during application of the plasma spray include gun-to-part standoff distance and rate of deposition. Too short of a spray distance generally causes overheating of the substrate. In addition, if the plasma torch is placed too close to the substrate, the powder has too short a dwell time and will not be completely molten upon impact with the substrate. Too large a spray distance is also undesirable since resolidification of the particle may occur prior to impact.

Based on the above considerations, the latest generation of Plasmatron (R) plasma spray equipment provided by the Plasmadyne, was selected for use in the APS process feasibility study. This equipment included a control console which could be interfaced with the APS process microprocessor by the simple addition of five interface relays. The plasma spray gun was supplied with two separate powder input ports to handle both constituents of the specified thermal barrier coatings. The powder supply hoppers use a volumetric control principle to accurately deliver the desired powder quantity without burdening the microprocessor with additional control functions. Powder delivery is determined by the rotational speed of the powder collection wheel inside the hopper canister.

Another feature of the equipment is the use of critical flow orifices instead of flowmeters to accurately control gas mass flows. A flowmeter is a mechanical device which depends on the mass and configuration of a float and tube to regulate flow past the float. The major drawback to this type device is dependence on back pressure. Each flowmeter is calibrated at some given back pressure and the calibration is only valid at that back pressure. Since different plasma conditions require different chamber pressures, the flowmeter does not accurately indicate the true gas flow. The critical flow orifice, on the other hand, will deliver a constant mass flow of the arc gas start after start as long as the orifice downstream pressure stays below the critical level. The mass flow level can be accurately set with the orifice upstream pressure regulator without actually firing the gun.

#### Process Parameters

The process parameters investigated in the preliminary deposition process study were those normally associated with plasma spray equipment:

1. Gun type and operating power level
2. Powder injection angle
3. Powder feed rates
4. Powder gas flow rates
5. Plasma gas flow rates
6. Plasma gun to substrate distance
7. Plasma gun traverse speed
8. Powder deposit rate

---

(R) Registered trademark of Plasmadyne, Inc., Santa Ana, CA.

The scope of investigation was concerned only with maintaining a coating quality similar to that produced at NASA (Ref. 1), not optimization. Major emphasis was on establishing control parameters amenable to the APS process.

All samples were sprayed with the spray pattern normal to the surface. Other investigators had previously found no noticeable effect on the deposited coating with spray angles varying up to 0.79 radian (45 degrees) from the normal (Ref. 2). For the APS process, the major concern over the effect of substrate geometry on deposited coating morphology is the lens effect on concave surfaces of the target airfoils. The incident material around the periphery of the spray pattern may be reflected off the blade and back into the spray and then onto the substrate. This could result in cold particles entrapped in the deposited coating. For this reason, it was thought desirable to keep the spray pattern or beam as narrow as possible for the APS process to minimize this effect. It was likewise desirable to keep the gun relatively normal to the surface,  $\pm 0.35$  radian ( $\pm 20$  degrees), to maintain tighter control over the coating deposition thickness uniformity.

In establishing the process parameters, only the 40 kW subsonic and 40 kW mach I electrodes were evaluated. Several combinations of spray techniques (foreward and backward powder injection), power levels and anodes were evaluated both with and without auxiliary gas. From these investigations the 40 kW subsonic electrode with foreward powder injection was selected. The combinations of parameters shown in Tables I and II, for NiCrAlY and 12%  $Y_2O_3$  -  $ZrO_2$ , respectively, seemed to closely duplicate the microstructure presented in reference 1. These were therefore selected for use in the APS feasibility demonstration.

### Evaluations

Experimental evaluations during the deposition process study were of two types — those for establishing the process parameters and those for determining the deposition profiles and rates. For establishing the process parameters, 300-series stainless steel metallographic evaluation specimens 5.08 cm (2 inch) square by 0.23 cm (0.090 inch) thick were coated with each of the coating materials (NiCrAlY and 12%  $Y_2O_3$  -  $ZrO_2$ ) as well as with the two-layer composite. For the deposition profile and rate measurements, carbon steel specimens 15.24 cm (6 inch) square by 0.32 cm (0.125 inch) thick were used. Each of these specimens contained a two-pass buildup and a four-pass buildup of plasma-sprayed coating over separate traverse lines.

The evaluation specimens were all sprayed by hand. To obtain the accuracy required for the profile determination specimens, the plasma gun was fixtured on a pneumatic drive device. The surface speed of the drive was 40.6 cm/s (16 in/s), and the specimen to be coated was fixtured at a 6.35 cm (2.5 inch) standoff distance.  $Co_2$  cover gas was used while coating all specimens, and the substrate temperatures were kept below  $204^\circ C$  ( $400^\circ F$ ). All specimens were prepared for spraying by grit blasting with 80 mesh aluminum oxide at 6.33 to 7.03 kgm/cm<sup>2</sup> (90 to 100 psig).

TABLE I  
PLASMA SPRAY PARAMETERS FOR NiCrAlY

<u>OPERATING MODE</u>	Subsonic
<u>GUN TYPE</u>	SG-100
Anode:	2083-135
Cathode:	1083A-129
Gas Injector:	1083A-113
<u>OPERATING PARAMETERS</u>	
Power:	21 kW
Voltage:	30 volts $\pm$ 3 volts
Current:	700 amps $\pm$ 25 amps
Arc Gas:	Argon
Flow Rate:	0.77 l/s (98 scfh)
Auxiliary Gas:	None
Power Gas:	Argon
Flow Rate:	0.9 l/s (12 scfh)
Powder Feed Rate:	0.70 g/s (42 g/min)
Standoff Distance:	6.35 cm $\pm$ 0.89 cm (2.5 in $\pm$ 0.35 in)
Surface Speed:	40.6 cm/s $\pm$ 5 cm/s (16 in/s $\pm$ 2 in/s)
Normal:	$\pm$ 0.35 rad ( $\pm$ 20°)
Cover Gas:	CO <sub>2</sub>



TABLE II  
PLASMA SPRAY PARAMETERS FOR 12%  $Y_2O_3$  -  $ZrO_2$

<u>OPERATING MODE</u>	Subsonic
<u>GUN TYPE</u>	SG-100
Anode:	2083-135
Cathode:	1083A-129
Gas Injector:	1083A-113
<u>OPERATING PARAMETERS</u>	
Power:	32 kW
Voltage:	37 volts $\pm$ 3 volts
Current:	800 amps $\pm$ 25 amps
Arc Gas:	Argon
Flow Rate:	0.77 l/s (98 scfh)
Auxiliary Gas:	Helium
Flow Rate:	0.20 l/s (25 scfh)
Powder Gas:	Argon
Flow Rate:	0.09 l/s (12 scfh)
Powder Feed Rate:	0.63 g/s (37.6 g/min)
Deposit Rate:	0.23 g/s (13.8 g/min)
Stand-Off Distance:	6.35 cm $\pm$ 0.89 cm (2.5 in $\pm$ 0.35 in)
Surface Speed:	40.6 cm/s $\pm$ 5 cm/s
Normal:	$\pm$ 0.35 rad ( $\pm$ 20°)
Cover Gas:	CO <sub>2</sub>

Figure 1 shows the microstructure of the two-layer composite coating deposited by Plasmadyne on one of the 5.08 cm (2 inch) square specimens using the process parameters selected for use in the APS process feasibility demonstration. Figure 2 shows the microstructure of a typical coating applied by NASA at that time. A comparison of these two photomicrographs indicates that the two coatings are very similar in structure and density. The as-sprayed surface finish of the Plasmadyne-coated samples is 10  $\mu\text{m}$  RMS. By light sanding, using 400 grit silicon carbide paper, the surface finish went below 3  $\mu\text{m}$  RMS.

Eight composite 50X photomicrographs were prepared from each of the 15.2 cm (6 inch) square specimens used to determine spray deposition profiles. Data was subsequently taken from the photomicrographs and subjected to a computer statistical analysis. The purpose of this analysis was to determine the optimum traverse or scan line spacing for each of the coatings to achieve maximum overall coating thickness uniformity. The effective coating thickness per pass using the optimum scan line spacing was also desired. The curve shown in Figure 3 was generated by the computer using a polynomial regression program to fit a second order curve through the data obtained for the 12%  $\text{Y}_2\text{O}_3$  -  $\text{ZrO}_2$  coating. No significant difference was found between the two-pass and four-pass data. Therefore, the curve shown is applicable to any single traverse of the plasma spray gun.

The curve shown in Figure 3 was then used by the computer to determine the optimum spacing between scan lines for overall coating thickness uniformity. This spacing was determined to be approximately 5 mm (195 mils) for the 12%  $\text{Y}_2\text{O}_3$  -  $\text{ZrO}_2$  coating. Figure 4 shows profiles generated by the computer assuming six passes of the plasma gun along each scan line. The lower (solid) curves are the deposition profiles which would result along each scan line in the absence of the others. The resultant overall coating thickness profile from summing all the scan line depositions is shown by the crosses at the top of the figure. The overall coating thickness from six passes per scan line is almost 127  $\mu\text{m}$  (5 mils) with peak-to-valley variations of approximately 7.5  $\mu\text{m}$  (0.3 mils). The effective overall coating thickness per scan line pass is thus approximately 21  $\mu\text{m}$  (0.82 mil). In actual coating applications a slight "feathering" (slight off-setting of the scan line from nominal between passes of a multiple pass application) would probably further minimize the surface ripples in the overall coating thickness.

The same type analysis was performed on the data for the NiCrAlY alloy coating. There was a significant difference between the data for the two-pass coating buildup and that for the four-pass buildup. Plasmadyne stated that it was not unusual for the first pass to result in a thicker coating buildup than subsequent passes, although the exact reason was not identified. The computer analysis therefore resulted in different deposition profiles for the first pass and subsequent passes for the NiCrAlY. These two curves are shown in Figures 5 and 6 respectively.

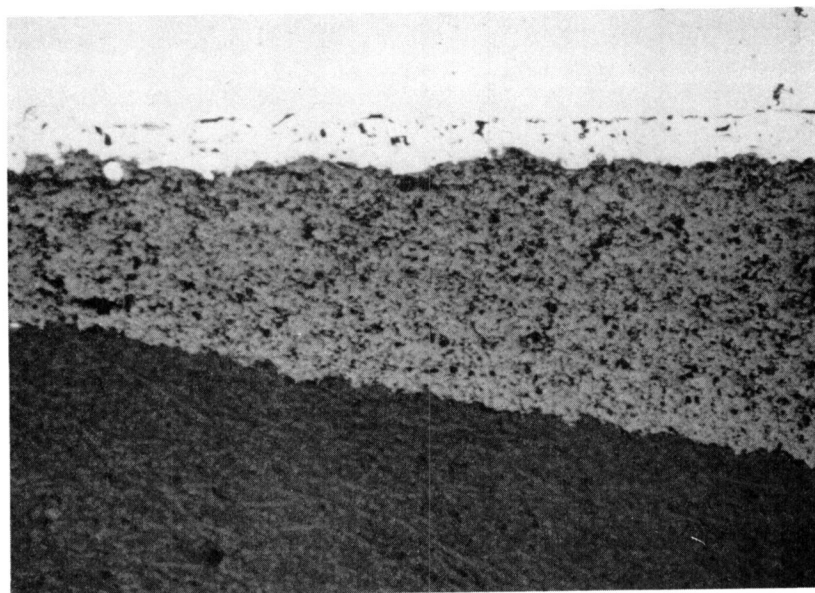


Figure 1. Microstructure of Two-layer (NiCrAlY/12%  $Y_2O_3$  -  $ZrO_2$ ) Plasma-sprayed Specimen Prepared by Plasmadyne Using Parameters Selected for APS Process. (100X)

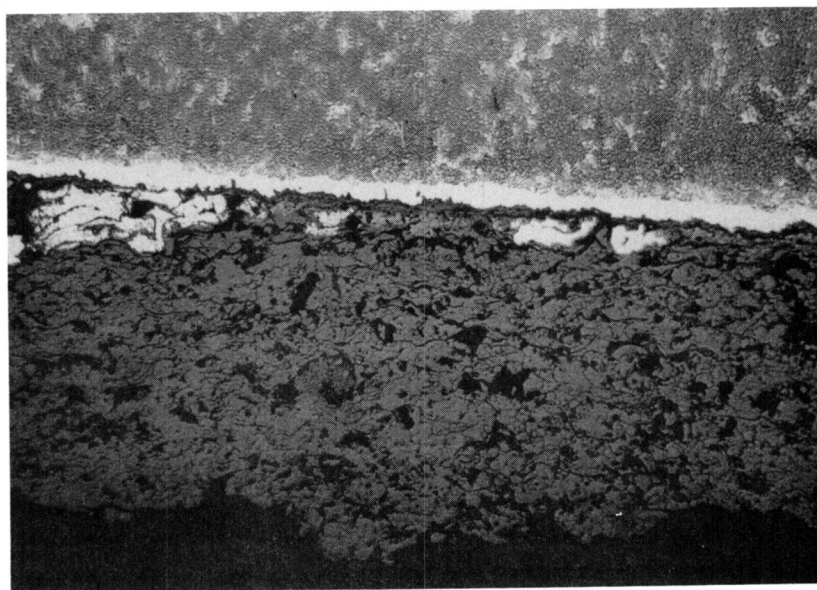


Figure 2. Microstructure of Typical Specimen Prepared by NASA in 1976 (Reference No. 1). (100X)

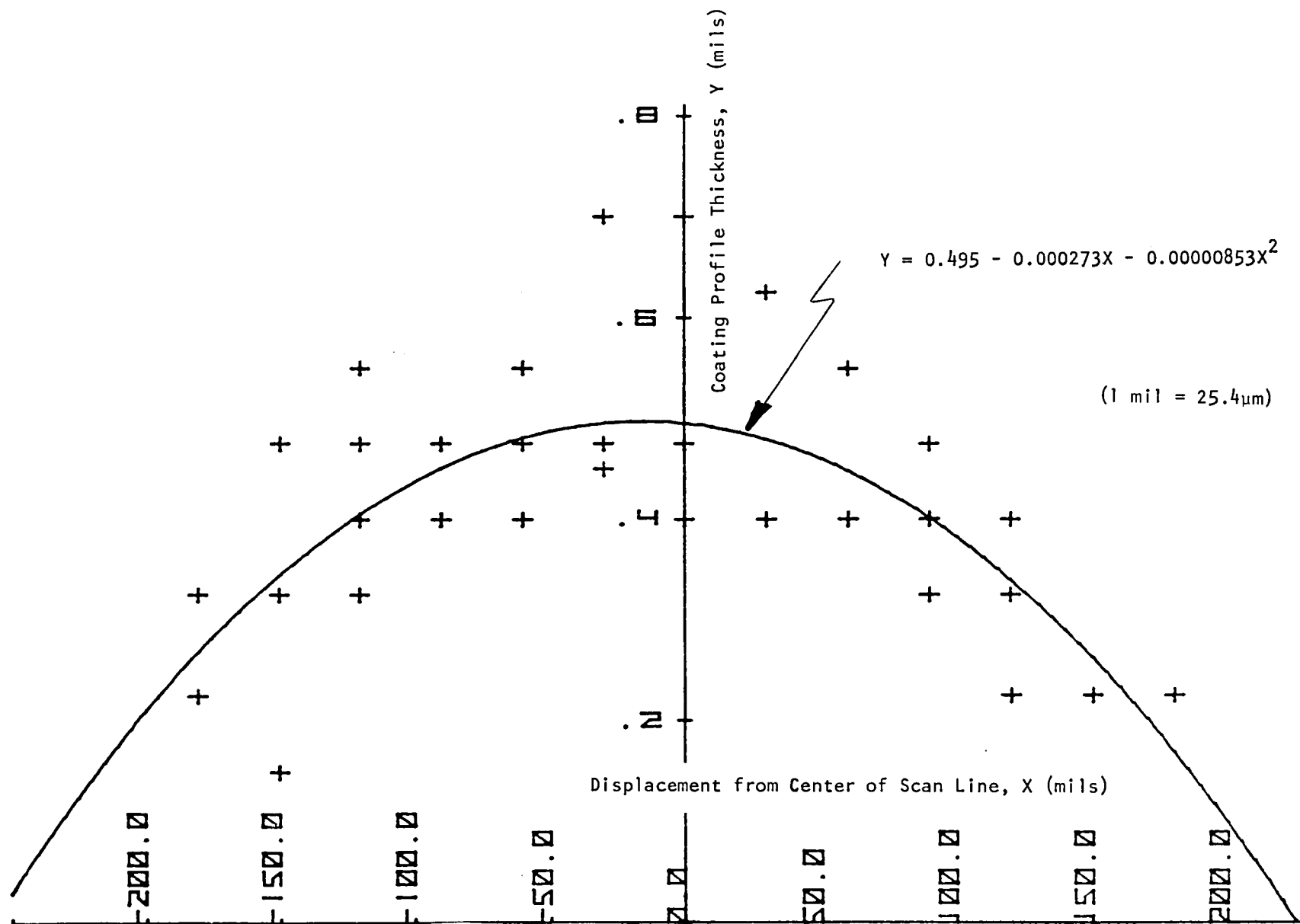


Figure 3. Computer-calculated Plasma-sprayed Coating Deposition Profile for a Single Scan Line Pass Using 12%  $\text{Y}_2\text{O}_3$  -  $\text{ZrO}_2$ .

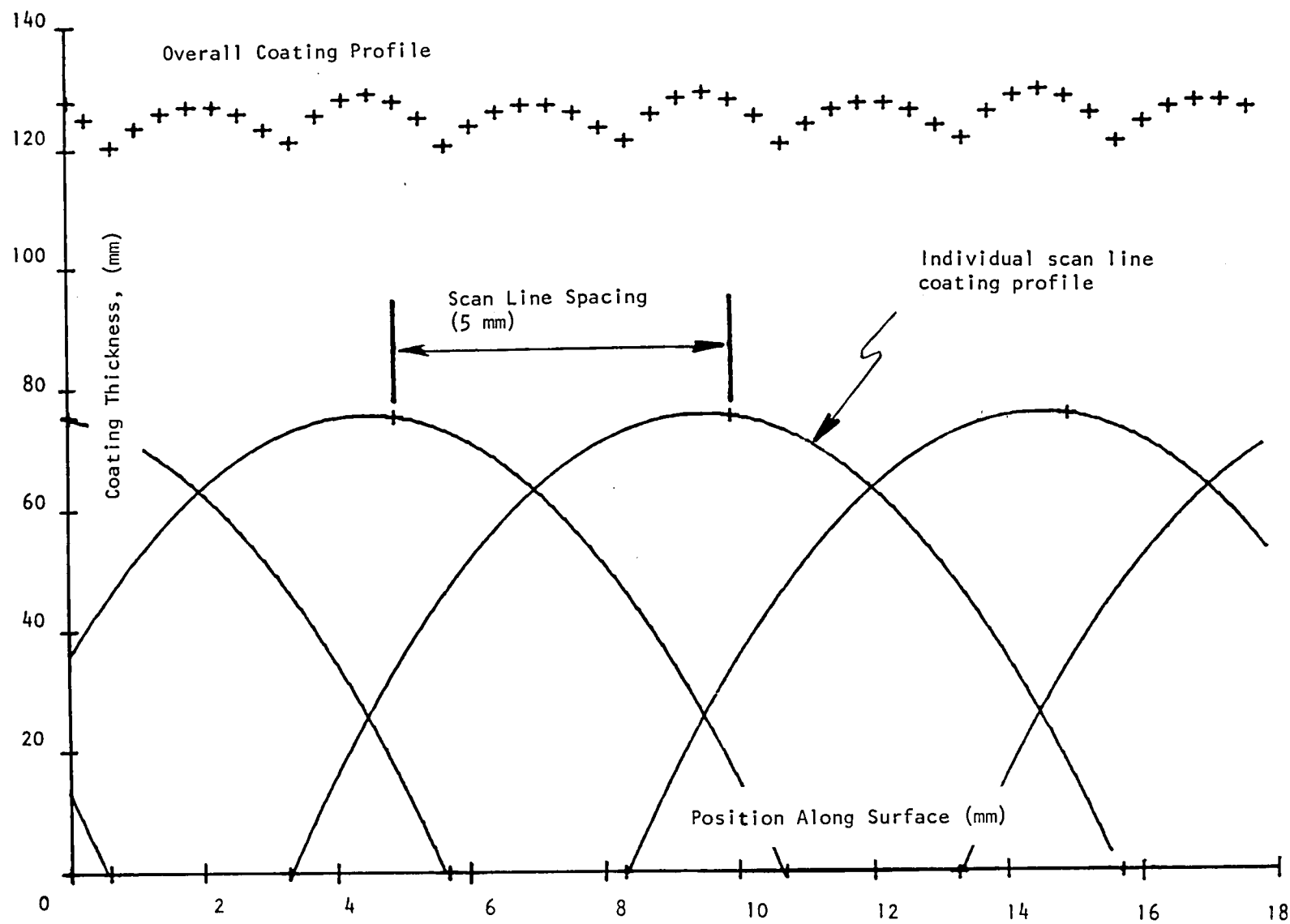


Figure 4. Computer-calculated Plasma-sprayed Coating Deposition Profiles for 12%  $Y_2O_3$  -  $ZrO_2$  (6 coating passes per scan line).

The computer determined the optimum scan line spacing for the NiCrAlY. However, in this case, both of the curves shown in Figures 5 and 6 had to be used. The optimum scan line spacing was found to be approximately 5mm (195 mils). Figure 7 shows profiles generated by the computer assuming four passes of the plasma gun along each scan line. The lower solid curves are again the deposition profiles which would result along each scan line in the absence of the others. The crosses again designate the summation of all the individual scan line depositions. For the NiCrAlY four passes on each scan line results in a total coating thickness of approximately 127  $\mu\text{m}$  (5 mils) with peak-to-valley variations of approximately 5.5  $\mu\text{m}$  (0.2 mil). The effective overall coating thickness was approximately 75  $\mu\text{m}$  (3 mils) for the first scan on all the scan lines and 16  $\mu\text{m}$  (0.64 mil) for each subsequent pass.

Based on the initial spray deposition process development phase results, the specific plasma spray hardware configuration and the associated process and control parameters to be used for the initial APS process feasibility investigations were selected.

#### APS Process Parameters

The APS process is being operated under normal ambient atmosphere conditions. No vacuum or other sealed chamber is being used. An inert cover gas ( $\text{CO}_2$ ) is being directed at the specimen being coated while the process is operational.

Coating deposition is accomplished using one plasma spray gun having two powder injection ports, each being independently fed by its own powder hopper. One powder hopper supplies the NiCrAlY material; the other supplies the Yttria-stabilized zirconium oxide material. Essentially the same plasma spray hardware parameters were specified for both materials. The differences were the torch power, use of an auxiliary gas with the zirconium oxide material, and use of different powder feed rates on the two hoppers. Most of the plasma spray operating parameters may therefore be manually preset; very few control interfaces are required with the APS process control hardware. In a production system, of course, it may be desirable to control additional parameters automatically. For this feasibility demonstration only five interface relays needed to be added to the plasma spray control console. The five signal interfaces were:

1. Start (or Run)
2. Hopper #1 Activate
3. Hopper #2 Activate
4. Power Level (#1 or #2)
5. Stop (or Purge)

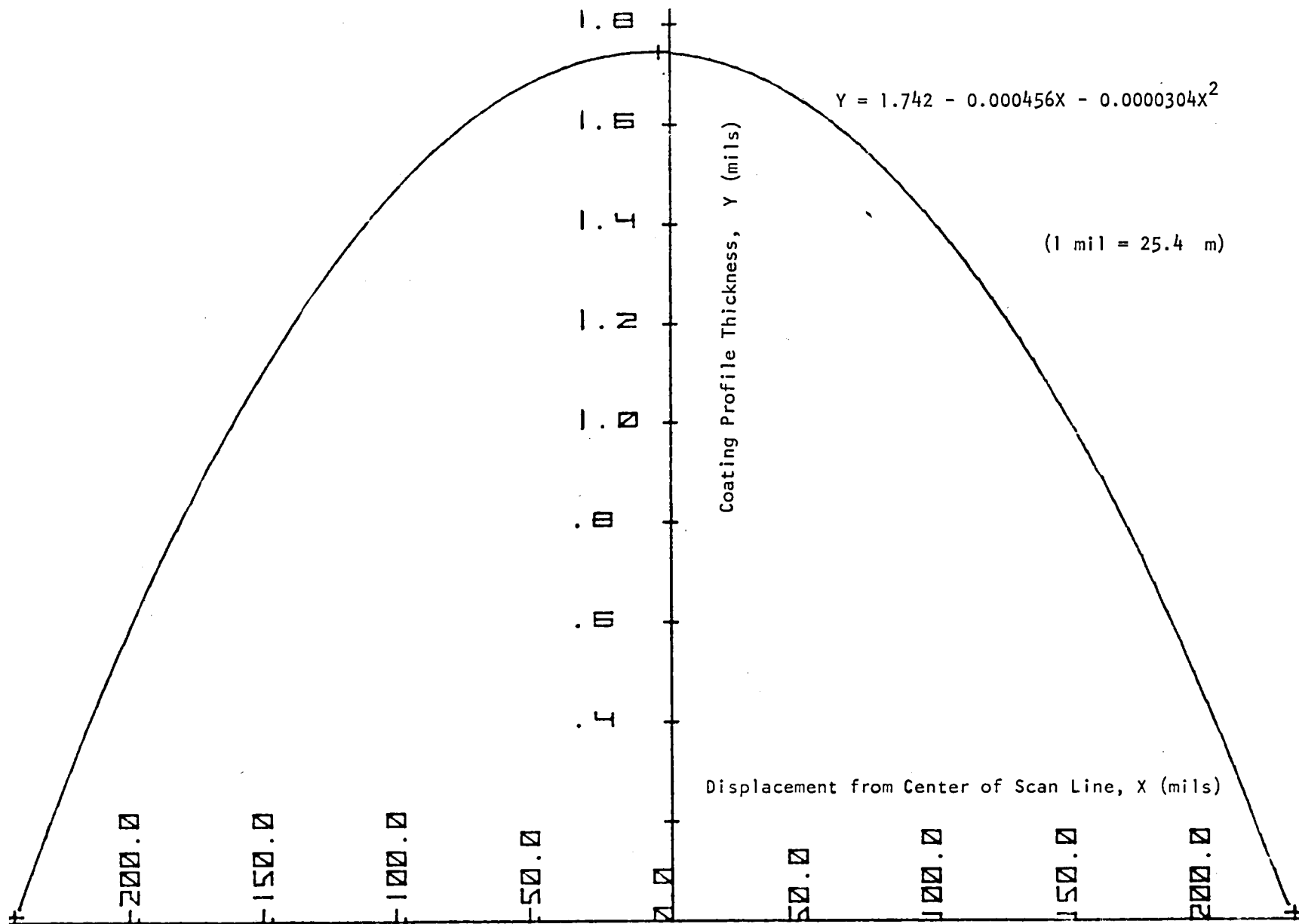


Figure 5. Computer-calculated Plasma-sprayed Coating Deposition Profile for a Single Scan Line First Pass Using NiCrAlY.

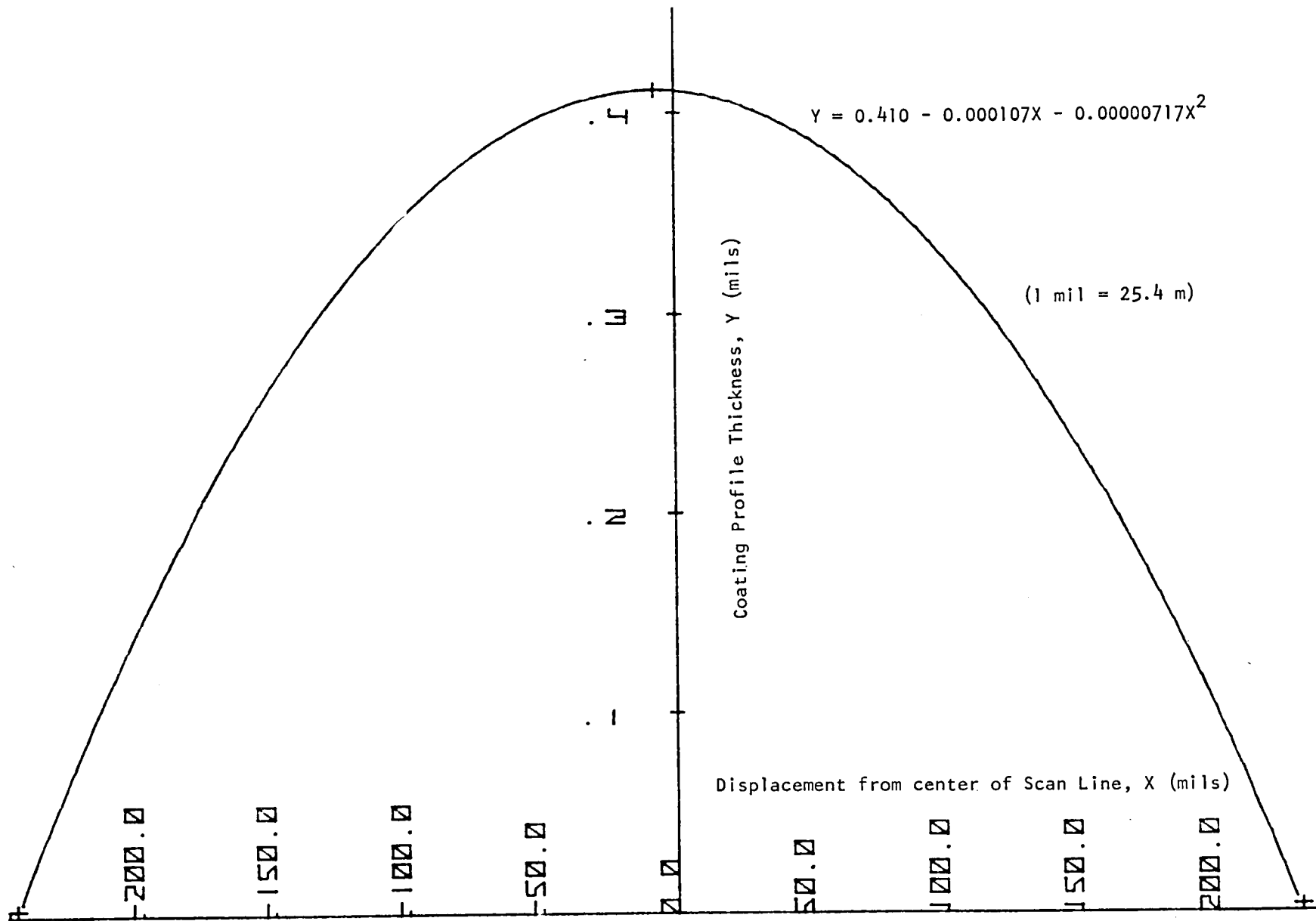


Figure 6. Computer-calculated Plasma-sprayed Coating Deposition Profile for Passes Other Than First for a Single Scan Line Using NiCrAlY.



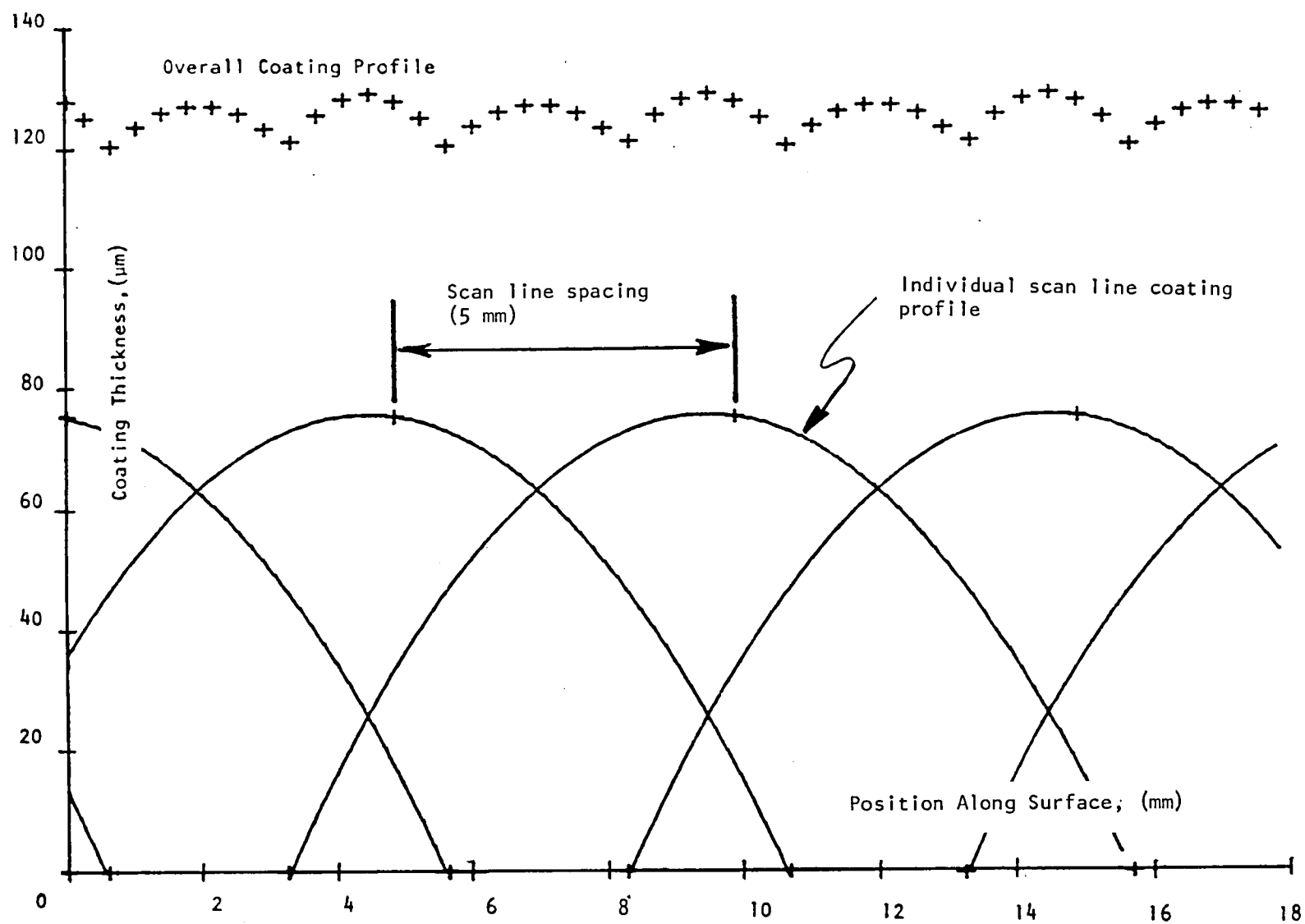


Figure 7. Computer-calculated Plasma-sprayed Coating Deposition Profiles for NiCrAlY (4 coating passes per scan line).

Various control parameters were also provided for use in initial process software preparation. The nominal scan line spacing and the number of passes required to build up a desired coating thickness are typical of these. Since the coating buildup per pass is relatively thin (16  $\mu\text{m}$  for the NiCrAlY and 21 for the zirconia) it is possible to control coating buildup on the various specimens surfaces to the desired  $\pm 38.1 \mu\text{m}$  ( $\pm 1.5$  mils). The possibility of using the same scan line spacing for both materials also reduced the burden on process firmware tables, since separate coordinate tables were not required.

The study did indicate that a slight amount of "feathering" may be required during coating deposition to maximize coating thickness uniformity over the specimen. However, it was felt that normal slight variations in the process parameters and in positioning system tolerances may provide adequate natural "feathering." The effects of surface curvature on the turbine blade specimens would also contribute in providing some blending of the theoretical profiles generated by the computer.

Finally, it should be emphasized again that this initial deposition process study was not intended to optimize the system parameters. It was intended to select parameters to be utilized in demonstrating feasibility of automatically controlling plasma spray deposition with tight control of thickness uniformity on (turbine airfoils).

#### 4.2 APS System Development

This phase of the APS process development effort was concerned with development of the various hardware and software subsystems with the exception of the specific plasma spray equipment (commercial items) selected during the initial deposition process study. The hardware subsystems include the various mechanical positioning subsystems and fixturing, the metrology subsystem for in-process monitoring of coating thickness buildup on the specimens, and the microprocessor-based process control subsystem. The software includes both the software subroutines used by the microprocessor to control the overall APS process and the firmware tables which define specific process and specimen characteristics. This phase of the program was conducted in parallel with the initial deposition process study and incorporated results of that study as they became available.

#### Technical Approach

The conventional approach in attempting to deposit uniform thickness plasma-sprayed coatings has been to utilize large stand-off distances between the gun and specimen. The spray pattern diverges as it leaves the gun and tends to become more uniform as it fans out over larger and larger areas. If a large enough stand-off distance is used, and the specimen being sprayed is not too large, an entire side of the specimen can be coated at one sweep. Vacuum chambers are often used to allow even greater stand-off distances.

The stand-off distance cannot be increased, however, without a trade-off in coating quality, and frequently the optimum stand-off distance will not yield desired uniformity in coating thicknesses. The conventional approach, therefore, is not amenable to close control of the localized uniformity variations over a specimen surface. This is particularly true for specimens having complex geometries and small radii of curvature.

The approach selected is diametrically opposite to the conventional approach. The APS process utilizes relatively small gun-to-part standoff distances and normal ambient atmospheres. This produces a minimum instantaneous deposition spot size which can be controlled to more uniformly coat curved geometries. An in-process optical gage is utilized to monitor the localized coating thickness buildup over the specimen. Feedback from this gage to the process controller allows the process to adapt to process variations and vary the deposition patterns until the desired coating thickness and uniformity are achieved over the entire specimen.

A simplified functional block diagram of the APS process, defining the major subsystems of the approach, is shown in Figure 8. The system is seen to consist of four major subsystems -- a mechanical positioning and scanning subsystem, a metrology subsystem for deposited coating thickness monitoring, the plasma spray hardware, and the overall process control subsystem. The plasma spray equipment consists of essentially standard commercial items with the exception of the interface modifications to allow APS process control. The other three subsystems, developed for the APS process, will be discussed in the following paragraphs.

A microprocessor was selected as the basis for the system controller. This provides an intelligence unique among the various alternatives considered -- i.e., hard-wired logic, relay controllers, numerical control, etc. The microprocessor is capable of making decisions based on the desired thicknesses and the data from the in-process optical gage. It can then automatically initiate iterations of the coating deposition cycle over selected portions of the specimen surface to produce the desired thicknesses. By utilizing firmware lookup tables (i.e., a single erasable programmable read-only memory (EPROM) of geometric coordinates and process specifications) unique to each type of specimen, a single set of process control software can accommodate almost all types of parts to be coated. Changes in the process are readily incorporated by relatively easy software changes rather than hardware changes.

In this APS process application for coating turbine parts, the microprocessor-based system proceeds as follows:

1. The part is loaded in the fixture and the plasma gun readied for operation.
2. When the run button is activated, the microprocessor indexes the part to the gaging station and records the bare part reference values at specified locations.

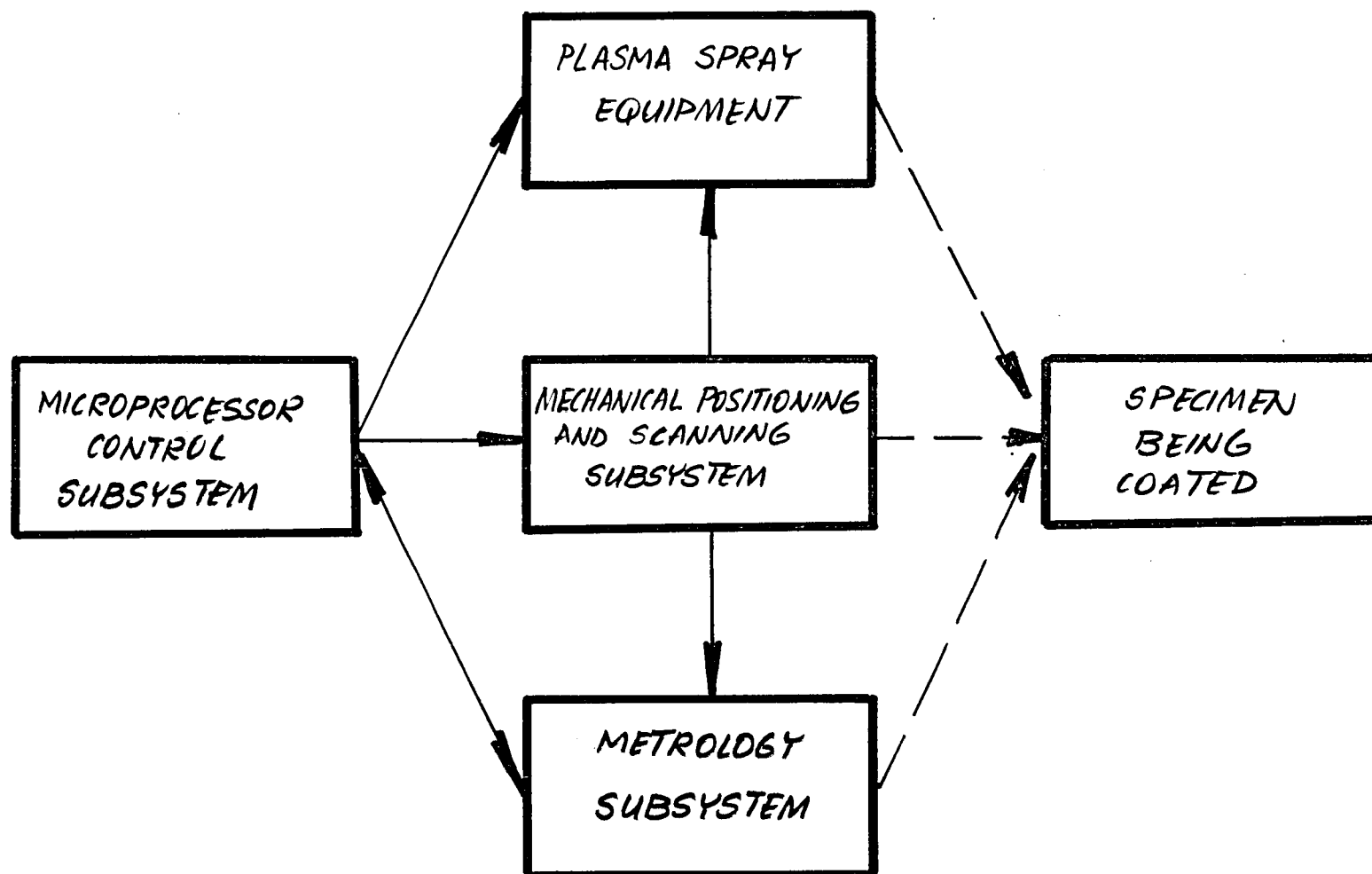


Figure 8 . APS System Functional Block Diagram.

3. The part is indexed through specified scan orientations while the plasma spray gun is automatically activated at the proper time intervals.
4. After completion of a percentage of spray scans slightly under the required number, the part is indexed to the gage position and the thickness values are measured at the specified locations.
5. The microprocessor calculates the remaining scans required on each line to achieve the required coating thickness and uniformity.
6. Step 3 is repeated for the required scan iterations.
7. The part is indexed through a final gage cycle to verify the coating thickness and uniformity.
8. If all portions of the part are not up to the required thickness, steps 5 through 7 are repeated until all are; the microprocessor then outputs the actual measured coating thickness at each gage point on a digital printout.
9. The part is indexed to the load position for removal and replacement with a new part.

The APS process subsystems developed to accomplish this procedure are described in the following paragraphs. The detail data is in Appendices 3, 4, 5 and 6.

#### Mechanical Subsystem

The mechanical subsystem provides the required component positioning and scanning functions as commanded by the system controller. These functions may be further subdivided into three subassemblies: the blade handling device (BHD), the spray gun scanning fixture (SGSF) and the coating thickness measurement device (CTMD) or optical detector positioner. Each of these subassemblies is described separately.

#### Blade Handling Device

The primary application for the APS process is coating turbine airfoil geometries. Therefore the blade profile characteristics to be accommodated had a strong influence on the concept selected for specimen orientation. A major portion of turbine airfoil profiles can be very closely generated by families of straight line segments lying within the blade surface. It therefore appeared reasonable to apply the plasma spray while scanning along these straight line segments. By sequentially positioning the various line segments, or scan lines, in front of the plasma spray gun so as to precisely control the spray deposition overlap between adjacent lines, very uniform surface coating thickness can be produced. Precise control of spray gun traverse speed provides coating uniformity along the scan lines. Since the coating thickness applied per scan line traverse is on the order of 13 to 25  $\mu\text{m}$  (0.5 to 1.0 mil),

the total coating thickness is built up of repetitive gun traverses over each scan line. Minor local surface thickness variations on the airfoil surface can therefore be minimized by slightly staggering the scan line locations between repetitive scans so as to "feather" the deposition profiles. All the motions required are implemented by relatively simple algorithms in the microprocessor logic controller.

To implement this APS process concept for the feasibility demonstration, a five axis BHD was designed and fabricated. The five axes of motion which the BHD can impart to the blade specimen are indicated in Figure 9. The two translational axes, X and Y, control blade motion transverse to the locations of the plasma spray gun and optical detector and blade standoff distance from the gun or detector respectively. The three rotational axes, A, B and C, provide blade rotations around the X and Y axes and around a longitudinal axis of the blade, respectively. With these five degrees of freedom any selected scan line on the surface of the blade airfoil may be positioned in a vertical orientation at a selected standoff distance from the spray gun. Only a single degree of freedom, an up/down scanning motion (ZZ), is therefore required on the plasma spray gun to spray the selected scan line. Likewise, only a single degree of freedom is required for the optical detector to allow it to be focused on any selected gage point on the airfoil surface. This is provided by the vertical translation axis Z.

The APS system concept illustrated in Figure 9 is thus seen to provide essentially two six-degree-of-freedom subsystems with only seven axes of motion. The five BHD axes plus the ZZ axis provide six degrees of freedom for plasma spray deposition on the specimen. The Z axis plus the five BHD axes provide six degrees of freedom for positioning the optical detector probe relative to the specimen surface during coating thickness metrology. This concept implementation appears to require the minimum number of control interfaces to provide the required six degrees of freedom between the blade specimens and both the spray gun and the optical detector. In the most basic operational mode, the motions required of the X, Y, A, B and C axes are all index motions between coating deposition traverses of the plasma spray gun. These index motions position the selected scan line in front of the gun. Coordinates for the scan line are selected from the firmware EPROM by the microprocessor. The firmware data also establish the limits of the gun traverse and the desired coating thickness to be applied. The gun traverse cycles along the ZZ axis are normally the only component motion during the actual coating deposition.

A photograph showing the BHD implementation for the APS process feasibility demonstration is presented in Figure 10. The system controller, the CTMD and SGSF, are also shown in this figure. The positioning subassemblies are mounted on a heavy duty machine base to provide the stiffness and ruggedness required for the high resolution measuring and positioning involved. The blade specimen (shown towards the right center of the assembly) is suspended upside down below the BHD translating cradle to minimize dust protection requirements during spray application. Actually, little additional dust protection is incorporated into the feasibility demonstration model. The leadscrews and gears are exposed. Covers would, of course, be required on a production model.

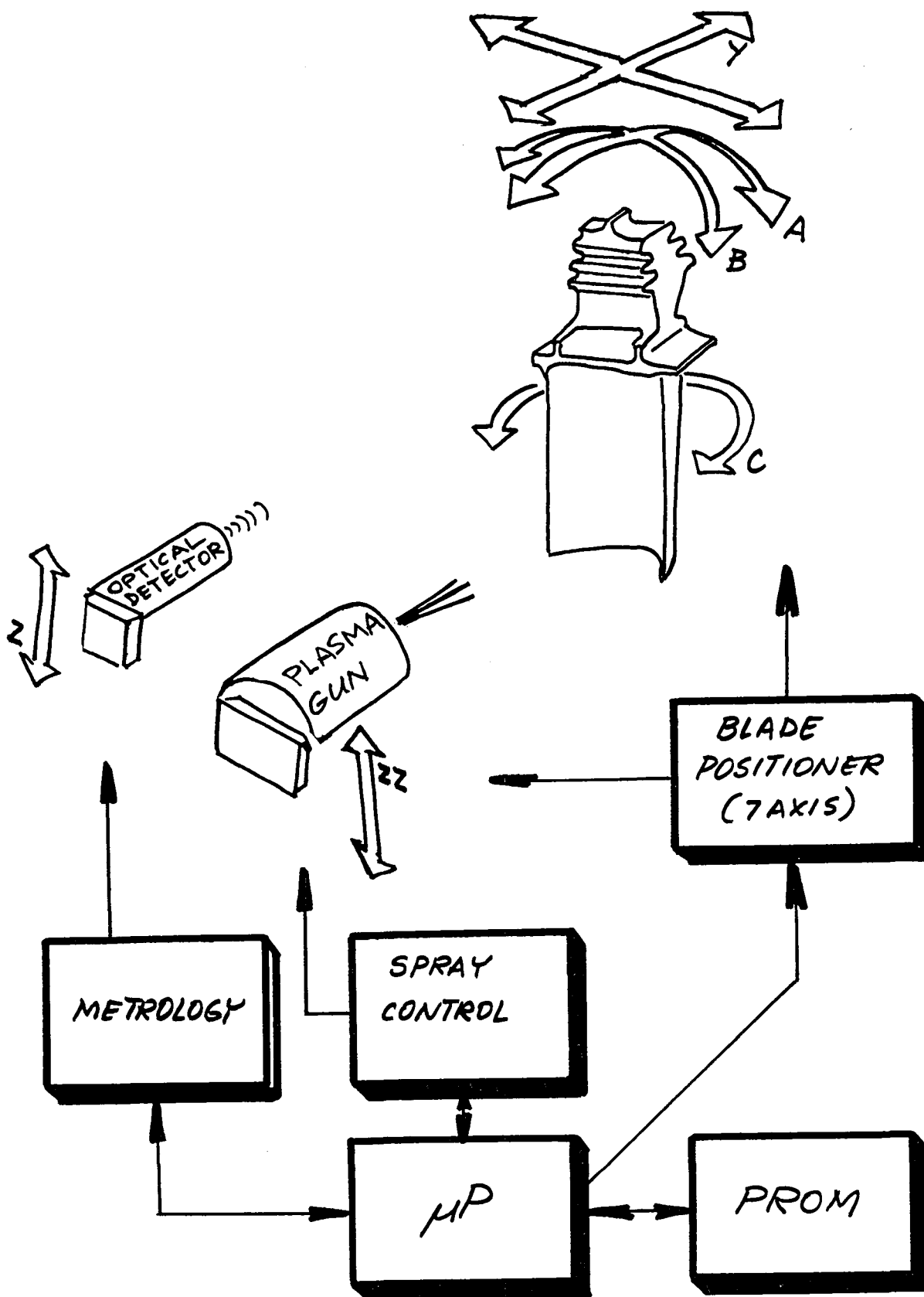


Figure 9 . APS System Concept Defining the Seven Axes of Motion

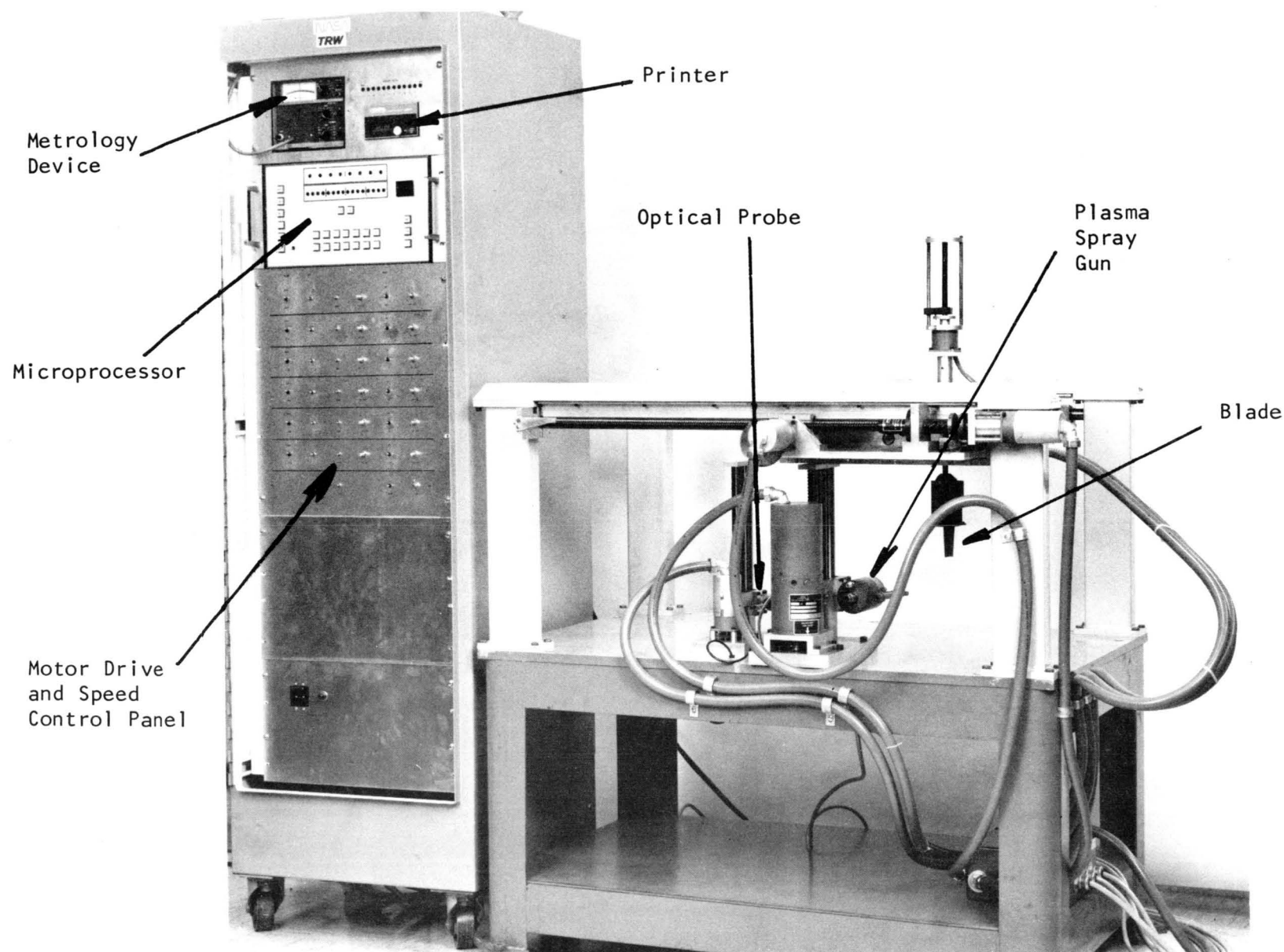


Figure 10. APS System Controller, Blade Handling Device, Coating Thickness Measurement Device and Spray Gun Scanning Fixture Assemblies as Implemented for APS Process Feasibility Demonstration.



### Mechanical Design Concept

The X and Y translational axes of the BHD are provided by preloaded ball-screw/ball-nut subassemblies. The A and B rotational axes are also driven by ball-screw/ball-nut subassemblies due to incorporation of a unique dual gimbel assembly supporting the blade holding fixture. The lower gimbel assembly is fixed in the cradle bottom plate. The upper gimbel assembly is translated in a fixed horizontal plane relative to the lower assembly by the two ball-screw assemblies thru a dual slide assembly. This results in the compound angle rotations required by the A and B axes. The C axis is a straight 180/1 rotational stepdown through a commercial speed reducer from the stepping motor to the blade holding fixture.

All five axes on the BHD are driven by digital stepping motors. The step size resolutions provided by the respective motors through the leadscrew and/or gear assemblies are  $25.4\text{ }\mu\text{m}$  (0.001 inch) for the X axis,  $5.08\text{ }\mu\text{m}$  (0.0002 inch) for the Y axis, and 0.175 milliradians (0.01 degree) for the three rotational axes. These resolutions are required to provide the desired  $\pm 38.1\text{ }\mu\text{m}$  ( $\pm 1.5$  mil) coating thickness tolerance on airfoils up to 25.4 cm (10 inches) square assuming a repeatability of  $\pm 1$  step for each axis.

Although very small resolutions are provided on the BHD axes, absolute accuracies of this magnitude are not critical. This is due to the technique of comparing differences in repetitive measurements to measure coating buildup. Repeatability of the positioning systems is a critical factor in the achievable measurement accuracy however. This means that all backlash in the positioning loops must be minimized. For these reasons it was possible to use rolled, rather than ground, ball screws on the BHD; but opposing, preloaded, ball nut pairs were utilized to minimize backlash. In addition, software compensation for the backlash was provided for the A, B and Y axes where the probability of problems was greatest.

### Electrical Design Concept

To avoid potential EMI (electromagnetic interference) problems in the plasma spray facility, no shaft encoders were incorporated into the BHD. Only the relatively high level motor drive electrical signals are in close proximity to the plasma arc. These are heavily shielded. Solid state integrated circuit counters for each axis are located back in the microprocessor chassis. These counters keep track of the absolute position of each axis. Since these counters have no memory when power is removed from the system, however, it was necessary to equip each axis with a "zero reference hard stop. After any system power up, each motor is automatically driven to its zero reference stop and the respective counter is cleared. The hard stop is provided at one extreme of ball screw travel for each axis. An auxiliary ball screw with a translating stop subassembly was mounted on the rear end of the C-axis motor to provide a zero reference stop for this motor. This subassembly is visible above the top of the BHD in Figure 10.

### Blade Holding Fixture

The blade holding fixture for supporting the specimen being sprayed mounts on the end of the C-axis shaft. One of the earlier models of this fixture for JT9D first stage turbine blades is visible in Figures 10 and 11. The specimen is slid into the clamp and locked by a single set screw. A cover drops down over the clamp, the blade root and the edges of the blade platform. This protects these areas from deposition of the sprayed coating without the need for masking. The current model of this fixture is a smaller, simplified, cylindrical design.

The BHD as shown in Figure 10 was designed for a feasibility demonstration. At that time it was planned that it would be operated for a period of two months instead of the present fifteen months. Many of the mechanical subassemblies are therefore a light duty, instrument quality utilizing commercially available off-the-shelf hardware. Also, items such as dust covers were not incorporated into the design. Although many maintenance-type problems are arising due to this extended operational service, the subassembly has held up surprisingly well.

### Gun Positioner

The gun positioner or spray gun scanning fixture (SGSF) is visible on Figure 10 and in greater detail on Figure 11. As discussed in the previous section, only a single degree of freedom is required for this subassembly, the ZZ-axis (Figure 9).

The spray gun motion is guided by two parallel vertical ball rod/ball bushing subassemblies. It is driven by a ball screw. The drive motor, unlike those on the BHD axes, is not a typical digital stepping motor. A stepping motor could not be found with a high enough torque/speed characteristic to handle the requirements of this axis. Instead, the SGSF motor is a dc servomotor/resolver subassembly with a digital interface driver. To the control microprocessor it appears almost identical to a digital stepping motor. In operation, the SGSF provides a cyclic up/down scanning motion to the plasma spray gun. To achieve uniform coating deposition along a scan line the motor speed is digitally controlled by a remote clock pulse generator in the process control console. For the 40.6 cm/s (16 in/s) traverse speed specified by the initial deposition process study (Tables I and II), the clock rate is 2667 Hz.

The motor used on the SGSF is considerably heavier duty than would normally be required for the specified speed and torque load. The reason is the extremely short stroke length utilized for small specimens such as the JT9D turbine blade. For this specimen the SGSF provides between 3 and 4 scan line traverses per second while depositing the coating. A major portion of the motor duty cycle consists of decelerating, reversing and accelerating the spray gun assembly at each end of the gun traverse. This must be done very rapidly to provide uniform speed and hence coating deposition on the specimen. The limiting characteristic of the motor is therefore the thermal duty cycle rating rather than the torque/speed characteristic. While the duty cycle requirement could be lessened by employing fewer part traverses per second, this would result in considerably lower powder utilization efficiency. It would also create thermal problems in the blade clamping fixture subassembly by increasing plasma beam dwell on this subassembly during gun reversal.

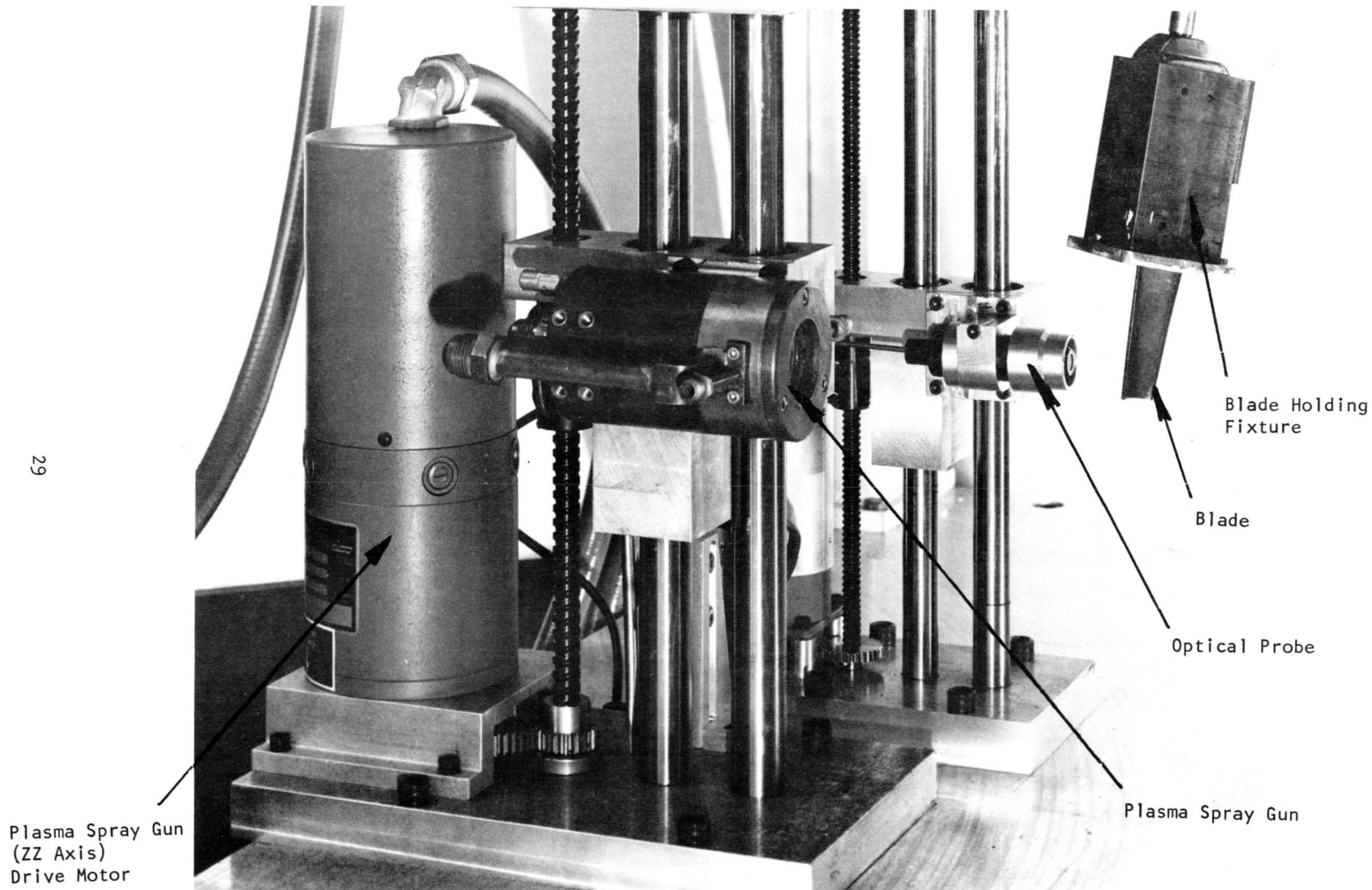


Figure 11. Closeup of Blade and Optical Probe During Gage Point Measurement Routine. Spray Gun Scanning Fixture also Shown in Left Foreground.

Because of the high speed scanning requirement for the SGSF and the lessened requirement for precise stationary positioning, the step size resolution for the ZZ axis is only 0.15 mm (6 mils). This is considerably coarser than all the other axes.

### Optical Detector Positioner

The optical detector positioner for the coating thickness measurement device (CTMD) is very similar to that for the spray gun. It is also visible in Figures 10 and 11. Again the motion is guided by two parallel vertical ball rod/ball bushing subassemblies and driven by a ball screw. A conventional stepping motor is used to drive the ball screw however. A finer ball screw subassembly is also employed, since precise positioning is required instead of high speed scanning. Step size resolution along the Z axis is 25.4  $\mu\text{m}$  (0.001 inch).

During gaging operation, the selected gage point on the specimen surface is positioned in front of the optical detector probe by simultaneously indexing the Z axis and the five BHD axes to the gage point coordinates selected from the EPROM firmware lookup table by the microprocessor. The Y-axis on the BHD then initiates a sequential stepping, or scanning, motion until the "valley point" in the optical detector response curve is located. The Y-axis coordinate position at which this valley point is detected is then stored in RAM (random access memory) by the microprocessor for use in coating thickness determination. (A detailed description of the metrology subsystem operation is discussed in the next section.) This procedure is repeated at each gage point specified for the particular specimen being coated.

The fiber optic probe utilized with the optical detector fits in with the general APS hardware design philosophy. It exposes no low signal level electronic circuitry to the high EMI ambient in the near vicinity of the plasma arc. Again the only electrical signals to the optical detector positioning subassembly are the relatively high level drive currents to the stepping motor.

### Metrology Subsystem

The metrology subsystem consists of the optical probe, the Y-axis of the BHD in the mechanical subsystem and selected portions of the microprocessor.

The optical probe is a commercially available instrument, the KD-100 Fotonics Sensor, manufactured by MTI Instruments, Latham, N.Y. It operates on a well-known principle illustrated in Figure 12. At one end a light source is used to illuminate half of the elements in a bundle of optical fibers, while a photo detector interrogates the other half of the fibers for returning light. At the other end of the fibers are mixed together to form the measurement probe. The relative amount of light received at the detector as a function of distance of the probe from a reflecting surface is shown in Figure 13. The received intensity, which is zero at contact, increases linearly with separation as more and more of the cone of light from each transmitting fiber is reflected onto a receiving fiber. When the receiving fibers are completely illuminated the intensity reaches a peak and then falls off as the square of the distance. This type of probe provides two regions of measurement. The rising side of the curve provides a region of high sensitivity but short range, while the following side of the curve provides considerably reduced sensitivity, but is fairly linear over a much wider range. In either case the probe must be in relatively close proximity to the target.

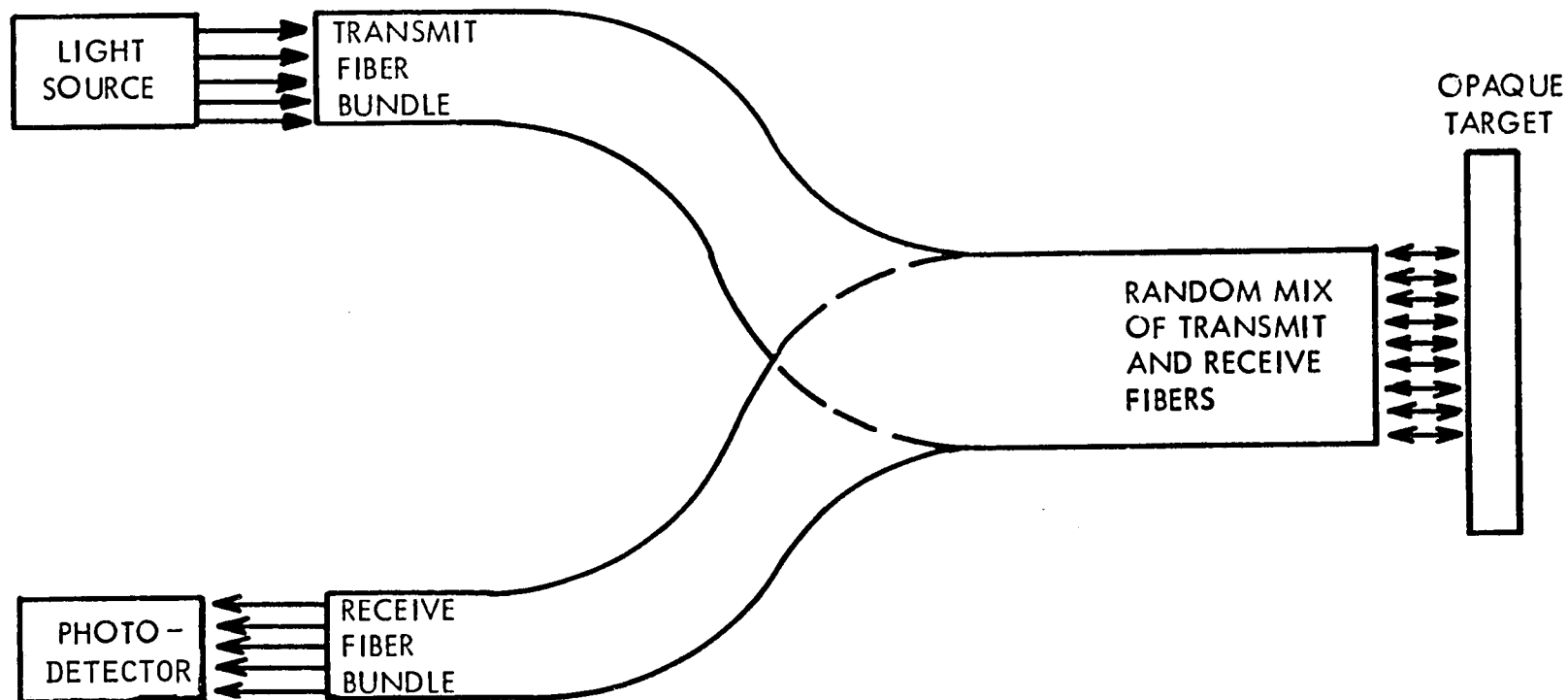


Figure 12. Concept Diagram of Non-coherent Optical Probe.

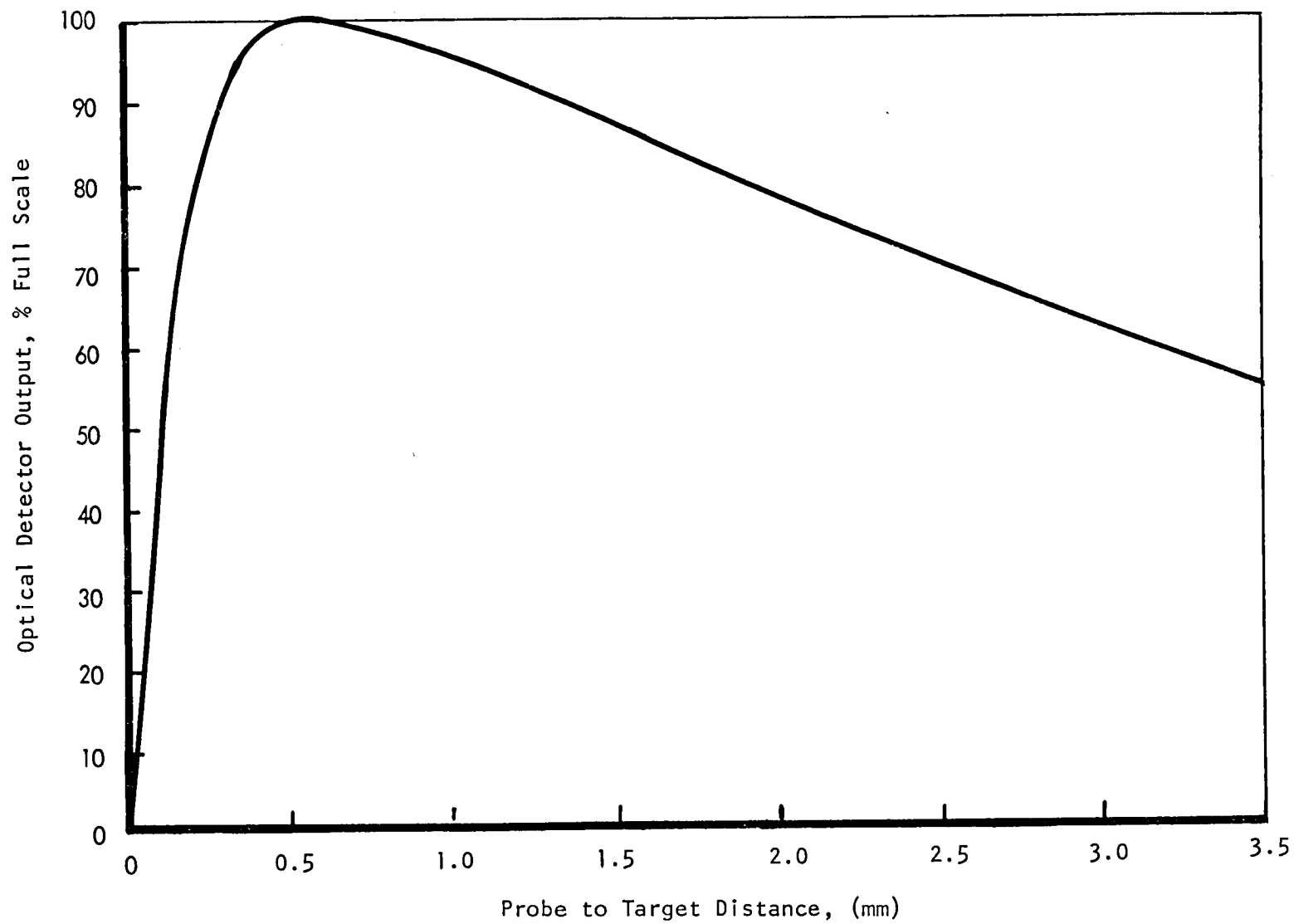


Figure 13. Typical Optical Detector Response With Bare Fiber Optic Probe.

A modification to this basic design is to add a lens system to the end of the probe to focus the end of the probe on the target. This allows a standoff distance which is a function of the optics and also allows the light spot to be made larger or smaller than the probe at the focal point of the optical extender. Figure 14 shows the intensity versus distance from the end of the lens system to the target. The portion of the curve from the focal point to the right is nearly the same as for the probe alone. A mirror image of this curve extends from the focal point in toward the target. Therefore there are two high sensitivity regions and two lower sensitivity regions. This makes it possible to make measurements with a significant standoff distance between the target and the probe.

Using the intensity versus displacement curve for measurement has a number of limitations, either with or without the optical extender. First, the intensity is a function of a number of factors other than the distance from the target. Among these factors are surface emissivity, color, texture and curvature. This means that accurate measurements can only be made on a uniform surface. Second, the measurements are affected by the long term drift of the electronic readout. Third, the range over which measurements can be made is still limited by the probe design.

These shortcomings can be overcome, however, by taking advantage of the characteristic curve created by the optical extender. At the focal point of the lens system, the intensity curve shows a sharp local minimum. The location of this minimum is independent of factors such as the color, texture and curvature of the target. It is a function only of the optical extender and the location of the probe with respect to the lens system. Using these principles the optical probe and extender are mounted on a precision axis of movement with position indication and the probe is moved with respect to the target until the local minimum, or valley, is detected. This technique is not affected by the target characteristics; its range depends only on the mechanical positioning device, and its accuracy depends on the precision of the positioning axis and the accuracy with which the valley can be located.

For the APS process this measurement scheme has been implemented for the particular case of a random bundle of 76  $\mu\text{m}$  (0.003 inch) diameter optical fibers with an optical extender providing a 1 cm (0.4 inch) standoff distance. This probe, which has an active diameter of 0.22 cm (0.086 inch), has a sensitivity of 0.2  $\mu\text{m}/\text{mV}$  (7.8  $\mu\text{in}/\text{mV}$ ) over a range of about 76  $\mu\text{m}$  (0.003 inches) on the rising curve and a sensitivity of 0.6  $\mu\text{m}/\text{mV}$  (23.2  $\mu\text{in}/\text{mV}$ ) over a range of about 0.18 cm (0.070 inches) on the falling curve. The noise level at a response frequency of 30 kHz is about  $\pm 35$  mV which limits the high speed measurement accuracy. However, with appropriate filtering the noise can be reduced to less than  $\pm 1$  mV.

The output of this probe with the optical extender is shown in Figure 15 over a limited range near the valley. The location of the valley is at 1.10 cm (0.433 inch) distance between the target and the end of the optical extender. With a maximum output of 9V the output at the valley is 0.5V. The width of the valley over which the

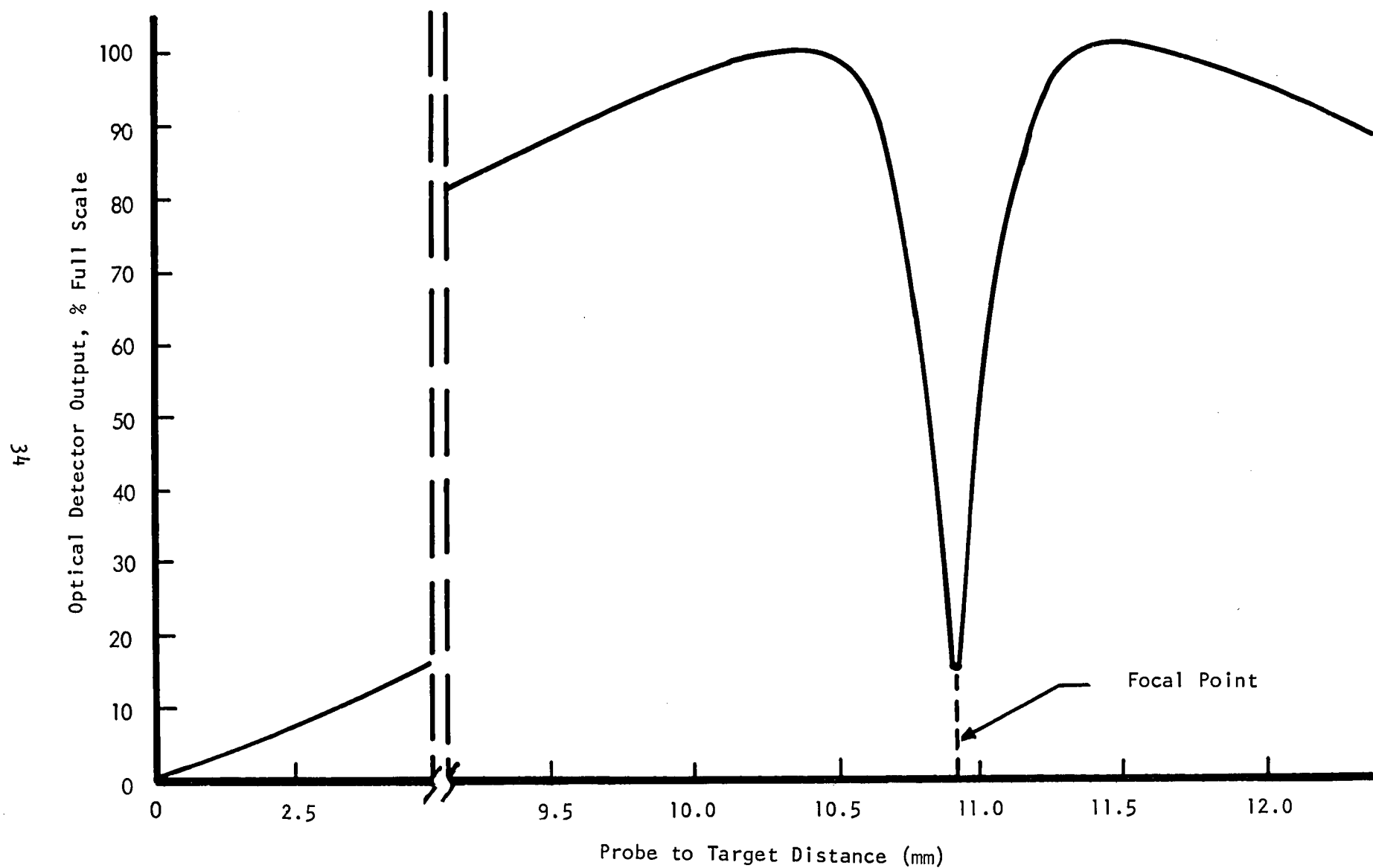


Figure 14. Typical Optical Detector Response With Fiber Optic Probe and Optical Extender.



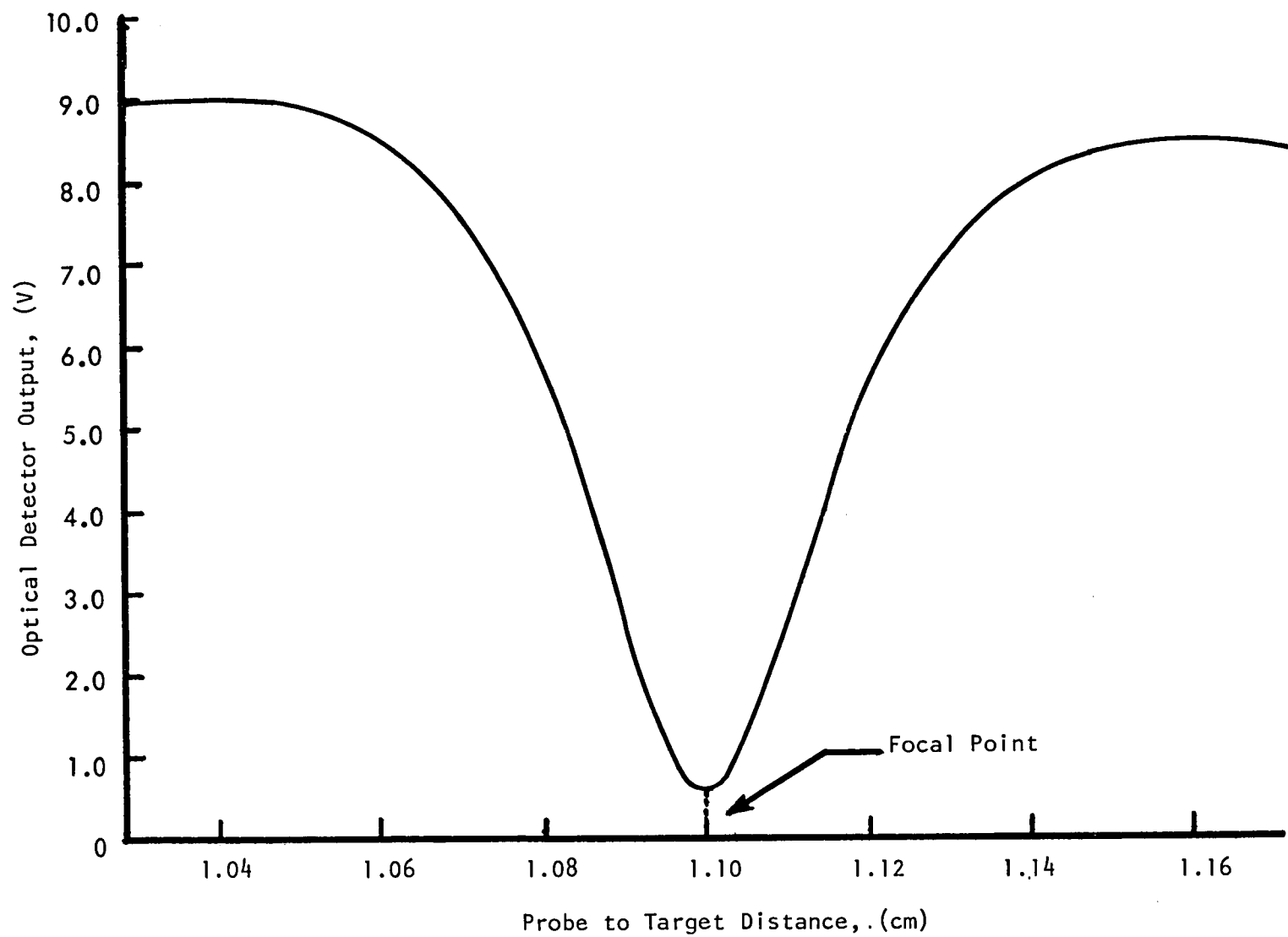


Figure 15. Optical Detector Output Response in the Valley Region.

voltage change is less than 1mV is about 10  $\mu\text{m}$  (0.0004 inches). The target in this case was a bright, flat, but fairly rough  $\text{ZrO}_2$  plasma sprayed surface. For changes in the brightness, curvature or surface texture of the target, the difference between the peak and valley voltages will increase or decrease having a small effect on the accuracy with which the valley can be detected, but the location of the valley does not change.

For the purpose of making measurements, the end of the fiber optic bundle and optical extender are mounted on the Z-axis, which positions the probe vertically along the length of the airfoil. The Z axis and the A, B, C, and X-axes of the BHD are used to position the gage point to be measured in front of the probe with the surface normal to the probe. The Y-axis is then used to change the probe to airfoil distance in 5.0  $\mu\text{m}$  (0.0002 inch) increments. The filtered analog voltage output from the probe is fed into an analog-to-digital (A/D) converter which can be sampled by the microprocessor ( $\mu\text{P}$ ) control system. The  $\mu\text{P}$  also controls the Y-axis stepping motor to change probe-to-target distance, and determines where the valley is. For safety purposes the target is brought in close to the probe and then valley detection is accomplished while backing away from the probe. The valley detection program is set up so that if the valley is not detected on the first pass, one or more parameters is incremented and another attempt is made. This allows measurements to be made at maximum sensitivity on targets which vary considerably in reflectivity.

The procedure by which the valley is detected by the  $\mu\text{P}$  is illustrated in Figure 16. A set of eleven memory locations, number 0 to 10, is set up to constitute a first-in-first-out (FIFO) memory. On the first step the voltage is read and entered into the first FIFO location. On each successive step of the motor a new voltage reading is entered into the first FIFO location and all previous measurements are moved back one location in memory. A reading which has reached the last memory location is lost on the next step. The FIFO, therefore, always contains the last eleven voltage readings and their corresponding probe coordinates in steps. When the first reading exceeds the last by a specified voltage, the valley is assumed to be detected and the coordinates of the sixth memory location is taken as the valley position. The program is also set up to detect the negative slope preceding the valley and the positive slope following the valley by looking for appropriate differences between the first and last FIFO readings. Parameters that can be varied automatically if searching for the valley are the voltage differences that define the slopes and the valley, and the position at which the valley detect routine starts. Another feature of the program is that the number of measurements taken at each step can be any multiple of 2 from 1 to 128. The value entered into the FIFO is then the average of the readings. This feature can be used to minimize the effect of noise spikes. In the final system software configuration, the FIFO length can also be varied up to 32 memory locations to further minimize noise sensitivity.

For measurement of coating thickness, the Y-coordinate at the valley for each measurement point on the bare blade is measured again and the new Y-coordinates are stored in a second memory location designated Table 1. The coating thickness of hexadecimal steps of the Y-axis is determined by subtracting the values in Table 0 from the corresponding values in Table 1. The  $\mu\text{P}$  converts this data into decimal values in mils and outputs it on the printer as a list of measurement point numbers and coating thicknesses.

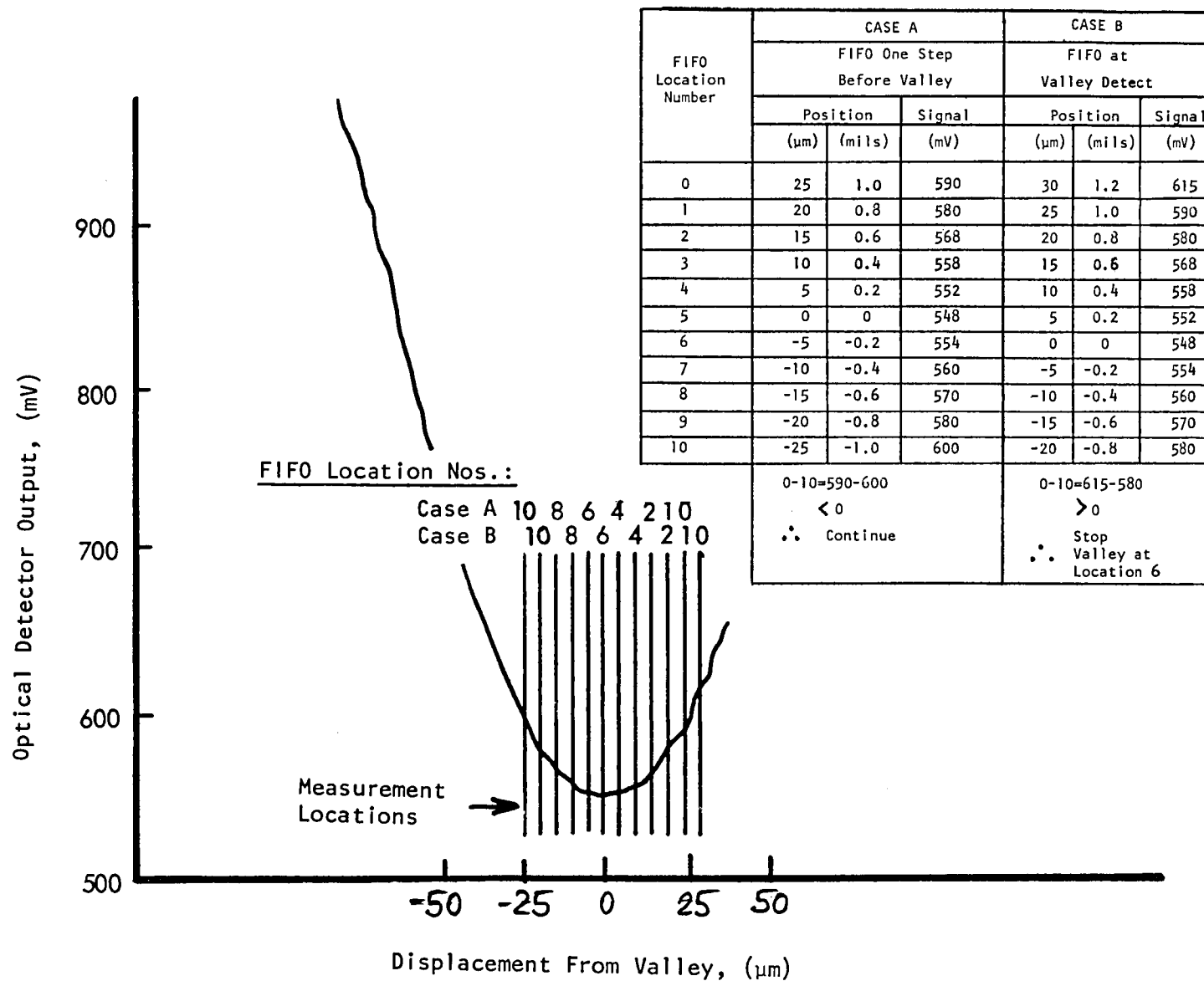


Figure 16. Example of FIFO Valley Detect Concept.

## Control Subsystem

The APS system controller is the subsystem that ties all the other subsystems together into one integrated system. Since the control subsystem is microprocessor-based, its development included both hardware and software efforts. These efforts are summarized in the following sections.

### General Discussion

The general configuration of the APS process control subsystem is shown in the simplified block diagram in Figure 17. The subsystem is configured around the bus concept; i.e., all system components interface into the microprocessor bus or motherboard. Each appears to the microprocessor as one or more memory address locations. Using standard memory addressing commands, the microprocessor may thus have two-way communication with any system device just as it would read from or write into memory.

Using the bus concept the system is readily expandable. The only limitation on the number of system devices is the maximum number of addressable memory locations — 64k. Thus, it was easy half way through system development, to add a digital printer to furnish hard copy inspection readouts of the actual coating thicknesses deposited on each specimen. It is also possible to plug a remote terminal into the bus during system checkout or modification to exercise keyboard control of any system device or the entire system. In a production model it would be a straightforward task to interface additional plasma spray console parameters into the bus. Some of the spray parameters manually preset on the current APS process implementation could thus be automatically preset or adjusted by the microprocessor as desired.

The devices interfaced into the microprocessor bus in the present feasibility model of the APS process controller are indicated in Figure 17. These include microprocessor memory for program control software, firmware and scratchpad. Control interfaces for seven motor-driven axes on the BHD, the CTMD and the SGSF are provided. A signal conditioning interface fabricated around an A/D converter allows the microprocessor to read the output of the optical detector on command. Five triac output interfaces allow the microprocessor to exercise control over the plasma spray console as previously described in Section 4.1. Finally, the microprocessor front panel also interfaces into the bus. This panel contains a number of control pushbuttons, a switch register and several LED (light emitting diode) status and data displays. The digital printer could also be grouped as one of the display outputs, though it is physically located on a separate panel.

Utilization of the printer could conceivably eliminate an entire operation in the production process. It can provide a record of the actual applied coating thicknesses as a byproduct of the deposition control process. This would eliminate the need for a subsequent gaging inspection station. Each of these interfaces is described in more detail in the following section on hardware development.

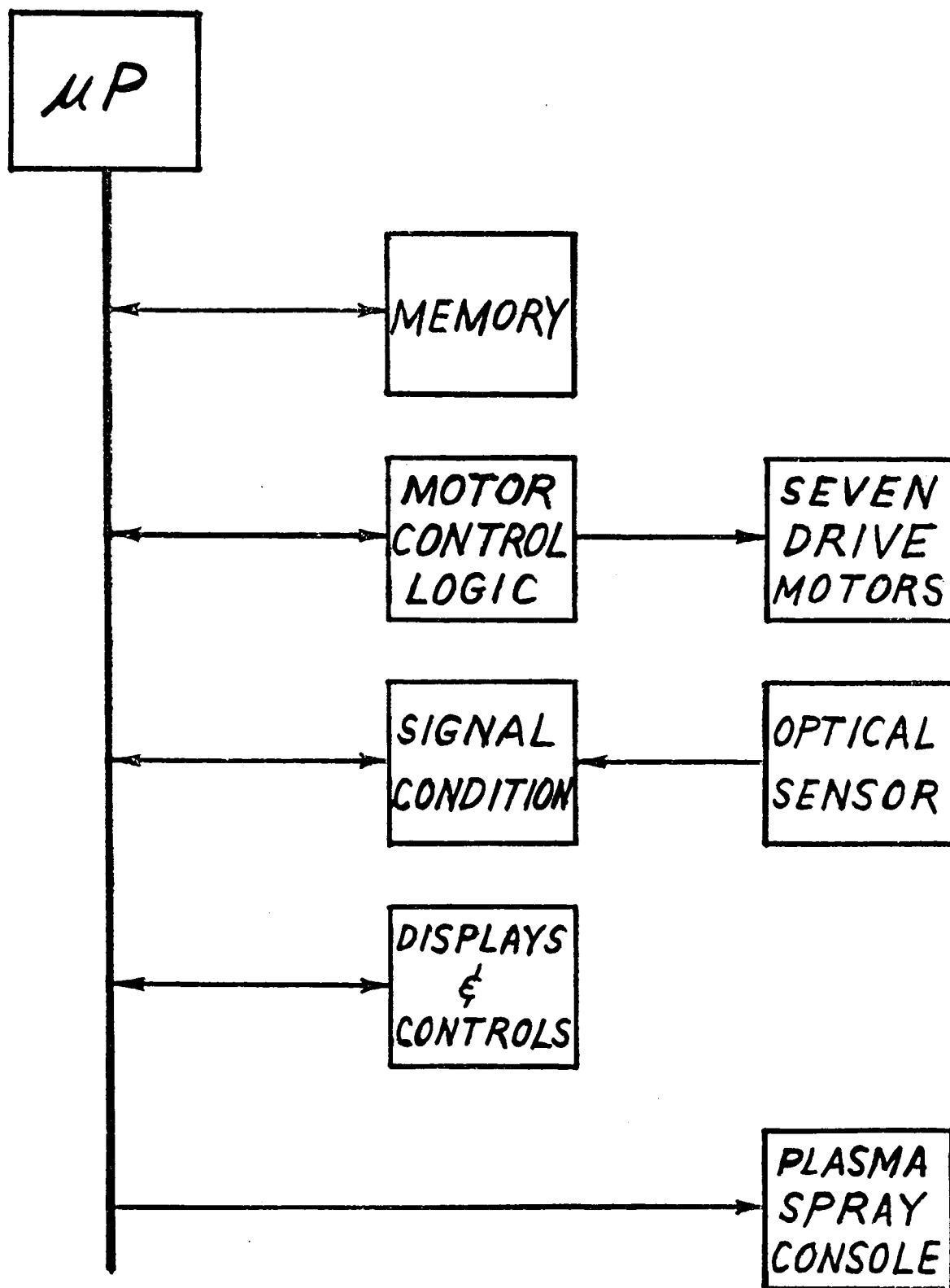


Figure 17. Block Diagram of APS Process Control Subsystem.

## Hardware Development

A more detailed functional block diagram of the APS system controller is shown in Figure 18. This figure summarizes the hardware configuration of the various interfaces.

A Motorola M6800 microprocessor is the heart of the APS system controller. At the time TRW was designing pc (printed circuit) boards to utilize this chip, a set of populated boards became available. The MMO2 CPU (central processor unit) board was subsequently selected for use on this project. Auxiliary pc boards provide for up to 16k of EPROM and 8k of dynamic RAM. The M6800 bus actually consists of three buses, a 16-bit address bus, an 8-bit bidirectional data bus and a control bus. These buses and a number of additional power supply, supervisory control and clock lines are all contained on a large pc motherboard located in the microprocessor chassis. The CPU board, the memory boards and all system device interface boards plug into this motherboard.

Each device interface contains a PIA (peripheral interface adaptor) chip to provide bus interface. Instead of the normal M6820 chip, an Intel 8255 PIA chip was used in the APS. This chip provides four extra I/O ports (24 instead of 20) which greatly simplified design of the motor interfaces.

Figure 18 indicates the functional block diagram of a typical stepping motor interface. The motor clock/driver board is a commercial board obtained from the stepping motor vendor. It contains adjustable clock pulse generators for high and low motor speeds, pulse rate ramping to accelerate and decelerate the motor without pole slippage, motor driver circuits and TTL (transistor-transistor logic) compatible remote control inputs. The interface board also contains a 16-bit integrated circuit axis position counter which counts the drive pulses fed to the motor to record instantaneous motor position. The counter counts up for motor steps away from the zero reference stop and down for motor steps toward the stop. During system startup initialization, the counter is cleared when the motor is driven against the reference stop. The counter output is fed to the PIA to allow it to be read by the microprocessor. It is also fed to one input of a 16-bit digital comparator. The other input of the digital comparator is a reference position register in the PIA.

In operation the microprocessor can set any desired position reference in the motor PIA register. The comparator indicates to the axis control logic circuits the motor direction required to move to the designated reference position. It will move in that direction upon receipt of a "motor enable" signal from the microprocessor. When the motor reaches the designated position, indicated by equality of the two digital inputs to the comparator, the comparator will signal the control logic circuits to cease motor motion. It will also flag the microprocessor that the motor has reached the commanded position. The digital comparator is of unique design, in that it supplies an "almost equal" output to the control logic as well as an "equal" output. This allows the logic to drive the motor at high speed until almost at the designated target position, then ramp down to a lower approach speed so as to stop without overshoot or pole slippage when comparator inputs equality is reached. During system startup initialization, the control logic circuits drive the motor in the negative direction into the zero reference stop to permit counter synchronization.

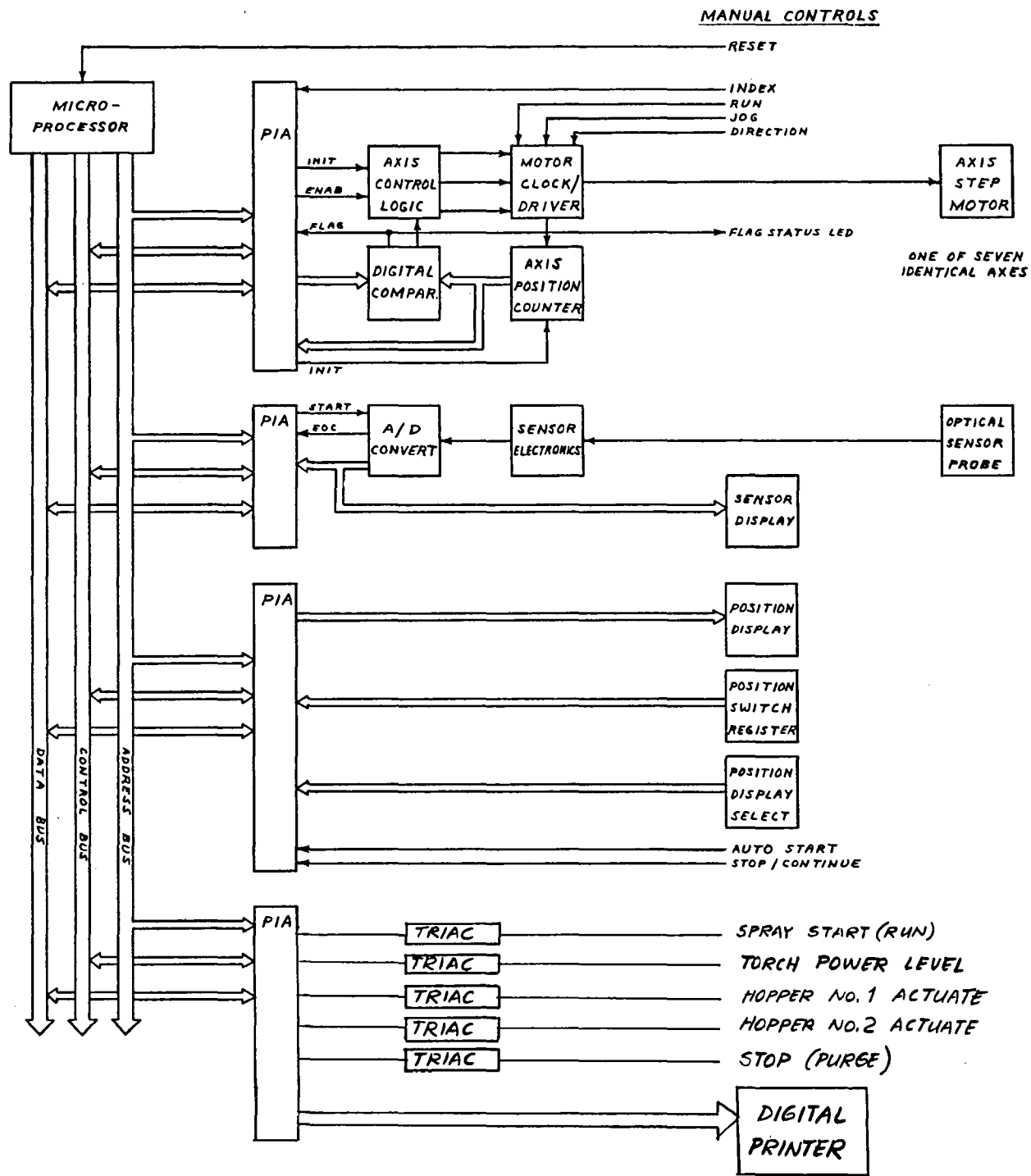


Figure 18. Functional Block Diagram of APS System Controller.

The combination of hardware and software logic utilized to control the axis drive motors combines some of the good features of each mode of control. The hardware logic circuits can be "tuned" to individually optimize the high and low speed performance of each axis without unnecessarily overcomplicating the software. The microprocessor can thus operate in a supervisory handshake mode by designating a target to each motor and then proceeding to other tasks until flagged by the axis hardware that the targets have been reached. Thus, all motors may simultaneously proceed at their individual optimum speeds. Not only does this provide better CPU utilization, but it allows the system to proceed at optimum speed regardless of specimen size or geometry. The same system software can thus be utilized with very different specimen geometries by providing firmware lookup tables of target coordinates unique to each specimen. The system will automatically proceed at maximum speed in each case without software modification.

The six interfaces for the stepping motor axes are identical. The seventh motor axis, for the SGSF servomotor, is very similar. The motor driver for this axis does not contain an internal clock pulse generator so an external clock circuit was fabricated. Also, only a standard digital comparator is required for this axis. It is not necessary to switch over to a lower speed clock upon approaching the target with the servomotor. The internal control loops within the motor translator accomplish the motor ramp to zero speed, without overshoot, automatically. Two motor interface circuits were fabricated on each interface board for insertion into the microprocessor motherboard. A total of 3-1/2 boards was therefore required to accommodate the seven motor interfaces. The motor driver boards are mounted directly on the motor power supplies, eliminating the need for separate card racks for these circuits.

The interface for the optical sensor contains a 12-bit A/D converter in addition to the PIA chip. The microprocessor can signal the A/D converter to initiate a sample of the detector output by sending a "start conversion" pulse. The conversion takes approximately 25 microseconds, after which the interface signals the microprocessor that the digitized data is ready to read. The rapid conversion time allows the microprocessor to take multiple samples of the detector output after each step of the Y-axis motor during gaging operations to average out the possible detrimental effects of noise spikes, interference, etc. The last digitized data output is also displayed on a front panel LED register for use in system checkout. It was also necessary to provide high frequency ripple filtering on the analog input to the A/D converter to utilize the full 2.44 millivolt/bit sensitivity of the A/D converter. The optical detector interface circuits also occupy one half of an interface board in the microprocessor chassis. These circuits are located on the same board as the SGSF servomotor interface logic circuits.

The interface circuits for the digital printer and the plasma spray console also share a common interface board. The interface for the printer is essentially just the 8255 PIA chip and associated address select logic. The interface for the plasma spray console consists of bistable latches with associated address select logic. The latches are set by the microprocessor to actuate the respective spray console functions. Heavy duty solid-state ac switches (TRIAC's), located at the bottom of the APS control console, are actuated by the interface latches through optical decouplers. The TRIAC's, in turn, actuate the remote interface relays in the plasma spray console. LED status lights are mounted on the rear inside of the APS control console to monitor the status of the control output signals to the plasma spray console.



The final interface board handles the various microprocessor front panel controls and displays. This board contains three 8255 PIA chips, associated address select logic, bistable latches and lamp drivers. The front panel displays consist of two LED status registers, one 8-bit and one 16-bit, which may be utilized to display contents of memory locations and registers such as the contents of the position counters. Status lights are also located in the front panel pushbuttons. A four hexadecimal digit thumbwheel switch register may be used to manually insert data to selected registers. These displays, the register, and most of the pushbuttons are strictly for use in system evaluation and/or setup when a remote terminal is not available. These pushbuttons may also be utilized to manually index the various axis motors to designated coordinates, but the remote alphanumeric terminal is much more convenient for this use. The only front panel controls normally used are the "Run" pushbutton and occasionally the microprocessor "Reset" pushbutton. The microprocessor front panel is visible in Figure 10.

Considerable attention was given to designing the hardware to provide insensitivity to the high EMI environment within the plasma spray facility. As mentioned previously, this was one of the major reasons for utilizing the remote position counters instead of axis encoders. All cabling outside the APS control console was shielded. The outputs to the plasma spray console were also optically decoupled to minimize EMI conducted back into the APS control console. These precautions paid off when the system was ultimately installed in the facility.

Manual controls for the seven axis drive motors are also provided on the front of the APS control console. (See Figure 10.) These controls bypass the microprocessor and interface directly into the motor drivers. With these controls each motor may be jogged (single-stepped) or run at high or low speed in either direction. The high and low speed adjustments are also located on this panel. These controls are often used in system setup and/or maintenance.

More detailed information on the design and fabrication of the various control hardware circuits can be found in the schematic diagrams appended to this report.

### Software Development

Development of the APS process software was in modular subroutine packages. These subroutines are linked together and/or called by the executive software program as required to formulate the system software program. This approach provides maximum flexibility for system update, modification and/or debug. It also subdivides the software development effort into more easily defined, easily handled subtasks. In all, there are well over 200 software subroutines which are utilized in the current version of the APS process software.

### General Executive Program Descriptions

Figure 19 is a simplified flow chart of the APS process software executive program. This flow chart defines the procedures which the APS process will follow in the automatic mode of operation to spray bond and barrier coatings separately or in sequence.

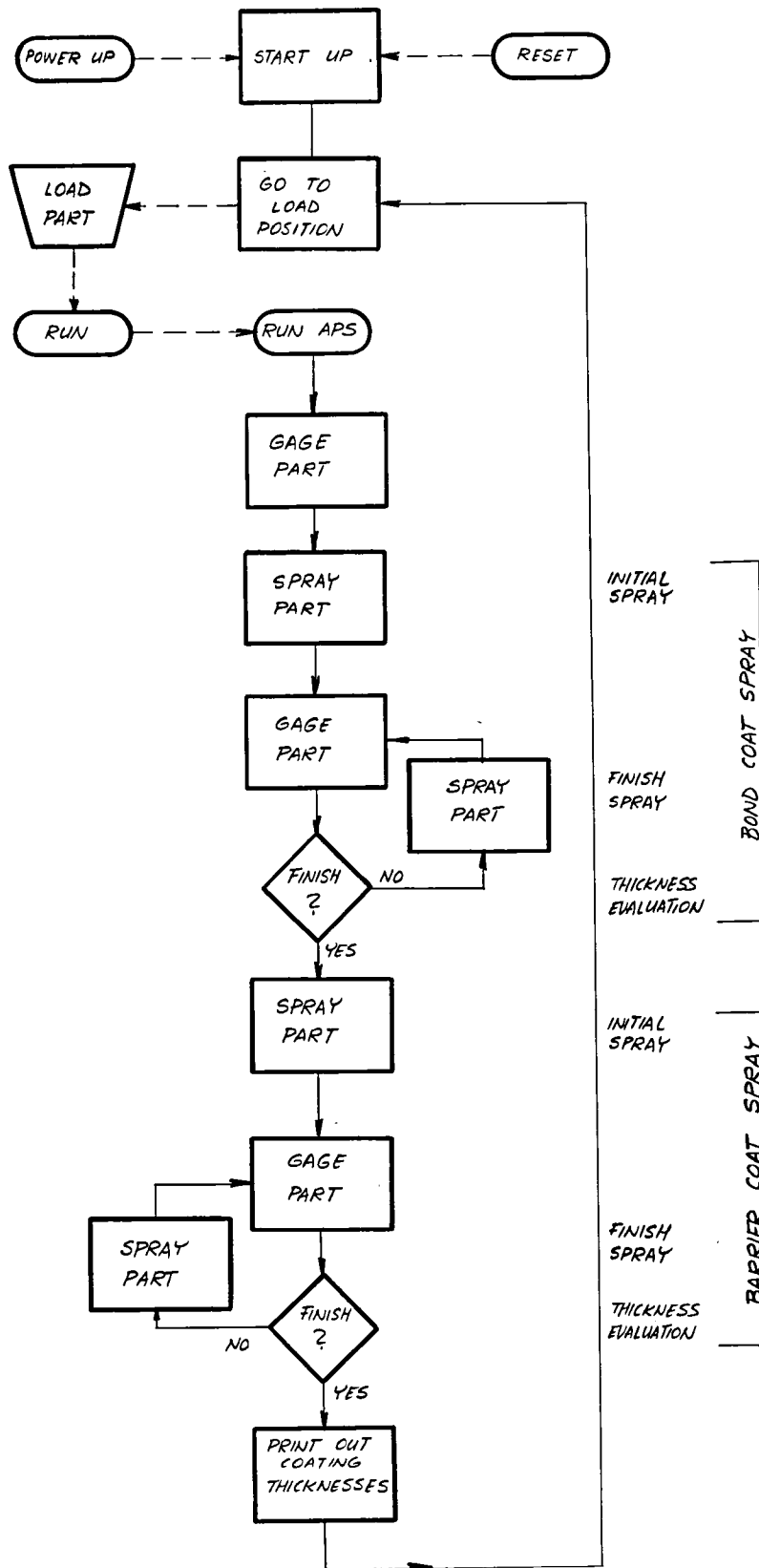


Figure 19. Simplified Flow Chart of APS Process Software Executive Program.

Depression of the reset pushbutton or powerup will cause the microprocessor to initiate the "startup" routine. This routine initializes the microprocessor stack pointer, initializes the modes of all the PIA interface registers, and performs a number of general housekeeping chores to ready the microprocessor subassembly for operation. It also drives all seven axis motors against the zero reference stops and clears the respective position counters to synchronize them with the motors. At the conclusion of the startup routine all system axes are automatically indexed to the "load" position. At this point the system will stop until directed by the operator to proceed. Several options are available to the operator at this point. He may utilize any of the front panel function pushbuttons to evaluate system status, or transfer system control to a remote video terminal for further evaluation. For continuation of automatic operation, he would load a specimen to be coated by the plasma spray subsystem and depress the "run" pushbutton. Depression of the "run" pushbutton causes the system to resume automatic operation. System operation is then controlled by the "run APS" routine in software. This routine is functionally described by the remainder of the flow chart in Figure 19.

The "gage part" subroutine is the first one to be exercised to gage the bare specimen. The BHD and CTMD motors are all sequentially indexed to the gage point coordinates as defined in an EPROM firmware lookup table. At each point the valley point coordinate is determined and stored in a RAM scratchpad table (Table 0) using the procedure described earlier. At the conclusion of this subroutine, Table 0 contains the bare blade coordinates at all the specified gage points.

The "initial spray" subroutine applies the bond coat constituent to the specimen. The thickness applied, specified by EPROM firmware, is typically slightly less than the final thickness desired to assure that no points are coated too heavy. Deposition is accomplished by sequentially indexing the BHD axes to the scan line coordinates specified for the specimen in an EPROM firmware lookup table. After each scan line is positioned vertically before the plasma spray gun at the required standoff distance, the gun is cycled up and down the required number of passes to deposit the nominal coating thickness specified. The microprocessor automatically signals the plasma spray console to initiate and terminate the gun power and powder flow at the proper instants.

The "gage part" subroutine is used to gage the thickness of the coating actually applied at each gage point. This is accomplished in the same manner as the initial bare specimen measurements were taken. In this case, however, the gage point valley location coordinates are stored in a different RAM table (Table 1).

In the thickness evaluation subroutine, the software directs the microprocessor to make a decision which way to proceed. By taking the difference between the respective coordinate values stored in Tables 1 and 0, the microprocessor determines the actual coating thickness applied on each scan line during the initial spray application of the bond coat constituent. Comparing these values to the desired thickness specified in EPROM, the microprocessor determines which lines, if any, require additional coating passes to bring the thickness up to the minimum acceptable value. The number of passes required on each line to achieve this minimum acceptable value is also calculated.

If all lines are not coated with at least the minimum required coating thickness, the respray subroutine for the bond coat constituent is utilized. This subroutine is actually the same subroutine used for initial spray application, except only the coordinates of the selected scan lines and the respective numbers of spray application passes calculated per line are utilized. At the conclusion of this subroutine the microprocessor loops back to the "gage part" subroutine for the bond coat constituent. This subroutine is executed the same as previously, updating the coordinate values stored in Table 1 where additional coating was deposited. This loop, alternately spraying and gaging the bond constituent, will be traversed as many times as necessary to bring all gage points up to the minimum acceptable coating thickness. Typically, however, no more than one respray should be required. One exception to this is in areas of extremely high curvature such as the leading edge of a JT9D first stage turbine blade. This will be discussed further in section 5.

After determining that all gage points have at least the minimum acceptable thickness of the bond coat constituent, the microprocessor will initiate the subroutine to deposit the initial application of the barrier coat constituent. This subroutine is actually the same subroutine used for application of the bond coat constituent, except a different desired coating thickness is specified by EPROM firmware. A different gun power level and the second powder hopper are also designated by the microprocessor. Again, as for the barrier constituent, the software will direct the microprocessor to deposit slightly less than the desired coating thickness on each line to assure that no lines are coated too heavy.

The software loop formed by the next three subroutines shown on Figure 19 for the barrier coat constituent is identical to the loop just discussed for the bond coat constituent. The coated part is gaged, the calculated coating thickness is compared to the desired thickness, and the respray or finish pass subroutine is utilized as required. When all gage points are determined to have at least the minimum acceptable total coating thickness, the microprocessor will emerge from the loop.

The final subroutine indicated on Figure 19 is the "print coating thickness" subroutine for the actual deposited coating thicknesses at each gage point as determined by the optical detector. These are tabulated to tenths of a mil (1 mil = 25.4  $\mu\text{m}$ ) by gage point number on the digital printer. The thicknesses of the bond constituent coating may be tabulated as well as the total applied coating deposition.

While the printout is being generated, the specimen is indexed back to the load position. It may then be removed and replaced by a new bare specimen. The entire process may then be automatically repeated by again depressing the "run" pushbutton.

As discussed above, spraying on each scan line is terminated when a "minimum acceptable coating thickness" is measured. To achieve a statistically acceptable confidence level that the actual applied coating thickness exceeds the minimum tolerance level, the "minimum acceptable thickness" has generally been taken as the minimum tolerance level plus  $12.7\text{ }\mu\text{m}$  (0.5 mil). The remainder of the tolerance band (e.g.,  $63.5\text{ }\mu\text{m}$  (2.5 mils) for a  $+38.1\text{ }\mu\text{m}$  (+1.5 mils) tolerance band) is the resultant process high-side tolerance before the deposited coating is too thick. It is desirable to keep this process high-side tolerance as large as practical.

All system software and firmware is stored in the type 2708 (1k x 8 bits) EPROM's. At this time, approximately 8k of EPROM is being used. There is room for 16k on the memory board currently being used in the APS process microprocessor. The information stored on EPROM may be categorized into three types. Four of the eight devices are used to store the software subroutines. These include all the program instruction statements. One device stores the control firmware. This includes all the system constants, time delays, etc., utilized by the software with the exception of those unique to the type of specimen being sprayed. The remaining three devices contain the specimen firmware: one, the spray scan line coordinate lookup table for the base coat constituent; the second, the spray scan line coordinate lookup table for the barrier coat constituent; and the third, the gage point lookup table. Separating the software and firmware data in this manner greatly eases the task of updating and/or modifying the process parameters. This also allows the software to be "universal." The parameters which are unique to the specimen type and geometry are all located in the firmware for that specimen.

#### Software Program Options

The previous section described the general executive program flow chart for the APS process software. There are, however, a number of options provided in the software. The options selected are normally specified in the process firmware or the specimen firmware. The firmware specification, however, may be overridden from either a remote terminal or from the microprocessor front panel controls. Unless overridden, however, the firmware specification will prevail as the default option.

In the flow chart of Figure 19, four different spray subroutines are indicated — an initial and a finish spray for both the base coat constituent and the barrier coat constituent. As was mentioned in the discussion, however, the same software subroutine is actually used in all instances. The subroutine is configured different for the four cases by parameters specified in the control firmware. The configuration parameters specify four factors for the spray subroutine:

1. The powder hopper (or hoppers) to be actuated,
2. The spray scan line coordinate table to be used,

3. The calculation formula to be used in determining the number of deposition passes to be made by the spray gun on each scan line, and
4. A maximum repetition limit number which would limit the number of times a particular spray sequence configuration could be accessed in the absence of any other limiting control logic.

A spray pointer is utilized in the software to indicate the current configuration parameters to be used for the spray subroutine.

The firmware presently provides for specification of up to seven sets of spray subroutine configuration parameters for use in one automatic sequence. Thus there is provision to use different calculation formulae on different areas of the specimen should this be desirable. Another example would be deposition of a graded layer, or mixture of the two constituent powders, as a transition layer between the bond and barrier coats. It is also possible for the firmware to specify less than four spray sequences during automatic operation. In particular, either one or both of the finish spray loops on Figure 19 may be deleted. This would be practical, for example, if the tolerances on thickness uniformity of the bond coat layer were not extremely tight, or if this layer were thin enough that there would likely not be a need for finish passes. The desired coating thicknesses for the bond coat layer and for the total coating deposition are specification parameters to be stored in firmware. The fraction of the total desired coating thickness to be applied during the initial spray subroutine is also a firmware specification parameter. This may be specified as any number of eighths of the total desired thickness. As discussed previously, the initial spray thickness is usually less than the desired value to assure that no lines are coated too heavy due to unanticipated process variations.

The current firmware provides for specification of up to 128 scan lines or 128 gage points in each coordinate table. Any number of these gage points may be located on the same scan line. In the case of multiple gage points on the same scan line, the software will select the point with the minimum deposition thickness for use in calculating the number of finish passes required in the finish spray subroutine. The software also calculates the high, the low and the average coating thickness deposited on the blade for each layer along with the corresponding locations for the high and low spots. Although always available, this data is not used unless specifically called for. It could, for example, be utilized in a calculation formula for defining parameters in a finish spray subroutine.

The firmware may modify the number of coating thickness printouts generated on the digital printer. Thus printouts may be generated only for the total applied coating thickness, for each of the coating constituent layers, or after each spray sequence including each finish spray sequence. This latter option is useful during initial setup for a specimen to monitor process step-by-step performance.

Up to eight breakpoints may also be specified in the automatic sequence. This allows the automatic sequence to be interrupted at any place for intermediate evaluations. This is also primarily a diagnostic tool.

Two other options were previously discussed in the metrology subsystem section. These are the ability to specify the FIFO length and the number of optical detector readings averaged after each motor step in the optical detector measurement subroutines. These specifications allow the system sensitivity to electrical noise or fixture vibration to be minimized. There is, however, a tradeoff to be considered with system response time. The gaging subroutine can be slowed unnecessarily if these parameters are specified too large.

#### Options Used for JT9D Coating

In the feasibility demonstration efforts, coating deposition specimens have all been JT9D first stage turbine blades. This specimen was selected as representative of the most difficult specimens which would be encountered due to its small size and small radii of curvature. Only three configurations of the spray subroutine are currently being used on the JT9D specimens. The finish spray loop is not being used for the NiCrAlY bond coat. This coat is thin enough, 127  $\mu\text{m}$  (4.6 mils) that it is applied in two passes of the spray gun. The  $\pm 38 \mu\text{m}$  ( $\pm 1.5$  mil) tolerance thus represents a relatively loose percentage tolerance, even without finish passes. It was felt that proper specification of the scan line coordinates could achieve this percentage tolerance without the additional finish spray loop. Recently consideration has been directed toward the possibility of changing the NiCrAlY spray parameters to deposit a thinner coating layer per pass. If this is done, it may then prove desirable to incorporate the finish spray loop on the bond coat as it is for the barrier coat.

For the feasibility demonstration, the selection of the desired coating thicknesses was relatively arbitrary. The values which have been used for most recent specimens are 117  $\mu\text{m}$  (4.6 mils) for the NiCrAlY bond coat and 290  $\mu\text{m}$  (11.4 mils) for the yttria-stabilized zirconia barrier coat for a total coating thickness of 406  $\mu\text{m}$  (16 mils). This appeared to be a reasonable thickness without using excessive amounts of powders for the feasibility investigations. It may prove desirable to use somewhat thinner coatings for aircraft jet engine and thicker coatings for electric utility engine applications.

Since no finish spray subroutine was utilized on the bond coat, the initial spray subroutine was configured to deposit the nominal 117  $\mu\text{m}$  (4.6 mils). The calculation formula in the firmware therefore is only:

$$\text{No. of Passes} = 1 + \frac{T_B - 3}{1.6} = 1 + \frac{4.6 - 3}{1.6} = 2 \quad (1)$$

where  $T_B$  is the desired thickness of the bond coat in mils.

For the zirconia barrier coat the firmware for the JT9D specimens designates deposition of three-fourths of the desired barrier coat thickness on the initial spray subroutine. The calculation formula for this subroutine therefore is:

$$\text{No. of Passes} = \frac{(T_c - 1 - T_B \times 0.75)}{0.8} = \frac{(16 - 1 - 4.6) \times 0.75}{0.8} \approx 10 \quad (2)$$

where  $T_c$  is the desired total coating thickness in mils. For the finish spray subroutine the calculation formula used for each line is:

$$\text{No. of Passes} = \frac{(T_c - 1 - T_A)}{0.8} = \frac{15 - T_A}{0.8} \quad (3)$$

where  $T_A$  is the actual total coating thickness in mils previously deposited on that line as determined by the microprocessor during the last "gage part" subroutine.

In the various calculations used above, the calculation formula and the various specimen constants are taken from the firmware by the microprocessor. The nominal coating depositions per pass (i.e., 3 mils and 1.6 mils for the first and subsequent NiCrAlY passes, respectively, and 0.8 mils per zirconia pass) are constants in the control firmware. These values were determined in the latest spray deposition profile study. (See section 5.)

Many alternate possibilities could be considered for the calculation formulae. One interesting possibility would be for the microprocessor to compute the actual average deposition thickness per pass on previous scans on each line instead of using nominal values from the deposition profile study. This could conceivably reduce the process time required for the finish spray subroutine, but needs careful study to determine the probability of overspraying some lines if process variations occur. The present approach, while sometimes requiring multiple finish pass cycles on areas such as the blade leading edge, minimizes the danger of overspraying.

A total of 24 scan lines are presently being used on the JT9D specimens. This is based on results of the deposition study summarized in section 5. This number could probably be reduced somewhat, particularly for the NiCrAlY. Recent specimens have utilized only one gage point on each scan line for a total of 24 points. All thickness evaluations made to date have revealed little problem with thickness uniformity along a scan line. There is no problem adding additional points on each line should the need be determined. The penalty paid for more points is extra time spent in each "gage part" subroutine indexing to the additional measurement locations.



The FIFO length presently being used on the JT9D specimens is the full 32 memory locations. This provides maximum immunity to noise spikes prematurely indicating a "valley detect" during the gaging subroutines. The process could be speeded up somewhat by reducing the FIFO length. Only one optical detector "read" is currently being made after each Y-axis motor step during the gaging subroutine. Eight "reads" per step were used on many of the earlier specimens. There has not been any noticeable increase in noise or gaging repeatability problems since the change. This would indicate that the noise levels are not at a seriously high level in the present APS process facility.

One software option not previously mentioned is also being used on the present APS process configuration. The configuration developed considerable wear in many of the instrument-quality mechanical components. This has resulted in considerable backlash in several axes. The current software is therefore configured to remove this backlash during the gaging subroutines. This is done by "swinging" the suspect axes away from the gage point locations and back again before each measurement to "windup" the backlash in the same direction on all occasions. Again this extends the total process time. This option would probably not be required on a new mechanical fixture built for extended operational endurance. This option has demonstrated the capability to hold the repeatability of the gaging subroutine at a standard deviation of approximately  $\pm 7.5 \mu\text{m}$  ( $\pm 0.3$  mils).

Further detail may be obtained on the APS process firmware and software by referring to the detailed software flow charts and software assembly listings in the Appendix.

#### 4.3 APS System Operation

In order to utilize the APS system to coat a specimen, two preliminary steps must be accomplished:

- 1) A holding fixture must be fabricated to mount the specimen on the APS system BHD.
- 2) The firmware coordinates and constants defining the specific process and specimen options desired must be inserted into the microprocessor.

Establishment of the firmware parameters for a new specimen type has customarily been done using a "master reference blade." The master reference is a typical specimen on which the desired scan lines have been drawn. These lines are drawn on the specimen using the scan line spacing derived, in the deposition profile study. (See section 5.) The desired gage points are also marked on the specimen, including at least one on each scan line. Figure 20 is a photograph showing the latest master reference blade used for the JT9D specimen. The firmware tables are generated by placing the master reference blade in the blade holding fixture normally supporting the specimen being sprayed. Each scan line on the reference is positioned in front of the plasma spray gun in the orientation required for spray deposition. The coordinates for each axis are then obtained by reading the corresponding position counters. Either

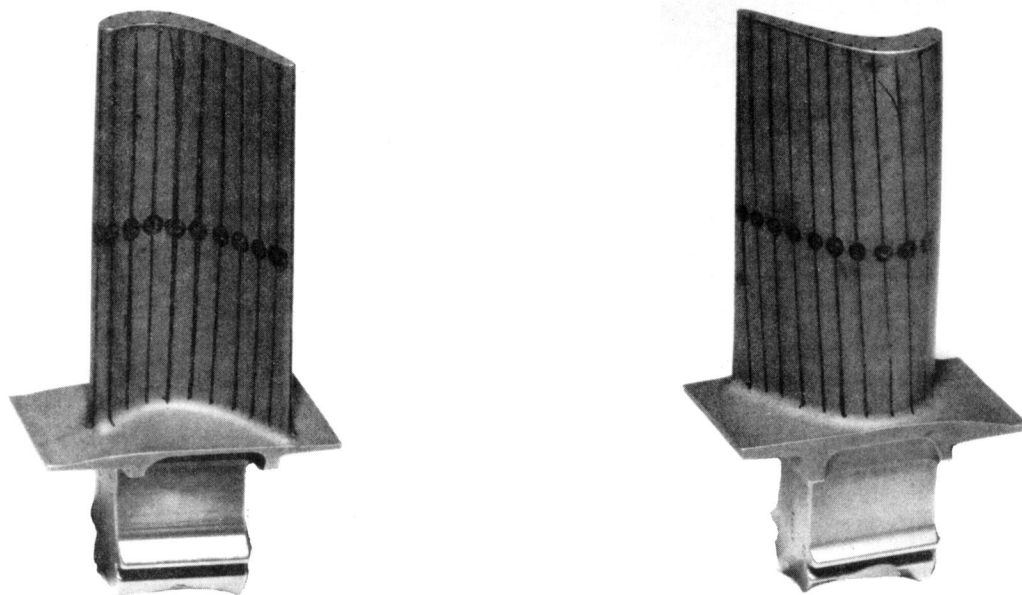


Figure 20. Photograph of JT9D First Stage Turbine Blade Used as Master Reference for Establishment of APS Process Firmware.

the remote video terminal or the microprocessor front panel controls may be used for this procedure. The gage point coordinates are obtained in a similar manner by positioning the reference blade in front of the optical detector and superimposing the optical detector light spot on the points marked on the reference blade. For a production system it would probably be feasible to replace this firmware specification procedure with a computer program. Digital data is available on most turbine blades which could be used in this program. The manual procedure described in the previous paragraph has proven adequate in experimental or development usage.

The APS system is readied for use by programming the specimen firmware obtained above in EPROM. The various process control parameters are also placed in firmware if different from those already in the control parameter EPROM. The EPROM's for various specimens can be readily interchanged in the plug-in sockets in the microprocessor chassis. A production system could have the firmware for many different specimens on one EPROM or on multiple EPROM's. Selection of the proper tables for the specimen being sprayed could then be by type number designation on a front panel switchregister or similar convenient technique.

Before initiating the automatic sequence on the present APS process feasibility implementation, the various spray parameters are manually preset on the plasma spray control console. These include parameters such as arc and auxiliary gas pressures, the feed rate settings on the two powder hoppers, the voltage levels for the two spray gun arc power conditions, etc. The spray control console is then switched over to remote control status. From that point on the APS process microprocessor will select the proper parameters, actuate the equipment at the proper instants and otherwise control the operation. On a production system it would be a straightforward task to have the APS process microprocessor also preset the various spray console parameters currently preset manually. This would be particularly advantageous if future process studies indicate the need or desirability for different settings for different applications. This would eliminate the possibility of a human error in process setup.

The specimen to be coated is currently prepared for spraying by grit blasting. A high purity alumina grit material is utilized. Relatively little attention was paid to the surface preparation process on the JT9D specimens sprayed to date. The concern on these specimens was obtaining deposition thickness uniformity. On the specimens for burner rig test and for coating quality evaluations in program Task III, however, the surface preparation task will be given careful attention. After grit blasting for surface preparation, the specimen is slipped into the blade holding fixture on the APS BHD. A single set screw locks the specimen in the fixture. The APS process is then initiated by depressing the "Run" pushbutton.

The remainder of the APS process is completely automatic. This includes determination of the actual bare specimen coordinates, deposition of controlled uniformity thicknesses of both the NiCrAlY bond coat and the yttria-stabilized zirconia barrier coat, printout of the actual deposition thicknesses deposited on each gage point as measured by the optical detector, and return of the specimen to the load position for removal and replacement by the next specimen to be coated. Figure 21 is a photograph

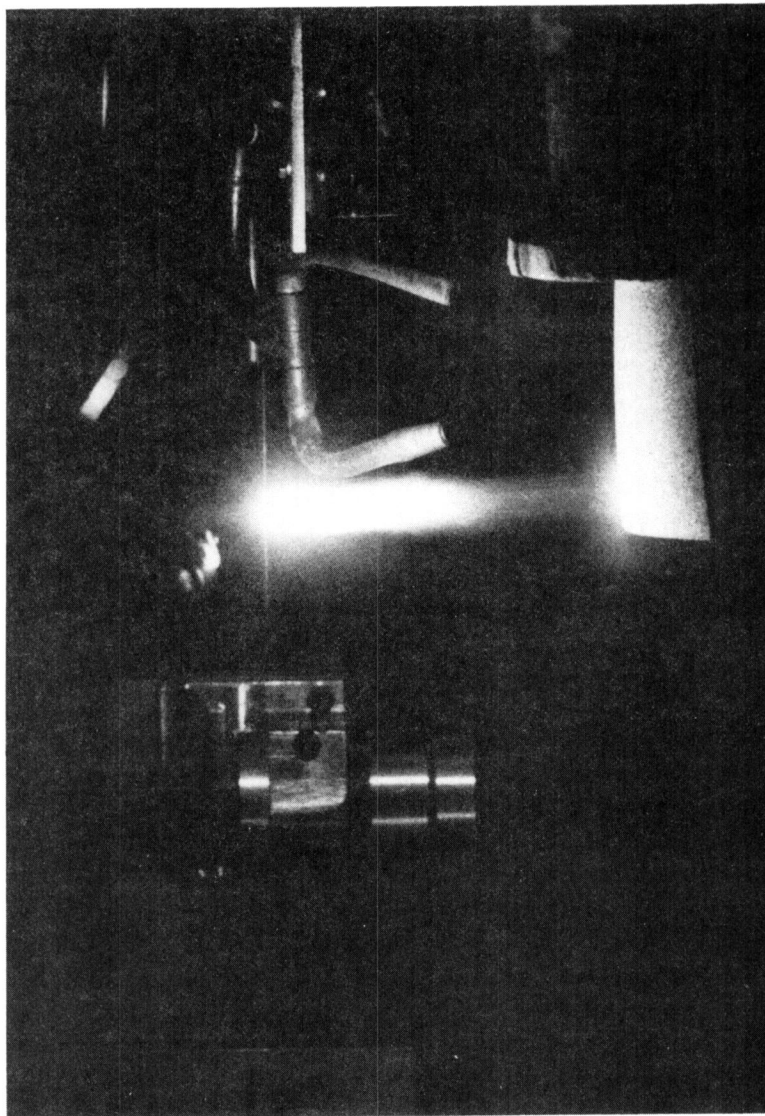


Figure 21. Photographs Taken During the Operation of the Automated Plasma Spray (APS) System (A JT9D engine 1st stage blade (right) is being sprayed by the plasma spray gun (left); the noncontact optical metrology sensor is in the background (lower center)).

of the APS system during automatic operation spraying a JT9D specimen. The gun, the optical detector and the specimen are visible in this figure. Also visible are tubes directing the CO<sub>2</sub> cover gas at the specimen during spray application.

The detailed consideration of the economics of the APS process are being considered under program Task IV. Results of this study will be presented in a subsequent report.

## 5.0 EVALUATIONS AND DISCUSSION OF RESULTS

This section describes evaluations both of the APS System and the process, i.e., the coating that it produces. These two elements must be considered in conjunction, since evaluation of the coating thickness was one of the major methods used to evaluate APS System performance. During the course of the program, the chronological sequence of events involved spraying blades, evaluating both the APS measurement data and the coating by metallurgical means, modifying the spray parameters, the mechanical subsystem and/or the control subsystem and then spraying more blades and repeating the evaluations. In order to provide a summary view of the end results, however, each of these activities is described in a separate section without regard to chronological order. All evaluations were carried out using the airfoil surfaces of JT9D 1st stage turbine blades.

During checkout and debug of the system, four blades were sprayed, Nos. 1 through 4. During initial system evaluation, seven more blades were sprayed, Nos. 5 through 11. An additional eighteen blades were sprayed during the course of the various system modifications. These are Nos. 12 through 29. Blades numbered 30 and higher were sprayed after addition of internal blade cooling and antibacklash software. Only the evaluation of blades 1 through 29 are included in this report.

### 5.1 Overall APS System Evaluation

The APS System underwent a series of evaluations to analyze the initial design and the effects of modifications to the system to improve its performance. During the initial evaluations, the measurement subsystem was evaluated separately to determine its ability to repeatably locate the airfoil surface. Then an initial set of blades was plasma sprayed and evaluated to determine the effectiveness of the spray application subsystem to apply the coating with the desired uniformity and also to determine the ability of the measurement subsystem to accurately measure the coating that had been applied. These initial evaluations identified a number of improvements in the design that were required in order to achieve the desired coating uniformity. As a result, a number of modifications were made to the mechanical subsystem, the control subsystem and to the spray deposition process parameters. An additional set of blades was then sprayed and evaluated, both to determine the uniformity of the coating deposited and to determine the accuracy with which the coating thickness had been measured. While the modifications made resulted in a substantial improvement in system performance, the evaluations also resulted in a number of ideas for improvements that could be incorporated into the present system or into a future system to further improve performance.

#### Measurement Subsystem Evaluations

Prior to overall system evaluation, the measurement subsystem was examined for its ability to make repeatable measurements. As described earlier, the measurement process consists of positioning the blade so that the optical probe is aimed

normal to the point on the blade to be measured and is within the focal length of the optical extender, and then moving the blade away from the probe in order to execute the measurement.

There are a number of variables within the system which can have an effect on the measurement process. These include the stepping rate measurement, the number of individual voltage measurements per step, the voltage difference used to identify the focal point and the time delay between stepping the motor and strobing the A-D converter to make a voltage measurement. Since the blade is mounted on a moving tower (BHD) and the BHD's natural frequency of vibration may be comparable to the stepping rate, the tower vibrations can also have an effect on measurement repeatability. The stepping rate during measurement is a function of the number of measurements per step so that the number of measurements influences the effect of resonance of the tower. In order to optimize these various parameters to achieve the best possible repeatability, a visicorder was used to record the analog output of the optical probe and the strobe pulse to the A/D converter during measurement. Repeatability was measured for a number of combinations of parameters for which visicorder traces were made. The results were then compared to determine the factors that affect repeatability and their optimum values.

The printer on the APS console is programmed to print out positive differences between two different tables in the microprocessor memory where the measurement values are stored prior to and after spraying. This approach works well for printing out coating thicknesses, but is not suitable for recording repeatability data because the printer has limited capacity to print out the entire value stored in memory, nor is it capable of printing out the negative numbers which occur. In order to determine repeatability, it was necessary to read the measured values out of the microprocessor memory using either a teletype or an alpha-numeric CRT terminal. These values were read out as four digit hexadecimal numbers representing the number of steps from the zero position of the Y-axis, the difference in two readings being the measured difference. This is the form in which the repeatability data is presented.

For repeatability testing the system was set up to measure four points on a blade, the last one twice. Repeatability runs consisted of five sets of measurements of each point at rates of 1, 2, 4, 8, 16, 32, 64 and 128 measurements per step (mt/st). It was found that 8 and 128 (mt/st) gave the best results, followed closely by 1 mt/st and then 16 mt/st. Visicorder runs were made during measurement of the fourth point at rates of 1, 8, 16 and 128 mt/st. An analysis of the visicorder data resulted in the following conclusions:

1. The system makes correct measurements. In each case studied, the measurement stopped at the point where the value entering the FIFO was greater than the value in the tenth location. The point selected as the focal point was either the point of minimum voltage or one of two equal points of minimum voltage.

2. At 1 mt/st, the voltage curve was smooth with occasional ripples. There were no oscillations where the voltage slope actually changed from increasing to decreasing or vice versa. As a result, the measured values went down steadily to a minimum and then up again. The stepping rate was 333 Hz.
3. At 8 mt/st, the voltage curve had definite ripples on it, which, near the valley, resulted in plateaus or even slight reversals of slope. The frequency of these humps was 117 Hz. The stepping rate was 237 Hz. This means that the two frequencies maintained an essentially constant phase relationship throughout the measurement, with two successive sets of measurements being taken  $180^\circ$  apart on each cycle of the voltage curve. The average voltage measured at each step went smoothly down to a minimum and then up again in spite of the ripples because of this constant phase relationship.
4. At 16 mt/st, the voltage curve had irregular ripples, or peaks for which no set frequency was assigned. The fluctuations were small, resulting in occasional plateaus near the curve's minimum, but more commonly resulting in variations in the predominant slope. The stepping rate was 182 Hz. At this stepping rate, visicorder data was also taken after the movement of the Y-axis stopped, and the tower was found to oscillate in two modes, one with a frequency of 20 Hz and the other with a frequency of 114 Hz.
5. At 128 mt/st the voltage curve oscillated continuously. It appeared that for each step the blade moved and then went through one complete cycle of overshoot before either damping out or receiving the next step pulse. The frequency of these oscillations was 42 Hz, the same as the stepping rate, so that for each step the 128 measurements were averaged over the same portion of the voltage oscillation. The average voltage moved smoothly down and then up.

If the stepping rate during measurement is independent of the number of measurements per step, the repeatability can be expected to improve in direct proportion to the square root of the number of measurements averaged. This expected improvement due to averaging was not achieved because of the effect of the interaction of the varying stepping rate with the resonant frequency of the mechanism. The best results were not obtained when the stepping rate was out of phase with the natural frequency of the mechanism, but were obtained when the stepping rate was a harmonic of the natural frequency so that relatively large voltage oscillations occurred. The explanation is that the voltage measurements are always taken at the same relative position on the oscillation, so the voltage readings themselves formed a smooth curve. The evaluation of measurement system repeatability at 8 mt/st is listed in Table III. The standard deviations at each point range from 0.9 to 1.5 steps with the average being 1.1 steps. This is  $\pm 0.005$  mm ( $\pm 0.0002$  inches).



TABLE III

Measurement System Repeatability Data at 8 MT/ST

Run No.	Point No.				
	1	2	3	4a	4b
1	119F	ODC6	09A5	0A5B	0A5A
2	119F	ODC7	09A5	0A5B	0A5C
3	11A0	ODC4	09A6	0A5B	0A59
4	119E	ODC7	09A7	0A5D	0A5A
5	119D	ODC4	09A4	0A5C	0A5B
Ave.	119F	ODC6	09A5	0A5C	0A5A
St. Dev.	<u>+1.1</u>	<u>+1.5</u>	<u>+1.1</u>	<u>+0.9</u>	<u>+1.1</u>
Ave. St. Dev.	<u>+1.1</u>				

NOTE: The data values are expressed in hexadecimal number of steps from the zero position of the Y-axis.

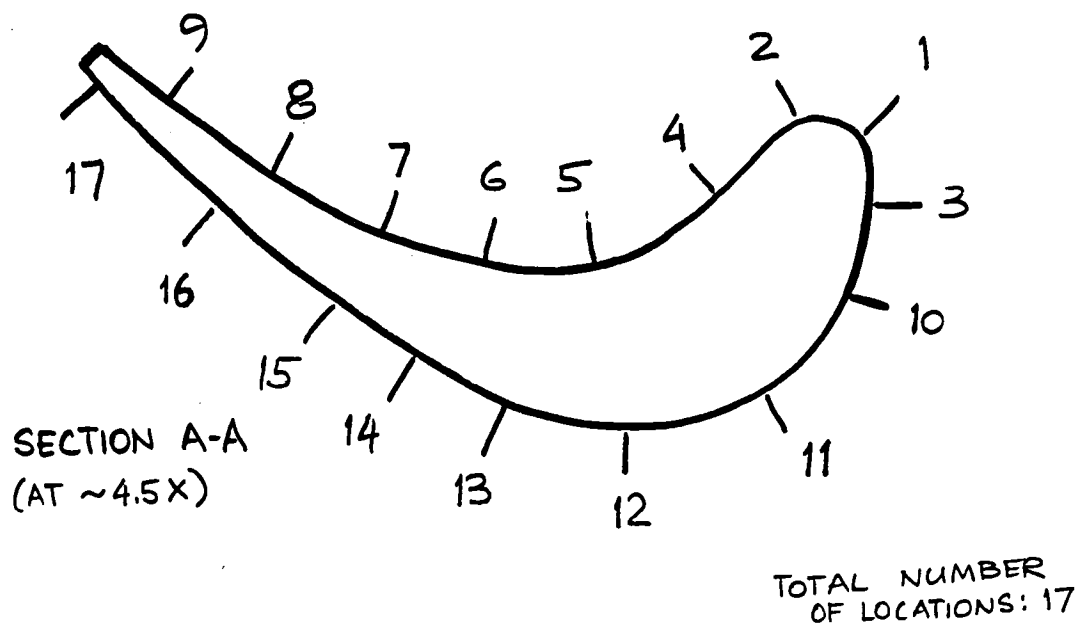
## Plasma Spray Subsystem Evaluations

After verification of the measurement system operation, it was possible to perform the initial evaluation of the plasma spray subsystem itself. The initial spray pattern, which was based on the spray deposition data from Plasmadyne, consisted of seventeen vertical spray lines around the blade with one measurement point on each line as shown in Figure 22. The measurement points alternated from one scan line to the next between two cross-sections of the airfoil, one near the center and one near the tip. This was done to allow evaluations of the uniformity of the coating along the length of the airfoil.

The first two blades in the initial evaluation, blades No. 5 and No. 6, were sprayed without using the finish routine for zirconia, so that each spray line received four passes of NiCrAlY and ten passes of  $ZrO_2$ . These were sectioned to evaluate the performance of both the spray subsystem and the measurement subsystem. The No. 5 blade was cut at five cross-sections along the length of the airfoil and 100X micrographs were taken at five locations on each cross-section in order to take coating thickness measurements. The results are shown in Table IV. This table shows the NiCrAlY thickness, the zirconia thickness and the total thickness for each point on each blade cross-section. It also shows the average total thickness for each cross-section. The NiCrAlY varies from 0.0 to 254  $\mu m$  (0.0 to 10.0 mils) and the zirconia from 177.8 to 340.4  $\mu m$  (7.0 to 13.4 mils). The total thickness varies from 188 to 543.6  $\mu m$  (7.4 to 21.4 mils). This is indicative of the fact that spray lines on the low end of the range for NiCrAlY are also on the low end of the range for zirconia and those on the high end of the range for NiCrAlY are also on the high end of the range for zirconia. In spite of the wide point to point variations on each cross-section, the thickness range is almost identical for each cross-section. This is to be expected since the spray gun is driven at constant speed along each spray line the entire length of the airfoil.

The No. 6 blade was cross-sectioned near the tip at the section where the optical measurements were made. The coating thickness measurements for blade No. 6 show the same general pattern as for blade No. 5. Thirteen 50X micrographs were taken around the airfoil, seven on spray line measurement points and six at locations between spray lines. Table V presents the coating thickness measurements made from the micrographs of blade No. 6 and compares them with the optical probe measurements for those locations where both measurements were made. A comparison of the optical probe data with the micrograph data shows agreement within  $\pm 35.6 \mu m$  ( $\pm 1.4$  mils) for the NiCrAlY except for micrograph No. 10 where the coating was separated from the blade. There was much poorer agreement for the zirconia. It was concluded that not only was the coating not uniform enough from one spray line to the next, but the measurement accuracy was not within the  $\pm 12.7 \mu m$  ( $\pm 0.5$  mils).

Five additional blades were sprayed with similar results. Observation of the system during spraying of these blades, in which a time delay was added between spraying and measuring, lead to the conclusion that there were two major problems with the APS system. The first problem was that the plasma spray gun was not spraying along its centerline as assumed. Figure 23 shows the plasma gun in top view including



SCALE : NONE

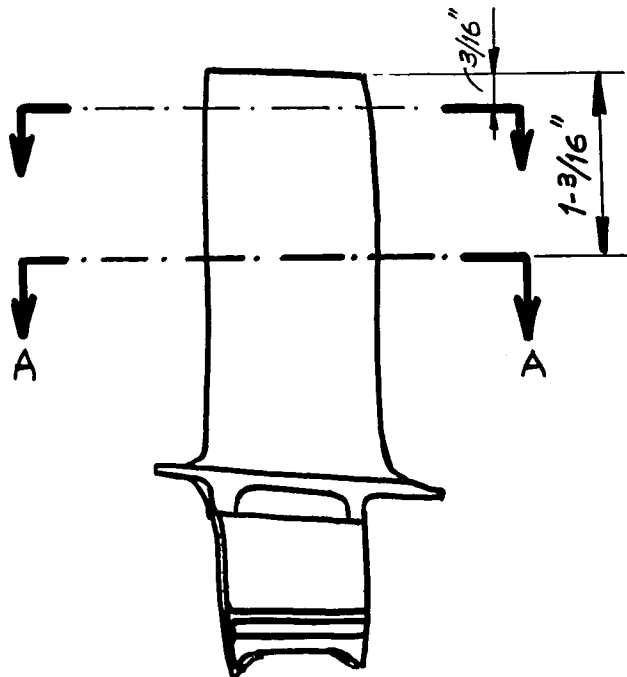


Figure 22. Initial Measurement Locations on JT9D First Stage Blade Airfoil Section.

TABLE IV

Coating Thickness Evaluation on Blade No. 5

Measurement Locations		Coating Thickness (mils)			
Section(1)	Location (2)	NiCrAlY	ZrO <sub>2</sub>	Total	Average
1	1	7.8	10.5	18.3	13.6
	2	0.3	8.0	8.3	
	3	1.5	9.0	10.5	
	4	0.0	10.0	10.0	
	5	7.5	13.4	20.9	
2	1	8.5	10.6	19.1	13.4
	2	0.2	8.2	8.4	
	3	0.8	7.0	7.8	
	4	2.0	8.5	10.5	
	5	8.2	13.2	21.4	
3	1	7.5	11.3	18.8	13.4
	2	0.2	8.0	8.2	
	3	0.0	9.0	9.0	
	4	1.0	9.8	10.8	
	5	10.0	10.0	20.0	
4	1	8.0	11.3	19.3	13.5
	2	0.2	7.2	7.4	
	3	0.6	7.4	8.0	
	4	4.4	11.0	15.4	
	5	7.0	10.5	17.5	
5	1	10.0	7.5	17.5	13.7
	2	0.1	10.1	10.2	
	3	0.7	8.0	8.7	
	4	1.8	13.0	14.8	
	5	8.0	9.5	17.5	

NOTES: 1. Blade sectioning was performed by NASA.

2. Approximate measurement locations:

- Location 1 - Convex side near trailing edge
- Location 2 - Convex side near center
- Location 3 - Convex side near leading edge
- Location 4 - Concave side near leading edge
- Location 5 - Concave side near trailing edge

TABLE V  
Coating Thickness Evaluation on Blade No. 6

Micrograph No. (1)	Coating Thickness, (mils)					
	NiCrAlY			ZrO <sub>2</sub>		
	Micrograph	Optical Probe	$\Delta$	Micrograph	Optical Probe	$\Delta$
1 (convex TE)	7.2	6.8	-0.4	15.6	10.1	-5.5
2	7.6	-		21.2	-	
3	6.4	5.2	-1.2	22.8	16.4	-6.4
4	6.0	-		23.0	-	
5	2.0	0.6	-1.4	17.4	12.4	-5.0
6	1.2	-		17.4	-	
7 (convex LE)	0.4	0.0	-0.4	16.0	14.8	-1.2
8 (concave TE)	0.0	0.0	0	17.4	19.8	+2.4
9	2.6	-		18.0	-	
10 (2)	8.0	4.6	-3.4	24.0	25.4	+1.4
11	7.4	-		32.6	-	
12	8.0	8.6	+0.6	32.0	-	
13 (concave LE)	7.4	-		29.2	-	

Notes: 1. Micrographs No. 1, 3, 5, 7, 8, 10 and 12 are at measurement points, Micrographs No. 2, 4 and 6 are to the left of the measurement points and Micrographs No. 9, 11 and 13 are to the right of the measurement points.

2. The NiCrAlY is pulled away from the blade in the area of Micrograph No. 10. The coating thickness measured off the micrograph was of the coating only.

the powder inlet tubes on its opposing sides. The NiCrAlY powder, which enters from the right, is sprayed to the left and slightly down. This is not a problem for manual spraying, nor is it even observable, because the operator aims the gun by looking at the spray. For automatic spraying, this situation must be accounted for, or when spraying for correcting coating thickness, the area needing the coating will not be sprayed. This was the prime cause of the leading and trailing edges not receiving uniform coating thickness.

The second problem was that the great amount of heat generated by the plasma gun was absorbed primarily by the blade, blade holder and C-axis shaft as the gun turned around at its upper extreme excursion point. Heat conduction up through the gimbals affected the A-axis and B-axis positions. This heat caused warpage of the blade and thermal shifting of the gimbals resulting in blade position changes and measurement errors. The total effect was larger than the desired coating uniformity. In order to improve the system, modifications were carried out which are described in the following sections.

#### Spray Deposition Process Modifications

In order to evaluate the extent to which the spray is off from the gun centerline, the system was set up to spray only three lines on a blade; one on the flat portion of the convex side, one on the highly curved portion of the convex side, and one on the highly curved portion of the concave side. The lines were located far enough apart on opposite sides of the blade so that they would not overlap. A bare blade (No. 21) was sprayed with four passes of NiCrAlY on each spray line. A previously sprayed blade (No. 7) was stripped of zirconia and sprayed with four passes of zirconia over the old NiCrAlY on each of the three spray lines. These blades were cut at two cross-sections, one near the tip and one near the center of the airfoil. Photomicrographs were taken at 50X over the entire width of the three spray lines. The coating thickness was measured every 254  $\mu\text{m}$  (10 mils) along the width of each pass. This provided six sets of data points per coating material. The data sets were processed using a second order polynomial regression program to obtain a curve of coating thickness versus position which was used to determine the centerline of each set of data. The data for each material were then averaged by matching centerlines and used to determine the average thickness at each distance from the centerline. This data was then processed using an eighth order polynomial regression program to obtain a curve of thickness versus position. The curves for both coatings (Figures 24 and 25) have the appearance of normal distributions. The curves show that the NiCrAlY is sprayed  $9.2^\circ$  to the right and the zirconia is sprayed  $2.8^\circ$  to the left. They were used to determine that the maximum allowable scan line spacing to provide a uniform coating is 3.5 mm (0.140 inches) for  $\text{ZrO}_2$  and 9.1 mm (0.360 inches) for NiCrAlY. It was also determined that a scan line spacing for NiCrAlY of 3.5 mm (0.140 inches) would also give a uniform coating. Therefore, to simplify the problem of setting up coordinate tables for spraying, it was decided to use a line spacing of 3.5 mm (0.140 inches) for both materials. It was also decided to increase the standoff distance of the blade from the spray gun from 6.35 to 7.62 cm (2.5 to 3 inches) in order to reduce the heat input to the blade.

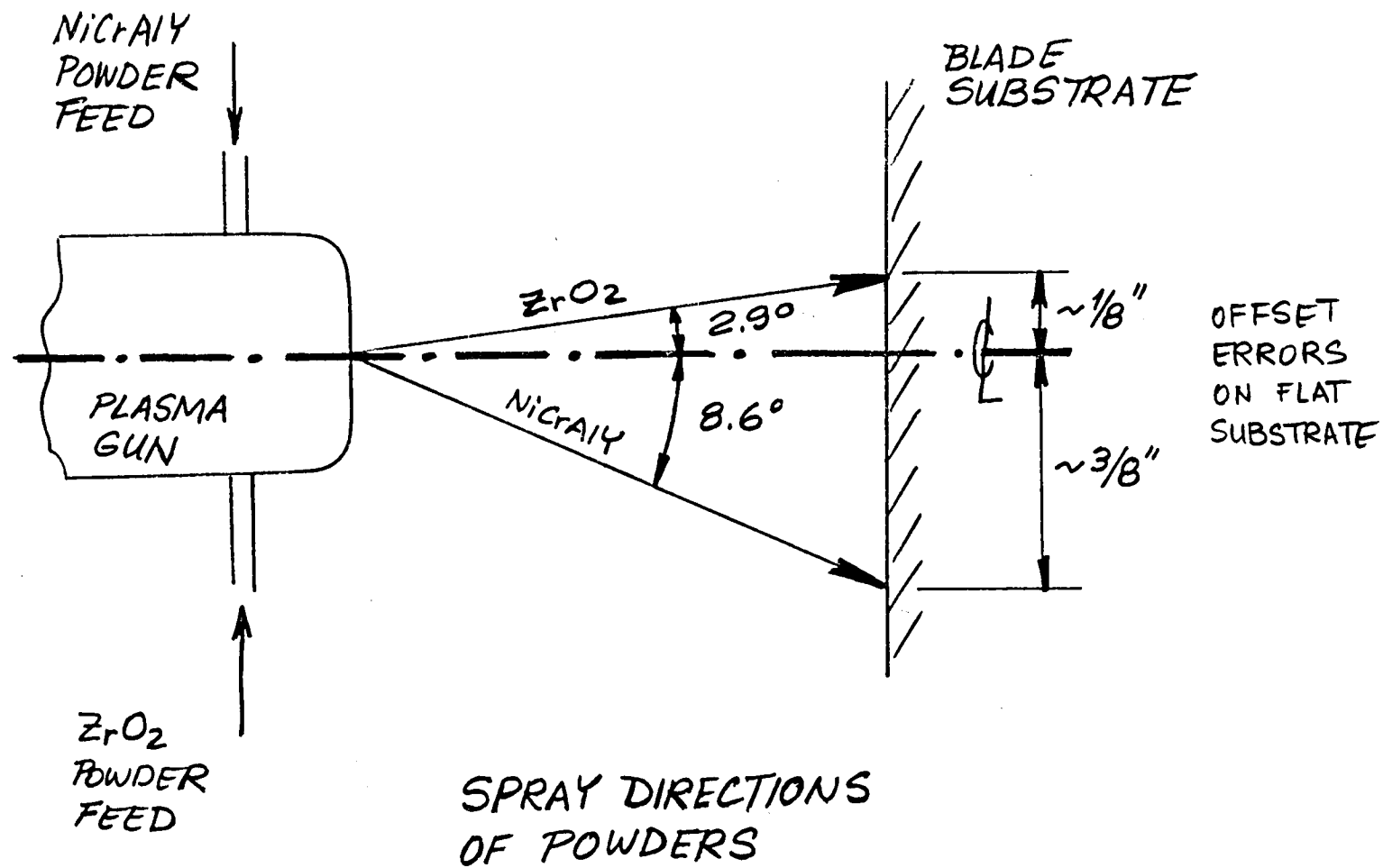


Figure 23. Spraying Pattern of Plasma Gun in APS

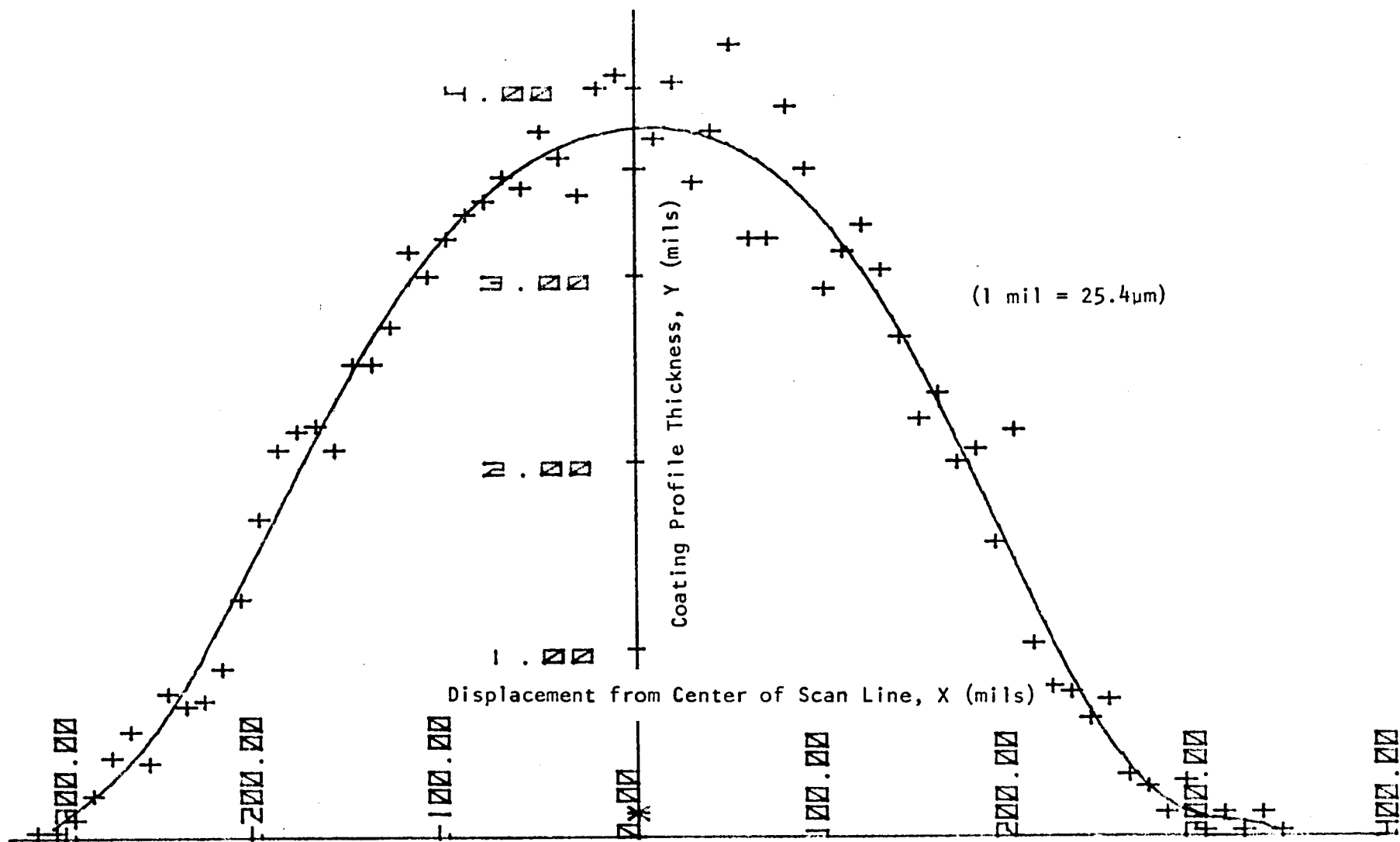


Figure 24. Average Beam Profile for  $\text{ZrO}_2$  Spray.



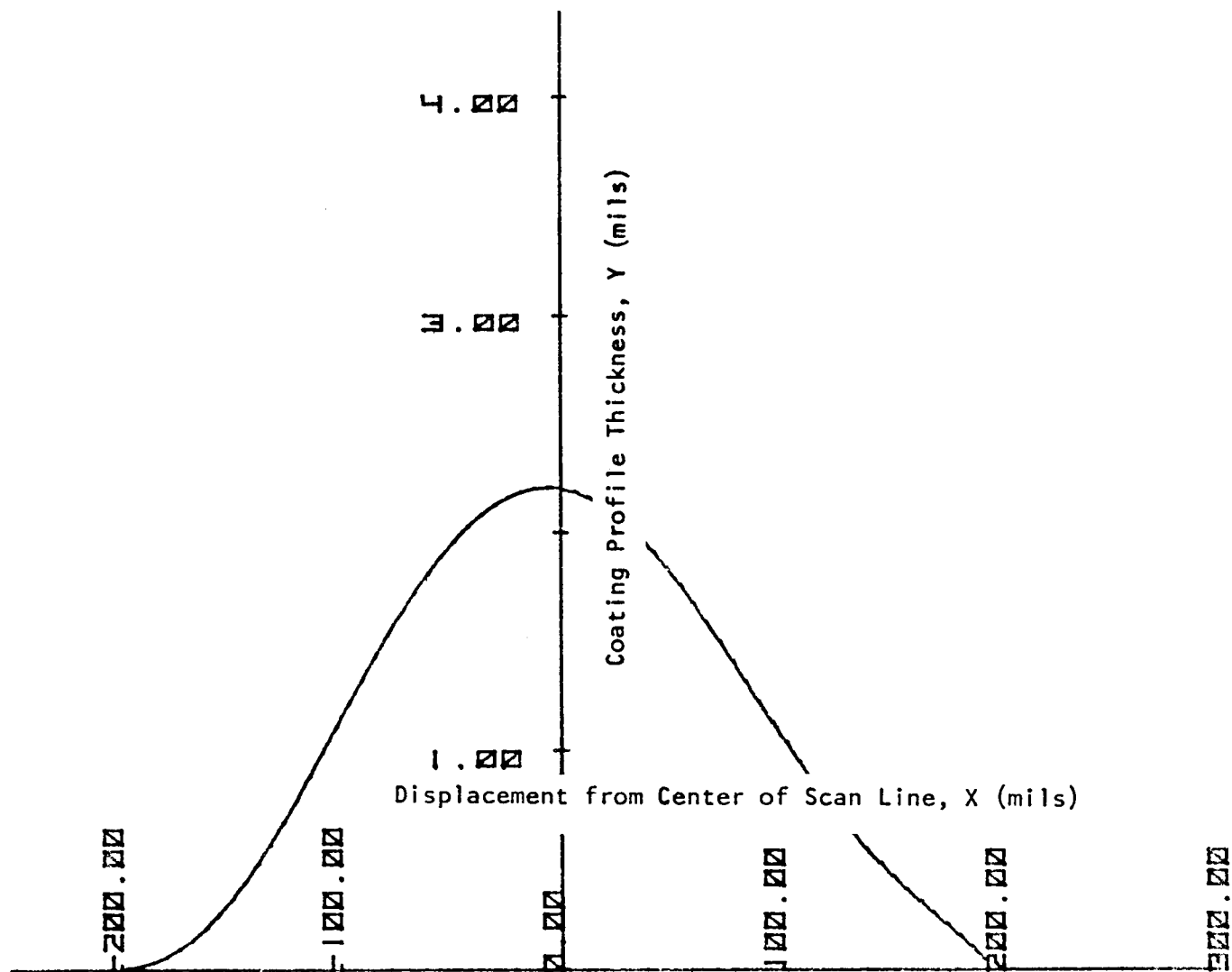


Figure 25. Average Beam Profile for NiCrAlY Spray.

The change in scan line spacing required increasing the number of scan lines from 18 to 24 as shown in Figure 26. Two of these scan lines, the ones at the trailing edge on the convex and concave sides, are aimed to miss the blade with the center of the beam so as to overlap the adjacent line enough to bring the trailing edges up to uniform thickness. The measurement points for these lines are at the trailing edges of the blade and are the only ones not centered on the scan line. The line on the convex side of the leading edge is sprayed with the blade turned slightly off-normal in order to avoid depositing spray at an oblique angle on the trailing edge of the concave side. The order of scan lines is such that spraying starts on the trailing edge of the convex side (scan line 0), moves around to the leading edge of the convex side (scan line 12), jumps to the trailing edge of the concave side (scan line 13) and moves around to the leading edge (scan line 23). This order was selected to minimize the amount of spray that strikes unsprayed surfaces at an oblique angle and to minimize the effects of backlash by reducing the number of reversals each axis must make during spraying.

#### Mechanical Subsystem Modifications

Mechanical subsystem modifications were carried out in order to eliminate, or compensate for, the blade and fixture thermal warpages which introduced a measurement inaccuracy too great to maintain  $+38.1 \mu\text{m}$  (+1.5 mils) coating thickness uniformity. Therefore, in addition to increasing the standoff distance used for spraying, a number of modifications were made:

1. A graphite barrier plate was installed between the plasma spray gun and the blade holder so that when the gun travels above the root platform of the blade and slows down, stops and reverses its direction, the plasma beam strikes the barrier plate rather than the cover of the blade holder. The barrier plate is angled so that the plasma sprayed beam is deflected to the side away from the blade and the gun.
2. The blade holder and cover were modified to reduce their size to make room for the addition of the graphite barrier plate.
3. A line was installed on the APS mechanism to provide  $\text{CO}_2$  cover gas to the area of the blade being sprayed.
4. An air line was also installed on the BHD to provide cooling air for the gimbal area of the carriage.
5. The C-axis shaft and blade holder were machined to accommodate an air line to provide cooling air through the inside of the blade.

Total number of locations: 24

TOP VIEW

SCALE: NONE

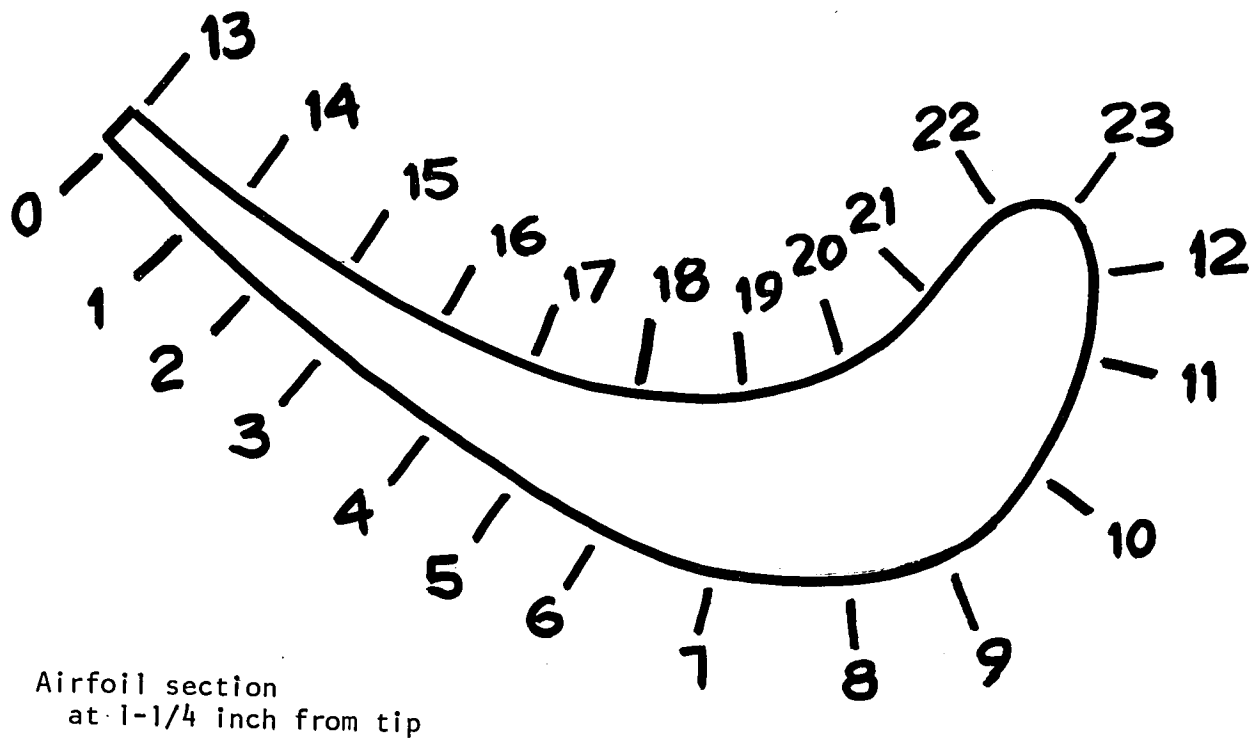


Figure 26. First Modified Measurement Locations on JT9D First Stage Blade Airfoil Section.

### Control System Modifications

Since the system was debugged and put into operation, no significant modifications to the control system hardware have been made. However, a number of modifications have been made in the software and firmware: 1) to reduce the heat input to the blade holder, the software was modified to allow only even numbers of passes; thereby the plasma gun is always spraying into an open space below the blade while the blade is being positioned from one scan line to the next; 2) to accommodate the difference in spray direction between NiCrAlY and  $ZrO_2$ , the one table of spray coordinates was replaced with two tables, one for each material; 3) to accommodate the difference in scan line spacing, the number of scan lines and measurement points was increased from 18 to 24; and 4) to minimize the effect on measurement accuracy of backlash caused by wear in the gimbal, a tilt of both the A and B axes was incorporated into the measurement routine before each point.

A number of software changes were also made to increase system flexibility so that process changes can be made or special tests can be run: 1) provision was made for programming the FIFO length for any value up to 32 steps; 2) provision was made for inserting offsets into the spray tables for any coordinate axis. This latter feature would allow the standoff distance to be changed, for example, and the offset of the spray tables to be adjusted to compensate for the angle of spray; and 3) special subroutines have also been devised, to use during manual operations such as establishing the measurement and spray tables.

### Evaluation of the Modified System

The modifications described in the earlier sections were carried out over a period of time. The modifications to the blade holder and to the C-axis shaft to allow internal cooling of the blade was a major modification and it resulted in a significant change in blade location in the mechanical positioner. This change required new tables of coordinates for both measurement and spray to be established. A total of eighteen blades, Nos. 12 through 29, were sprayed during this period, some to aid in re-establishing the coordinate tables and some to determine the effects of the modifications. The following paragraphs describe the details of the evaluations from which significant conclusions were drawn.

After all of the above modifications were made, except the addition of the line for internal cooling of the blade and the antibacklash software for the B-axis during measurement, blades No. 26 and No. 27 were sprayed. For blade No. 26, a cooldown period of 10 to 15 minutes was inserted after spraying and before measurements were taken. For blade No. 27, the entire operation was carried out continuously. The results of the optical probe measurements for these two blades are compared in Table VI for the NiCrAlY coating, the initial layer of zirconia and the total coating thickness after the finish passes of zirconia. The table shows that for blade No. 26, the NiCrAlY coating is  $96.5 \pm 35.6 \mu\text{m}$  ( $3.8 \pm 1.4$  mils) except for point 12, which is on the convex side of the leading edge and point 13, which is the trailing edge of the

TABLE VI

Evaluations of Modified APS System Using Blades No. 26 &amp; 27

Scan Line	Coating Thickness, mils <sup>(1)</sup>								
	NiCrAlY			1st ZrO <sub>2</sub> (10 pass)			Total		
	Blade No.		$\Delta$	Blade No.		$\Delta$	Blade No.		$\Delta$
	26	27		26	27		26	27	
0	3.0	2.8	0.2	7.4*	2.8*	4.6	14.0	14.8	-0.8
1	3.4	3.6	-0.2	8.4	4.0	4.4	16.2	17.8	-0.6
2	3.8	5.0	-1.2	10.6	5.6	5.0	17.0	18.4	-1.4
3	4.2	4.2	0.0	8.8	7.0	1.8	15.8	16.8	-1.0
4	4.6	4.6	0.0	8.4	6.8	1.6	15.8	16.0	-0.2
5	4.4	4.2	-0.2	8.4	6.6	1.8	16.0	16.4	-0.4
6	4.0	3.8	-0.2	8.2	7.0	1.2	15.2	16.4	-1.2
7	5.2	3.2	-2.0	8.0	7.0	1.0	15.8	16.2	-0.4
8	4.6	3.6	-1.0	8.8	6.6	2.2	16.0	16.2	-0.2
9	3.6	3.2	-0.4	9.0	5.8	3.2	14.8	15.6	-0.8
10	4.2	3.8	-0.4	10.0	6.0	4.0	16.0	17.2	-1.2
11	3.8	3.0	-0.8	11.6*	7.6*	4.0	18.6*	19.6*	-1.0
12	0.6*	1.2*	+0.6	6.0*	2.2*	3.8	11.8*	13.2*	-1.4
13	1.8*	2.2*	+0.4	9.4	5.4	4.0	14.0	14.6	-0.6
14	2.4	2.4	0.0	10.0	6.0	4.0	15.0	16.0	-1.0
15	3.2	3.2	0.0	9.4	6.2	3.2	14.8	16.2	-1.4
16	3.4	3.0	-0.4	10.0	5.8	4.2	14.8	15.6	-0.8
17	3.8	3.6	-0.2	10.2	5.4	4.8	15.2	16.6	-1.4
18	3.6	3.8	+0.2	9.6	5.6	3.0	14.8	17.0	-3.2
19	4.8	4.6	-0.2	10.0	5.4	4.6	15.0	18.0	-3.0
20	5.2	5.2	0.0	10.4	6.4	4.0	14.4	19.0	-4.6
21	4.4	4.8	-0.4	10.6	7.2	3.4	15.2	20.0	-4.8
22	-	2.4	-	-	4.0	-	13.6*	16.4	-2.8
23	2.8	1.8*	-1.0	5.6*	3.0*	2.6	14.0	14.0	0
Average	3.8	3.8		9.3	5.6		15.5	17.0	
Range	+1.4	+1.4		++1.3	+1.6		+1.5	+3.0	

\*Not included in Average or Range

(1) Measurement data is expressed in units of mils as printed by APS System.

concave side. Slight adjustments of the spray coordinates for these two lines would be expected to bring the NiCrAlY coating within the desired  $\pm 38.1 \mu\text{m}$  ( $\pm 1.5$  mils) tolerance band. The NiCrAlY measurements for blade No. 27 show the same uniformity, except that, in addition, point 23, which is right on the leading edge, is low. For the initial pass of zirconia, the pattern for blade No. 26 is about the same as for NiCrAlY. The zirconia layer is  $236.2 \pm 33 \mu\text{m}$  ( $9.3 \pm 1.3$  mils), except for line 0, which is on the trailing edge of the convex side and lines 11, 12 and 23. In this case the spray that missed line 12, hit line 11, causing it to be oversprayed. Blade No. 27 shows a similar pattern but an average of  $94.0 \mu\text{m}$  (3.7 mils) less coating. The total coating thickness for blade No. 26 came out  $393.7 \pm 1 \mu\text{m}$  ( $15.5 \pm 1.5$  mils) except for lines 11, 12 and 22. Additional finish passes would have brought lines 12 and 22 up to the desired coating, but would have caused line 11 to be badly oversprayed. It is reasonable to assume, however, that by adjusting line 12 and allowing an adequate number of finish passes, the entire blade could have been coated within the desired range. The results for blade No. 27 show similar results for lines 11 and 12, but a heavier coating and a larger range of values on the other lines,  $431.8 \mu\text{m}$   $\pm 76.2 \mu\text{m}$  ( $17.0 \pm 3.0$  mils).

It was concluded from these results that two corrections were needed in order to achieve a coating uniformity of  $\pm 38.1 \mu\text{m}$  ( $\pm 1.5$  mils):

1. A few scan lines needed adjustment to even out the deposition; and
2. The heat generated during plasma spraying needed to be removed more efficiently in order to eliminate measurement errors caused by the effects of thermal expansion.

The errors in measurement caused by thermal effects are illustrated by comparing the results for blades No. 26 and 27 listed in Table VI. The measurements after spraying two passes per line of NiCrAlY show very little difference between the two blades. The measurement after spraying ten passes per line of zirconia show a large error on almost every line. The total coating thickness, which is achieved with three sets of finish passes separated by measurements, with only a few selected lines sprayed the last time, show large differences on only a few lines on the high curvature part of the concave side of the blade.

These results are consistent with the theory that the measurement values are in error by an amount that is proportional to the amount of heat that the part is subjected to during the spray operation and the amount of time allowed for cooling before measurement. For blade No. 26, a sufficient cooldown period (10 to 15 minutes) was allowed, so that true measurements were obtained and the coating uniformity was limited only by a few minor errors in the spray coordinate tables. For blade No. 27, however, the measurements made after the first application of zirconia were low on some lines due to thermal warpage, causing too many finish passes to be applied on these lines the first time. During subsequent measurements, following finish passes in which only a few lines were sprayed, the blade had time to cool down, so that the measurements revealed the overspray. This can be seen by comparing the measurements taken after each zirconia pass which are presented in Table VII along with the number

of finish passes. Lines 19, 20 and 21 all had adequate coating after the first zirconia application and no finish passes were added. By the final measurement, all three lines had increased by about 88.9  $\mu\text{m}$  (3.5 mils) and were shown to be oversprayed. It can also be seen from the data in Table VII that the effect of warpage is more predominant near the edges of the blade. Lines 3 through 5 and 14 through 17, which are near the center of the airfoil and also had no finish passes after the first finish spray, show considerably less change after cooldown, an average of 17.8  $\mu\text{m}$  (0.7 mils). This indicates that the warpage includes a significant twisting of the airfoil.

In order to correct this problem, additional cooling was provided in the form of air flow through the inside of the blade. At the same time the antibacklash tilt was added to the B-axis to correct effects of wear in the gimbal.

## 5.2 APS Process Evaluation

### General Discussion

The automated plasma spray (APS) process developed in this program is designed to provide uniform and reproducible coatings on airfoils. Specifically, a two-layered thermal barrier coating of NiCrAlY and yttria stabilized zirconia was used to demonstrate the process. All efforts were carried out utilizing a single airfoil geometry; the JT9D first stage turbine blade. APS process evaluations, thus, were carried out in respect to three criteria: 1) coating thickness uniformity and reproducibility, 2) coating structure, and 3) coating integrity in torch exposure tests.

The prime objective in the APS process/system development was coating thickness uniformity and reproducibility. Since the APS system contains an optical dimensional metrology subsystem, the system evaluation relied heavily on this device. This approach was not only feasible but was cost-effective once initial calibrations proved the approach accurate. Subsequent blade sectioning and dimensional measurements obtained from photomicrographs were made to verify coating thickness performance.

Coating structure was to be maintained at the level of prior art demonstration (Ref. 1). Coating optimization, as such, was not the objective of the program. Evaluations of coating structure were performed relying on established procedures of part sectioning and metallography. A preliminary evaluation of coating integrity in a torch test was performed. The results of the various evaluations are discussed in the following sections.

### Coating Thickness Evaluation

Evaluations of coating thickness uniformity were performed by sectioning sprayed blades and making measurements on photomicrographs taken of the sections. Micrographs taken at 50X provided an area for coating thickness measurements comparable to the area measured by the optical probe. Coating thickness evaluations covered both manually sprayed and APS system coated JT9D first stage blades.

TABLE VII

## Effect of Blade/Fixture Thermal Warpage on Coating Thickness

Coating Thickness on Blade No. 27 (mils) <sup>(1)</sup>							
Scan Line	Total Coating After 1st ZrO <sub>2</sub>	Total No. of Finish Passes	Total Coating After 1st Finish	Total No. of Finish Passes	Total Coating After 2nd Finish	Total No. of Finish Passes	Total Coating After 3rd Finish
0	5.6	12	11.4	18	13.6	20	14.8
1	7.6	10	14.6	12	16.8	12	17.8
2	10.6	6	17.0	6	18.8	6	18.4
3	11.2	6	16.0	6	16.4	6	16.8
4	11.4	6	15.6	6	15.6	6	16.0
5	10.8	6	15.4	6	15.6	6	16.4
6	10.8	6	14.6	8	15.6	8	16.4
7	10.2	6	14.6	8	15.8	8	16.2
8	10.2	6	14.4	8	16.0	8	16.2
9	9.0	8	13.4	10	14.6	12	15.6
10	9.8	8	14.8	10	16.6	10	17.2
11	10.6	6	17.4	6	18.6	6	19.6
12	4.4	14	9.2	22	11.4	28	13.2
13	7.6	10	14.6	12	15.4	12	14.6
14	8.4	10	15.6	10	16.6	10	16.0
15	9.4	8	16.2	8	16.6	8	16.2
16	8.8	8	15.0	8	15.8	8	15.6
17	9.0	8	15.0	8	16.2	8	16.6
18	9.4	8	14.4	10	15.8	10	17.0
19	10.0	8	15.4	8	16.6	8	18.0
20	11.6	6	15.6	6	16.6	6	19.0
21	12.0	4	16.4	4	17.4	4	20.0
22	6.4	12	12.8	16	15.4	16	16.4
23	4.8	14	11.2	20	14.4	22	14.0

Notes: 1. Measurement data is expressed in units of mils as actual printouts of the APS hardware.



### Evaluation of Manually Sprayed Blades

Evaluations were performed on two blades (No. X and Y) hand sprayed by two operators, while the blades were vise-clamped. These blades are believed representative of manual plasma spray (MPS) production operations using no mechanization.

Figure 27 illustrates the blade sectioning scheme. Cuts were made perpendicular to the length of the airfoil at about 32mm (1-1/4 inch) and 50mm (2 inches) from the tip. The tip end portion of the airfoil was then sectioned along its length at about 7.6 mm (0.3 inch) from the leading edge. Surfaces "A" and "B" were polished and photographed. Figures 28 through 31 show surfaces "A" and "B" of blade No. X and Y, respectively. These provide an overall view of the coating distribution and uniformity. Figure 30 shows that the coating is pulled away from the blade on the concave side. Measurements of the coating thickness were made on surface "A" of each blade at the same points at which optical probe measurements are made on the automatically sprayed blades (Figure 26). Surface "B" of each blade was measured every 6.4 mm (0.25 inches) along its length on each side. The results of these measurements are presented in Table VIII. For both operators the uniformity along the length of a line is about  $\pm 38.1 \mu\text{m}$  (1.5 mils) for NiCrAlY and  $45.7 \mu\text{m}$  (1.8 mils) for total. The variation between points on the cross-section, however, is much greater;  $\pm 112 \mu\text{m}$  (4.4 mils) for NiCrAlY and  $\pm 417 \mu\text{m}$  (16.4 mils) total. The average NiCrAlY thickness is  $180 \mu\text{m}$  (7.1 mils) and the average total thickness is  $886 \mu\text{m}$  (35.9 mils). While the data is limited, it suggests that the spread in coating thickness is a relatively fixed percentage of the thickness rather than a fixed number, so that for a total coating thickness of  $406 \mu\text{m}$  (16.0 mils) the uniformity might be expected to be about  $\pm 190 \mu\text{m}$  (7.5 mils).

Although the average coating thicknesses and the spread in thicknesses are not drastically different between the two blades, there is a significant difference between the two blades as can be seen by comparing Figures 26 through 29. Blade No. Y has a fairly uniform coating except for a few locations which are considerably thinner or thicker. The concave side has only a slightly thicker coating than the convex. Blade No. X has a much thicker coating on the concave side and is very nonuniform on the convex side. These differences illustrate the fact, that for manually sprayed blades, the problem is not only the nonuniformity of the coating on a particular blade. An even greater problem is the lack of repeatability from one blade to another which can occur because of the many factors affecting human operator performance.

### Evaluation of the APS System Sprayed Blades

Of the many blades that were sprayed using the APS system about twenty were coated completely and had printouts of the coating thicknesses. Table IX lists the spread of the best blades done during the time when there was still a thermal warpage problem. The best uniformity achieved was  $\pm 43 \mu\text{m}$  (1.7 mils) for NiCrAlY and  $\pm 79 \mu\text{m}$  (3.1 mils) for total thickness. The average for ten blades is  $\pm 68.1 \mu\text{m}$  (2.68 mils) for NiCrAlY and  $\pm 98.3 \mu\text{m}$  (3.85 mils) for total thickness. The comparable results

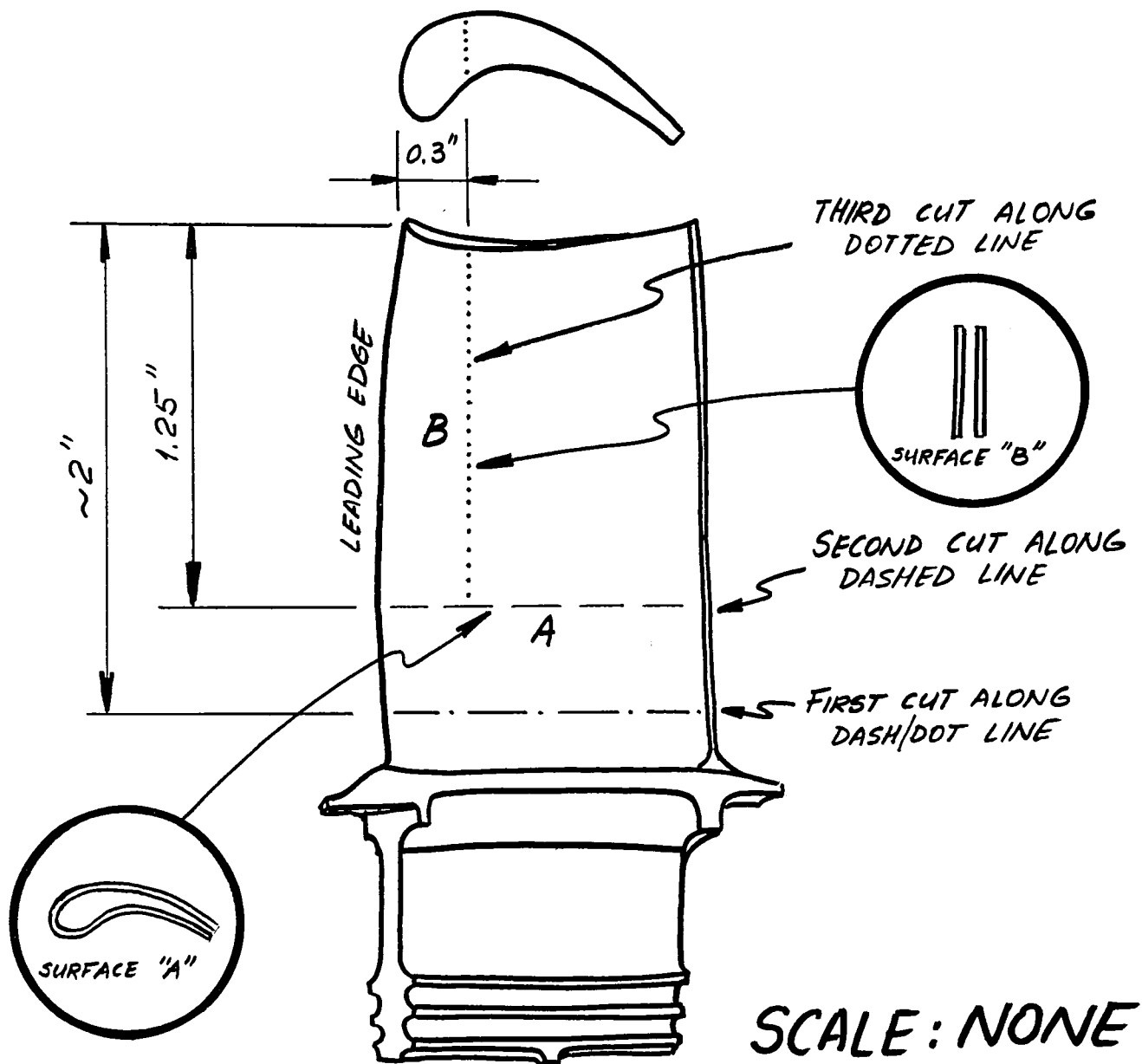


Figure 27. Locations of Sections Examined for Manually Sprayed Blades

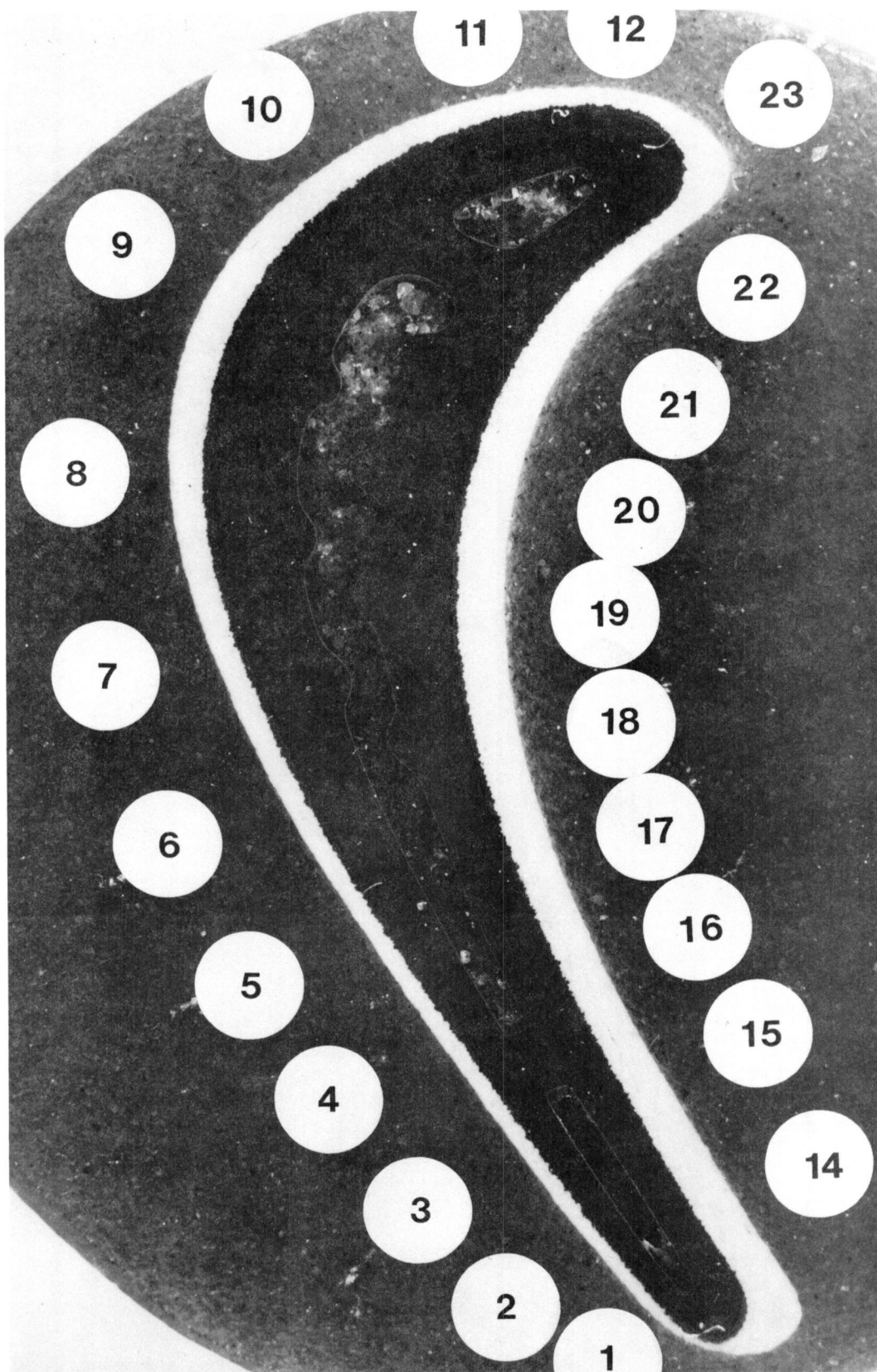


Figure 28. Photomicrograph Cross-section of Manually Sprayed JT9D Blade Specimen No. "X" at Surface Location "A".

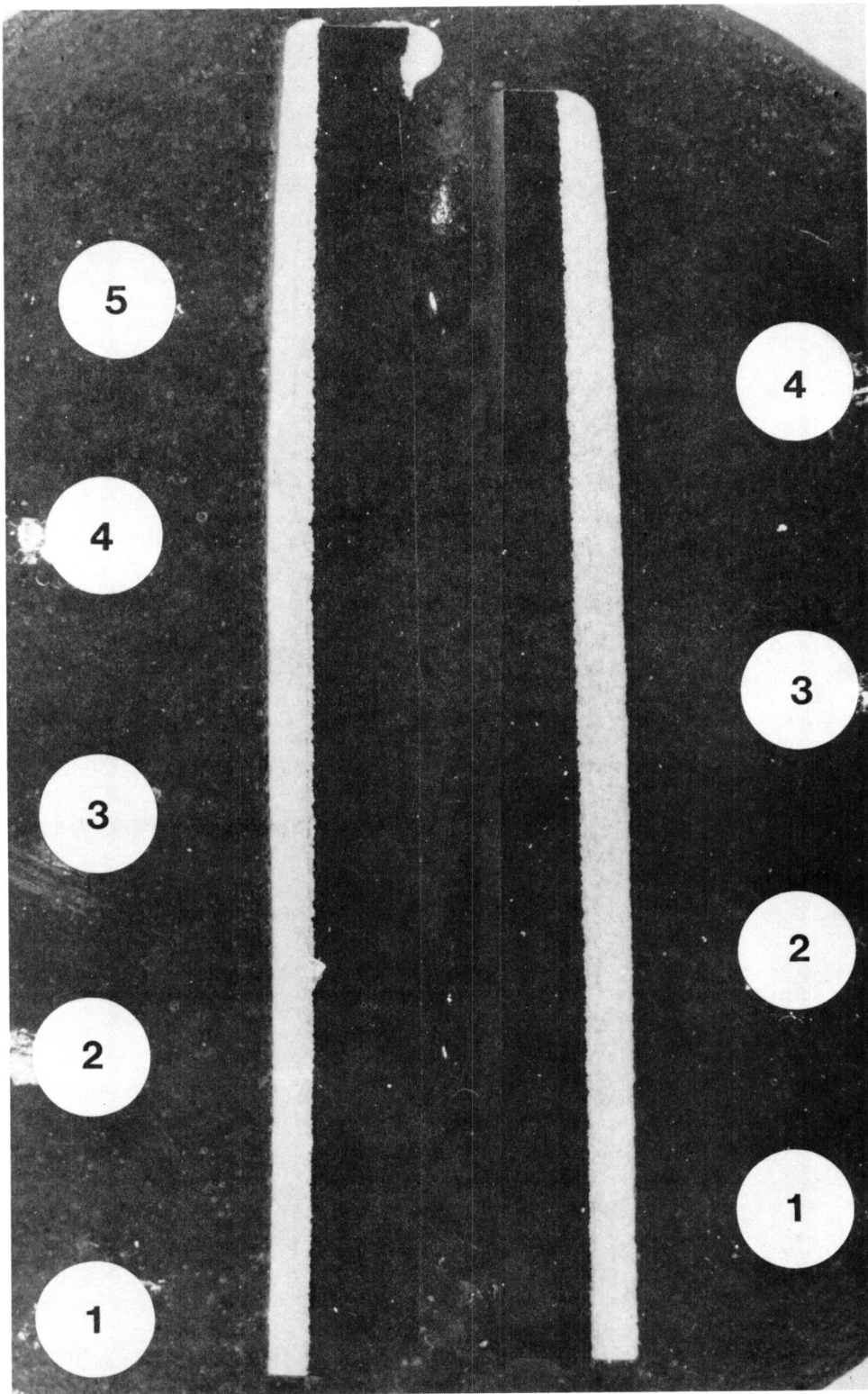


Figure 29. Photomicrograph Cross-section of Manually Sprayed JT9D Blade Specimen No. "X" at Surface Location "B".

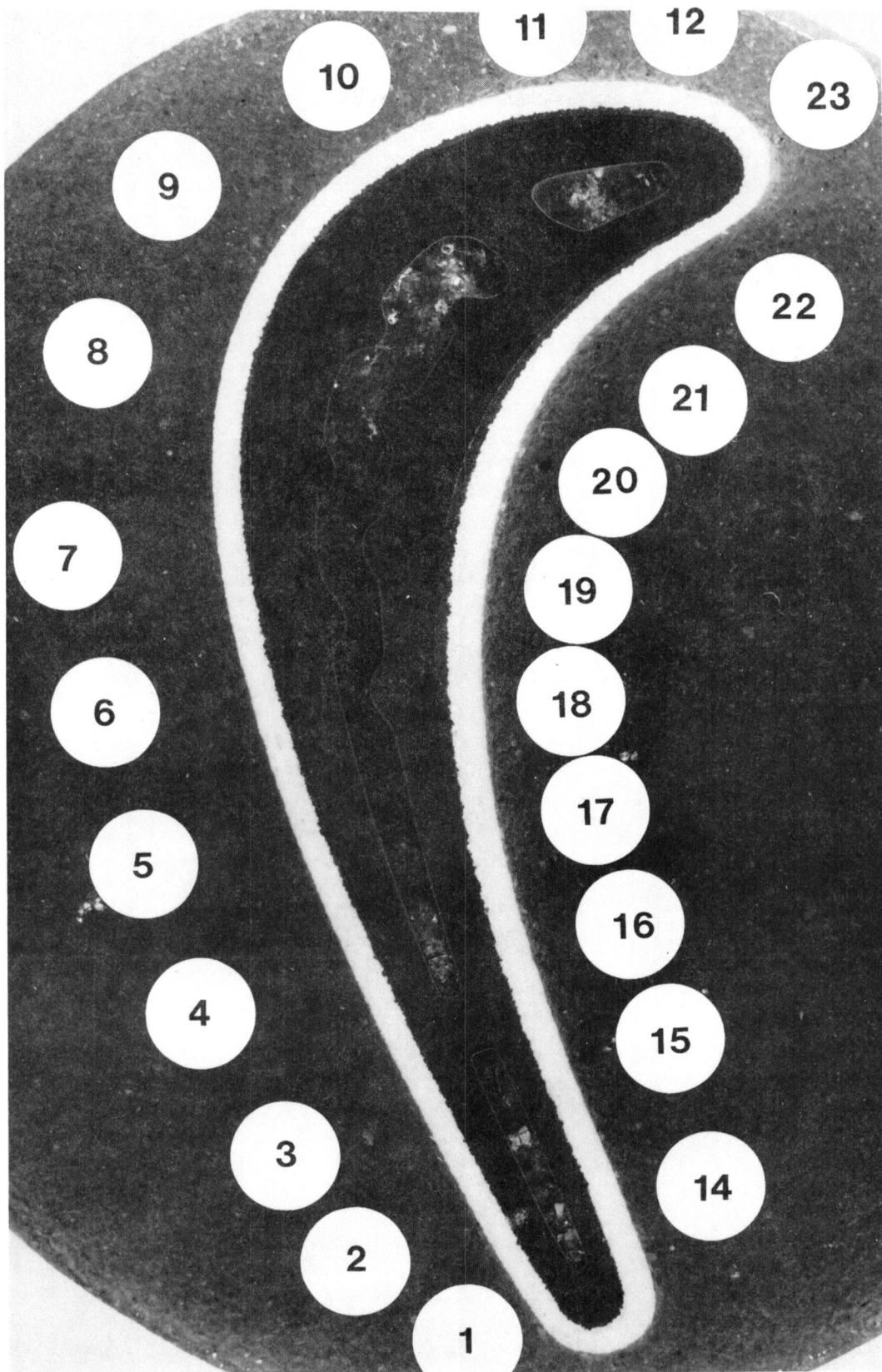


Figure 30. Photomacrograph Cross-section of Manually Sprayed JT9D Blade Specimen No. "Y" at Surface Location "A".



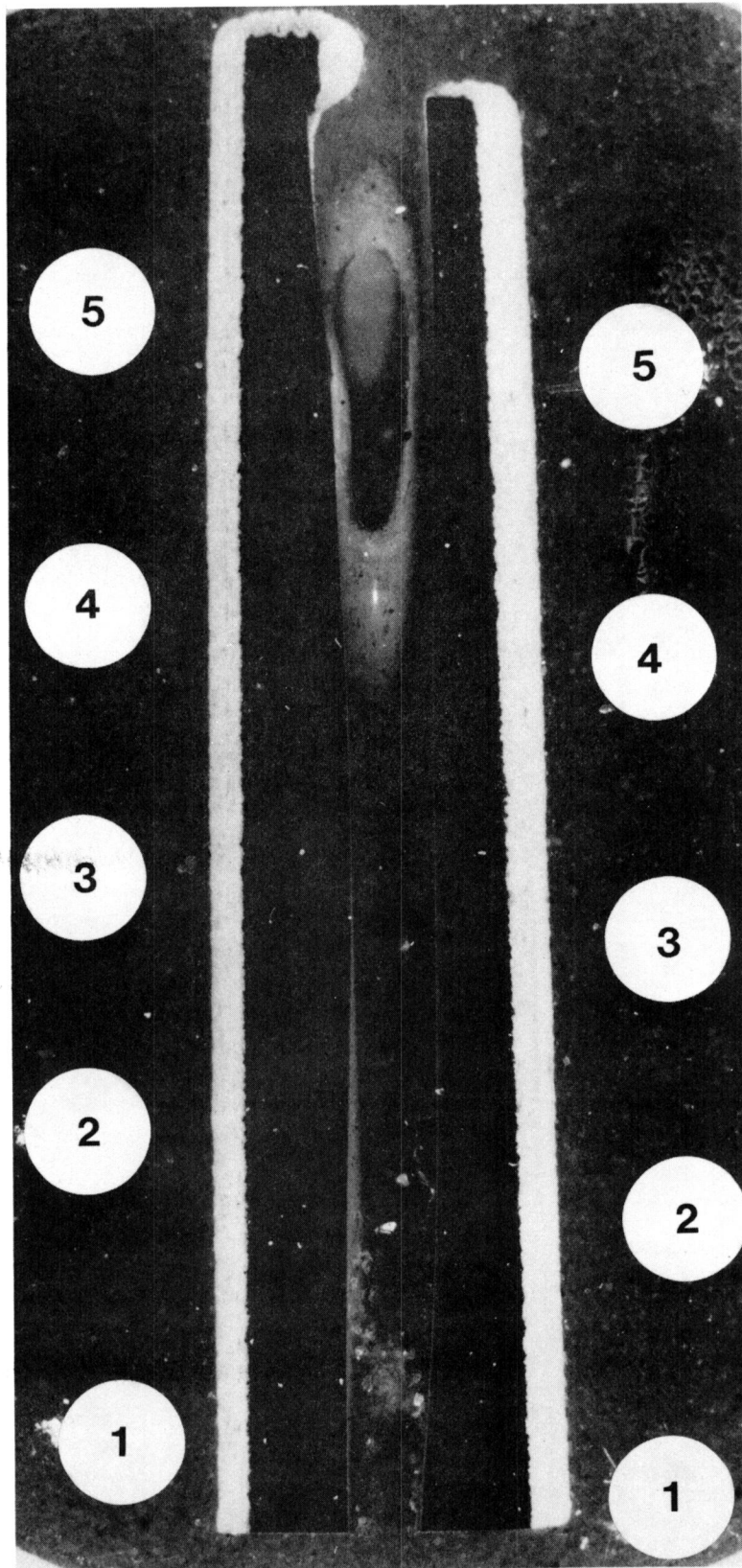


Figure 31. Photomicrograph Cross-section of Manually Sprayed JT9D Blade Specimen No. "Y" at Surface Location "B".

TABLE VIII

## Coating Thickness Measurements on Manually Sprayed Blades

Side	Coating Thickness (mils)										
	Surface A					Surface B					
	Location No.	Blade No.				Location No.	Blade No.				
		X		Y			X		Y		
NiCrAlY		Total	NiCrAlY	Total	NiCrAlY		Total	NiCrAlY	Total		
Suction (Convex)	1	3.9	15.0	2.4	26.0	1	3.9	43.3	3.9	33.1	
	2	5.5	18.1	4.7	30.7	2	5.5	47.3	3.9	31.5	
	3	5.5	22.1	4.7	31.5	3	5.5	44.9	4.7	31.5	
	4	6.3	22.1	3.9	31.5	4	6.3	44.1	5.5	34.7	
	5	6.3	23.6	3.9	32.3	5	8.7	45.7	4.7	30.7	
	6	7.1	28.4	5.5	32.3						
	7	8.7	33.5	6.3	33.9						
	8	9.5	43.3	4.7	31.5						
	9	9.5	47.3	5.5	32.3						
	10	9.5	39.4	5.5	33.9						
	11	7.1	27.6	7.1	31.5						
	12	7.9	23.6	7.9	30.7						
	median spread	6.70 +2.80	31.15 +16.15	5.15 +2.75	29.95 + 3.95		6.30 +2.40	45.3 + 2.0	4.70 +0.80	32.70 + 2.00	
	average std dev.	7.23 +1.83	28.67 +10.17	5.18 +1.49	31.50 + 2.02		5.98 +1.75	45.06 + 1.54	4.54 +0.67	32.30 + 1.60	
Pressure (Concave)	14	3.9	47.3	7.1	37.0	1	3.9	49.6	7.9	47.3	
	15	4.7	47.3	9.5	39.4	2	5.5	51.2	8.7	46.5	
	16	4.7	47.3	9.5	43.3	3	5.5	50.4	9.5	44.9	
	17	5.5	48.1	11.8	44.9	4	5.5	48.1	9.5	44.1	
	18	6.3	49.6	13.4	47.3	5	-	-	11.8	45.7	
	19	7.9	53.6	13.4	48.9						
	20	5.5	52.0	11.8	43.3						
	21	5.5	46.5	9.5	33.1						
	22	3.9	29.9	3.9	22.1						
	23	3.2	41.8	5.5	31.5						
		median spread	5.55 +2.35	41.75 +11.85	8.65 +4.75	35.5 +13.4		4.70 +0.80	49.65 + 1.55	9.85 +1.95	45.70 + 1.60
		average std dev.	5.11 +1.36	46.34 + 6.60	9.54 +3.23	39.08 + 8.30		5.10 +0.80	49.83 + 1.32	9.48 +1.46	45.70 + 1.26
Total	median spread	6.25 +3.25	34.30 +19.30	7.90 +5.50	35.50 +13.40		6.30 +2.40	47.25 + 3.95	7.85 +3.95	39.00 + 8.30	
	average std dev.	6.27 +1.93	36.70 +12.41	7.16 +3.25	34.95 + 6.82		5.59 +1.41	47.18 + 2.85	7.01 +2.81	39.00 + 7.19	

Notes: 1. Values listed for the column of "Total" are the sum of the NiCrAlY and ZrO<sub>2</sub> coatings.

TABLE IX

Spread of Optical Probe Data From  
Ten Best Uniformly Coated JT9D Blades  
(Sprayed Without Internal Air Cooling)

Blade No.	Coating Thickness, in Mils	
	NiCrAlY	Total
	Average/Spread	Average/Spread
22	4.7 $\pm$ 3.5	11.2 $\pm$ 3.2
23	4.9 $\pm$ 3.7	16.5 $\pm$ 3.7
26	2.9 $\pm$ 2.3	15.2 $\pm$ 3.4
27	3.2 $\pm$ 2.0	16.6 $\pm$ 3.4
29	2.4 $\pm$ 2.4	16.3 $\pm$ 3.1
30	4.2 $\pm$ 2.6	18.8 $\pm$ 3.8
31	7.3 $\pm$ 3.5	14.8 $\pm$ 4.2
34	3.5 $\pm$ 1.7	20.8 $\pm$ 5.0
35	3.9 $\pm$ 3.3	19.1 $\pm$ 4.9
37	4.2 $\pm$ 1.8	17.8 $\pm$ 3.8
Average	4.12 $\pm$ 2.68	16.71 $\pm$ 3.88



for manually sprayed blades are an average of  $+112\text{ }\mu\text{m}$  (4.4 mils) for NiCrAlY and an expected average of  $+190\text{ }\mu\text{m}$  (7.5 mils) at the same thickness for total. Therefore, these results not only show good consistency from one blade to another, but also better uniformity than can be achieved by manual spraying.

Blades No. 26 and 27 were sectioned and photographed to determine the actual coating uniformity. Section A (cross-section) on each blade was made in about the same location as on the hand sprayed blades. Section B was only cut on Blade No. 26 and it was located at approximately the center of the airfoil, rather than near the leading edge. Section A on Blade No. 26 only includes the part of the blade from Section B to the leading edge. Figures 32, 33 and 34 show photomicrographs of Sections A and B of Blade No. 26 and Section A of Blade No. 27, respectively. These provide an overall view of the coating distribution and uniformity. 50X photomicrographs were made around Section A of each blade approximately at the points where optical probe measurements were made during spraying, and along Section B of Blade No. 26 at 6.4 mm (0.25 inch) intervals on both sides. The coating thickness at each location, both for NiCrAlY and for total coating thickness, was measured on each photomicrograph. The results of these measurements are listed in Table X.

Figures 35 and 36 show two of the most difficult areas to spray on Blade No. 27. Figure 35 shows the area with the highest radius of curvature, the leading edge (point 23). Figure 36 shows one side of the trailing edge adjacent to the cooling passage opening (point 1). It can be seen that the coating tapers down to the edge of the cooling passage without blocking the opening. This excellent result was accomplished without masking. The data in Table X show that the uniformity along the length of a scan line (Section B) is  $+10\text{ }\mu\text{m}$  (0.4 mils) for NiCrAlY and  $+20\text{ }\mu\text{m}$  (0.8 mils) for total, which is about a factor of three better than on the manual sprayed blades. The uniformity between scan lines (Section A) is  $+57\text{ }\mu\text{m}$  (2.2 mils) for NiCrAlY and  $+66\text{ }\mu\text{m}$  (2.6 mils) for total thickness. Both of these values are considerably better than can be done by manual spraying. Also, the average coating thickness for each portion of a blade, and for each entire blade, is within the desired range of 79 to 155  $\mu\text{m}$  (3.1 to 6.1 mils) for NiCrAlY and 368 to 445  $\mu\text{m}$  (14.5 to 17.5 mils) for total coating thickness. These results demonstrate that, even with the problem of thermal warpage when these blades were sprayed, the APS system is considerably better than manual spraying in uniformity both over each blade and between blades.

Figure 37 is a graph comparing coating thickness taken from the optical probe data in Table VI with the photomicrograph data in Table X for Blade No. 27. The agreement is quite good. A carefully controlled experiment, in which special precautions are taken to identify the exact locations of the optical probe and metallurgical measurement points, would be required to determine whether or not the differences shown in Figure 37 are statistically significant.

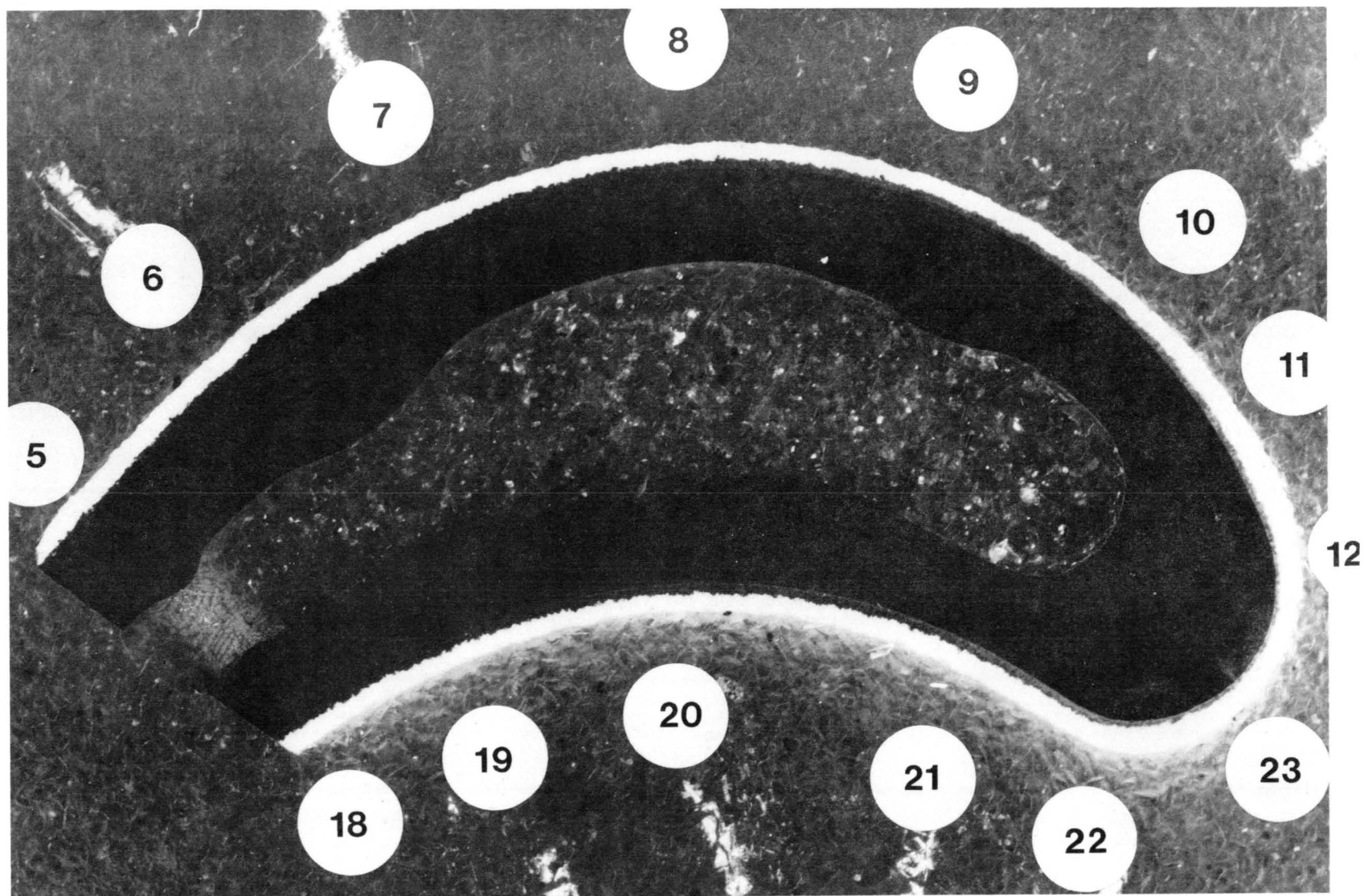


Figure 32. Cross-section of JT9D Blade Specimen No. 26 from Center to Leading Edge after Coating with APS System and Torch Test (Approximate locations where micrographs were taken are indicated by numbered arrows).

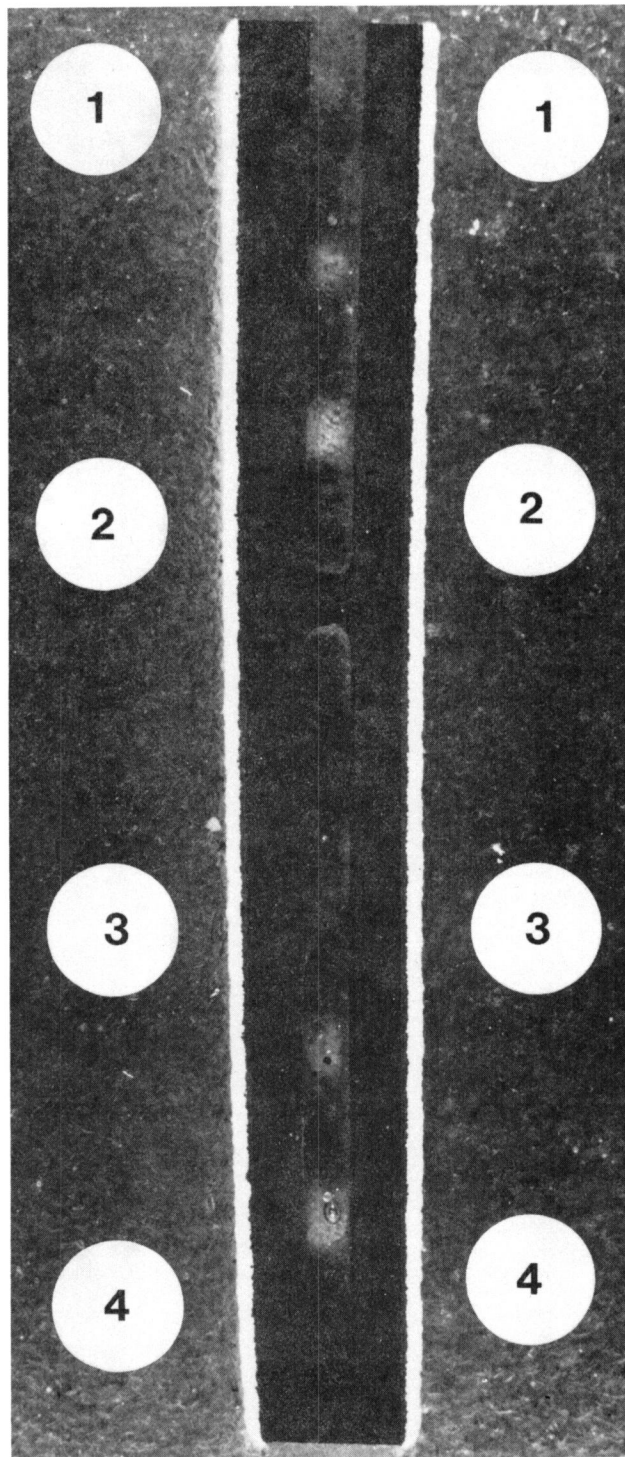


Figure 33. Length Section of JT9D Blade Specimen No. 26 from Tip to Section 'A' after Coating with APS System and Torch Test (Approximate locations where micrographs were taken are indicated by numbered arrows).

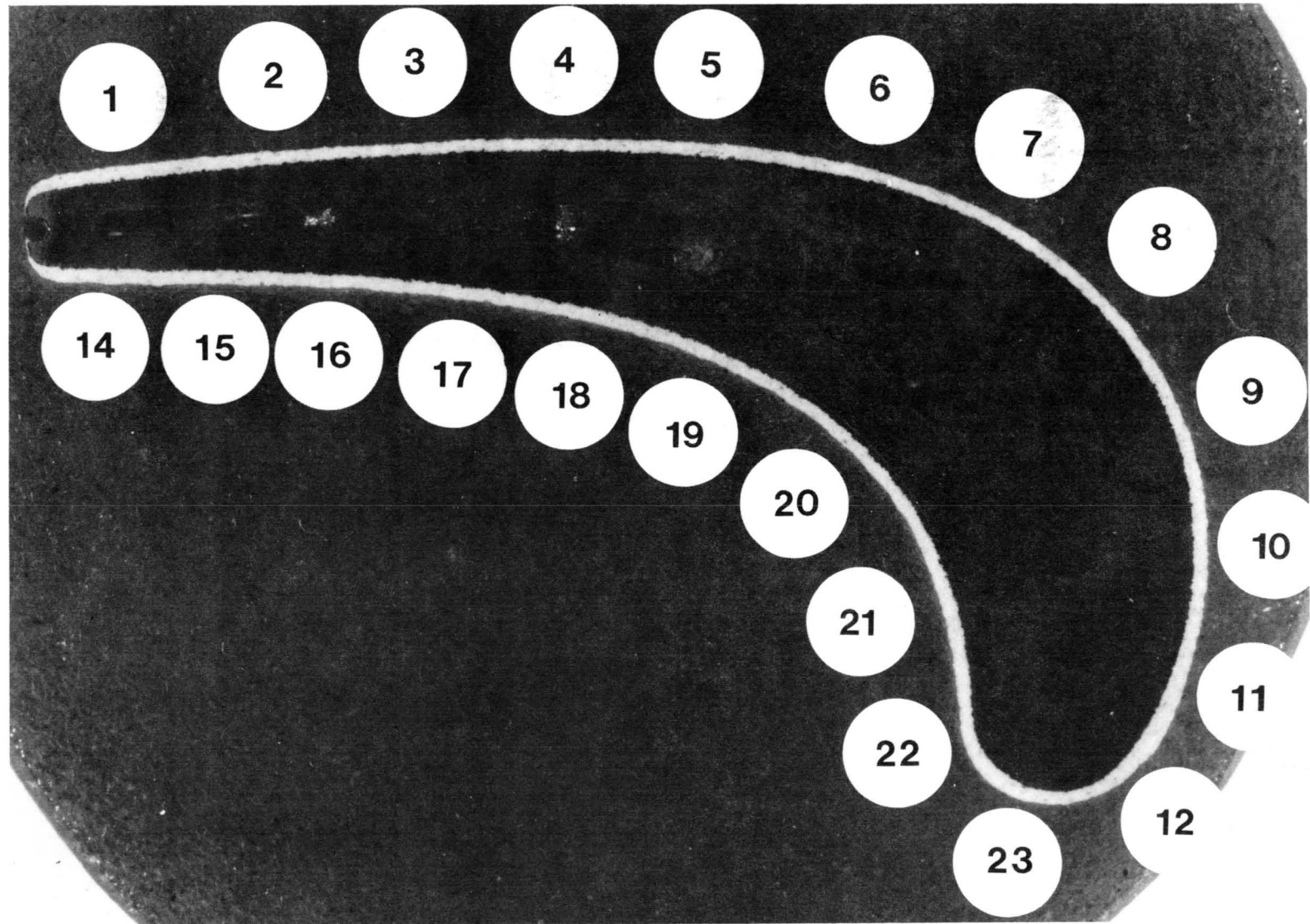


Figure 34. Cross-section of JT9D Blade Specimen No. 27 after Coating by APS System (Approximate locations where micrographs were taken are indicated by numbered arrows).

TABLE X

## Coating Thickness Measurements on APS System Sprayed Blades

Side	Coating Thickness (mils)								
	Surface A (Cross-Section)					Surface B (Length)			
	Location	Blade No.				Location	Blade No.		
		27		26			26		
		No.	NiCrAlY	Total	NiCrAlY		Total	No.	NiCrAlY
Convex	1	3.7	17.1			1	5.1	17.3	
	2	5.0	17.6			2	5.5	18.1	
	3	4.9	16.2			3	5.3	17.3	
	4	4.1	15.6			4	5.3	16.4	
	5	4.2	16.5	3.9	15.4				
	6	3.9	16.5	4.2	15.8				
	7	4.7	16.0	5.0	16.0				
	8	3.9	16.2	5.1	15.4				
	9	3.9	16.0	4.7	14.2				
	10	4.2	16.5	4.3	13.8				
	11	3.9	19.5	3.5	17.7				
	12	1.3	15.2	1.6	11.8				
	median	3.15	17.35	3.35	14.75		5.30	17.25	
	spread	+1.85	+ 2.15	+1.75	+ 2.95		+0.20	+0.85	
	average	3.98	16.58	4.03	15.01		5.30	17.28	
	std. dev.	+0.94	+ 1.11	+1.12	+ 1.76		+0.16	+ 0.70	
Concave	14	4.2	18.4			1	4.3	16.2	
	15	4.2	17.9			2	4.7	15.8	
	16	4.5	16.3			3	4.7	15.8	
	17	4.2	16.5			4	5.5	17.3	
	18	4.2	17.3	5.1	15.4				
	19	5.4	17.1	5.8	15.8				
	20	5.8	17.9	6.0	16.4				
	21	5.4	18.7	6.0	17.6				
	22	3.2	17.9	4.3	16.2				
	23	1.6	15.0	2.7	15.0				
		median	3.70	16.85	4.35	16.30		4.90	16.55
		spread	+2.10	+ 1.85	+1.65	+ 1.30		+0.60	+ 0.75
	average	4.27	17.30	4.98	16.07		4.80	16.28	
	std. dev.	+1.21	+ 1.12	+1.30	+ 0.91		+0.50	+ 0.71	
Total	median	3.55	17.25	3.80	14.75		4.90	16.95	
	spread	+2.25	+ 2.25	+2.20	+ 2.95		+0.60	+ 1.15	
	average	4.11	16.90	4.44	15.46		5.05	16.78	
	std. dev.	+1.06	+ 1.15	+1.25	+ 1.51		+0.44	+ 0.84	

Notes: 1. Values listed for columns of "Total" are the sum of the NiCrAlY and ZrO<sub>2</sub> coatings.

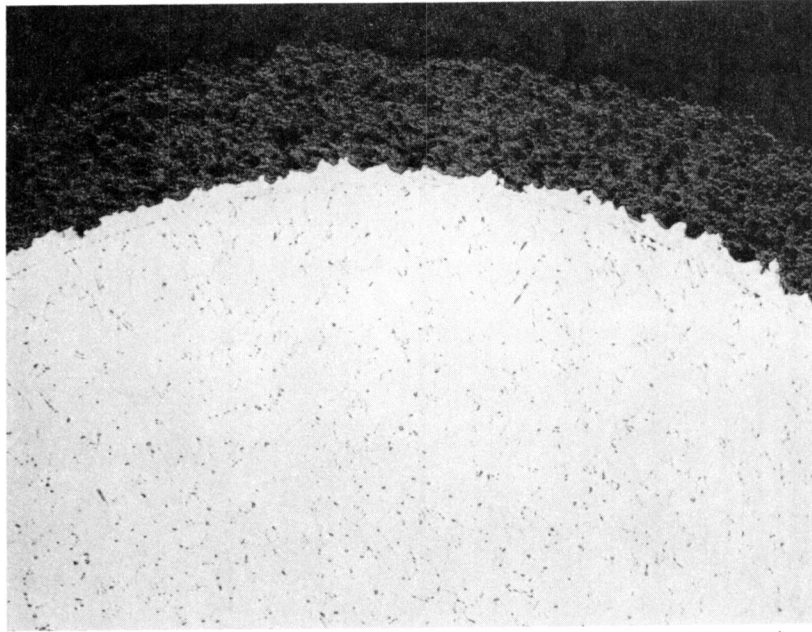


Figure 35. Photomicrograph of APS-Coated JT9D Blade Specimen No. 27 at Point No. 23 (Leading Edge) (50X).



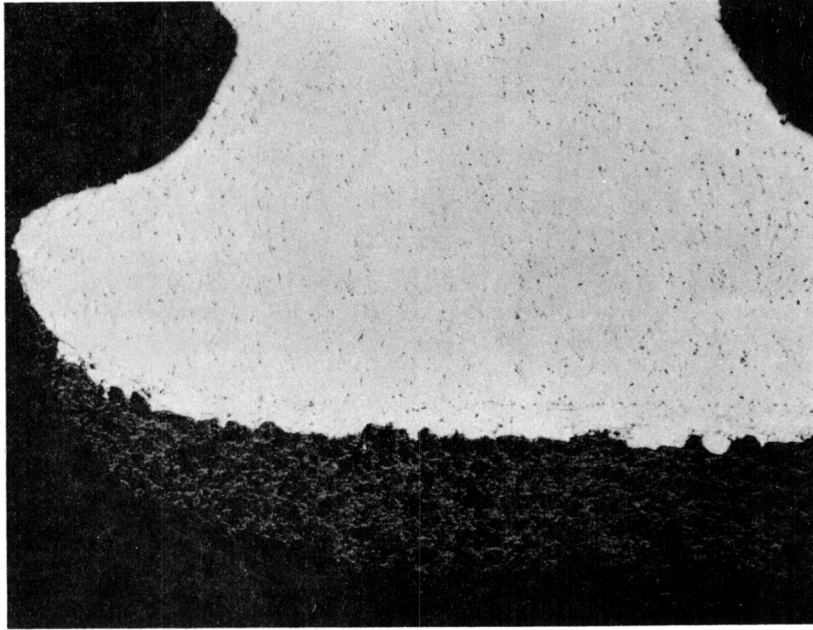


Figure 36. Photomicrograph of APS-Coated JT9D Blade Specimen No. 27 at Point No. 1 (Trailing Edge) (50X).

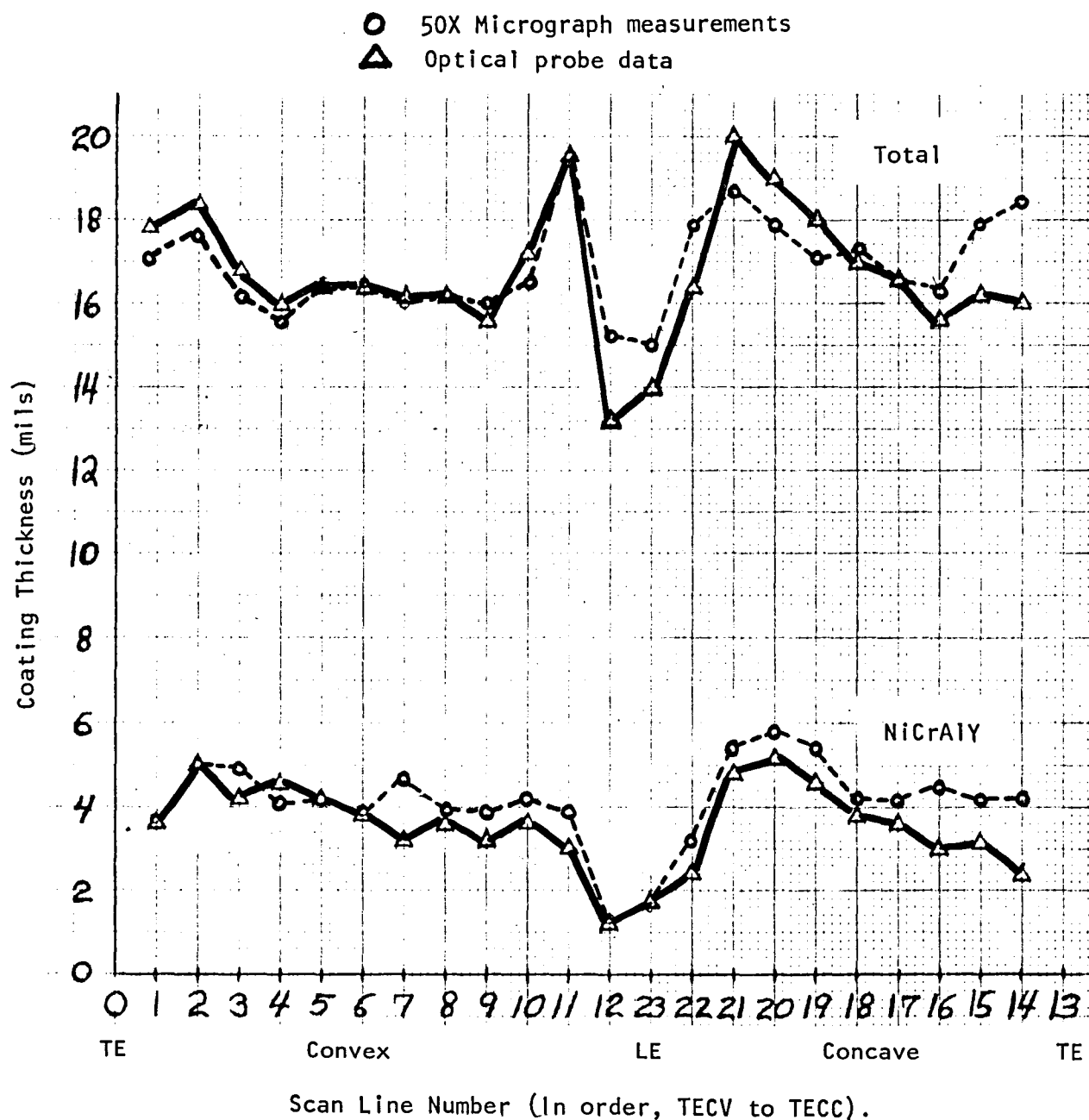


Figure 37. Comparison of Photomicrograph and Optical Probe Coating Thickness Measurements on Blade No. 27.



Another comparison that can be made is the coating uniformity as indicated by the two types of measurements. If the results for blades Nos. 26 and 27 are compared over the regions where data is available by both methods, the average spread for the two types of coatings on the two blades is found to be  $+64\text{ }\mu\text{m}$  (2.5 mils) based on photomicrograph measurements and  $+71\text{ }\mu\text{m}$  (2.8 mils) based on the optical probe measurements. These results indicate that the optical probe provides a reliable indication of the coating uniformity.

#### Macro Coating Characteristics

In addition to evaluating the APS system and manually sprayed coatings for thickness uniformity, the coatings were visually examined at 50X for evidence of cracking, oxides, interface quality, etc. Figures 38 through 45 illustrate the features observed in the coatings on blades X and Y which were manually sprayed. On these blades the coating was applied over an aluminide coating on the blade surface. The photomicrographs show the variation in the substrate/bond coat interface quality and the range of porosity and cracking found in the zirconia coating. Figures 46 through 49 cover the substrate/bond coat interface quality and the porosity found in the zirconia coating as deposited by the APS system. It should be noted that there is no cracking in the APS coatings while there is in the manually applied coating. The photomicrographs illustrate that neither coating process was optimized, although as a whole, the APS coatings appeared to be of better quality.

#### Torch Test Evaluation

One of the APS cooled blades (No. 26) was submitted to a torch test at NASA to determine coating integrity. After 23 one-hour thermal exposures, the test was stopped because of surface spallation. The localized thermal barrier spallation on the leading edge (see arrow) is shown in Figure 50. Under macroscopic examination, three small localized spallation areas on the leading edge were observed. Figure 51 shows the spallation areas at 40X and 100X. In the spalled area just to the right of the arrow in Figure 50 (the area closest to the root platform), the total coating thickness was reduced approximately 20%.

Microscopic examination of the spalled region showed a thin bond coat, varying from one to three mils in thickness. This corresponds with the printouts obtained from the APS system optical detector for the NiCrAlY coating on the leading edge (Figure 52, at lines 12 to 23). No cracks, either parallel to or at an angle to the bond/zirconia interface are present in the area of spallation. The localized spallation was probably due to exfoliation of loosely bonded outer layers of the ceramic.

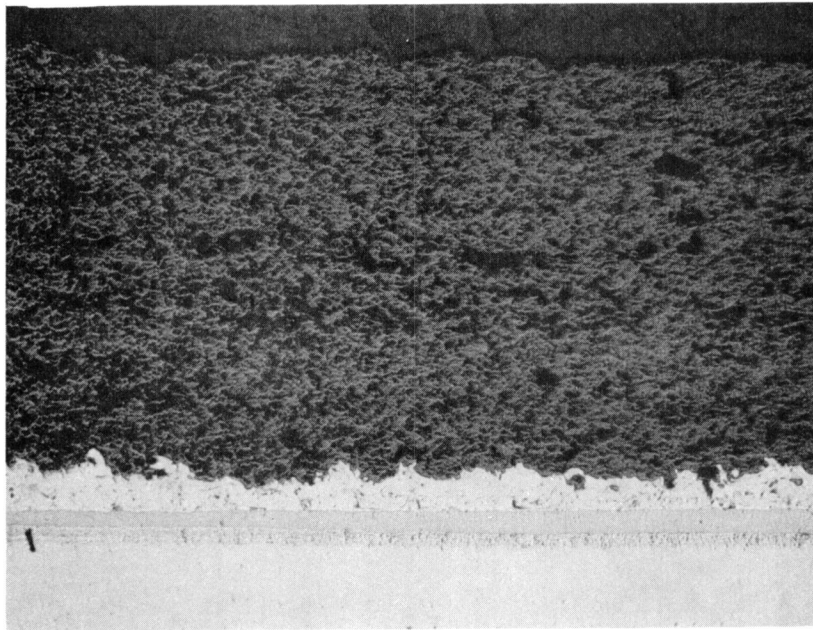


Figure 38. Photomicrograph of Manually Coated JT9D Blade No. "X", Surface "A" at Location 14 (50X).

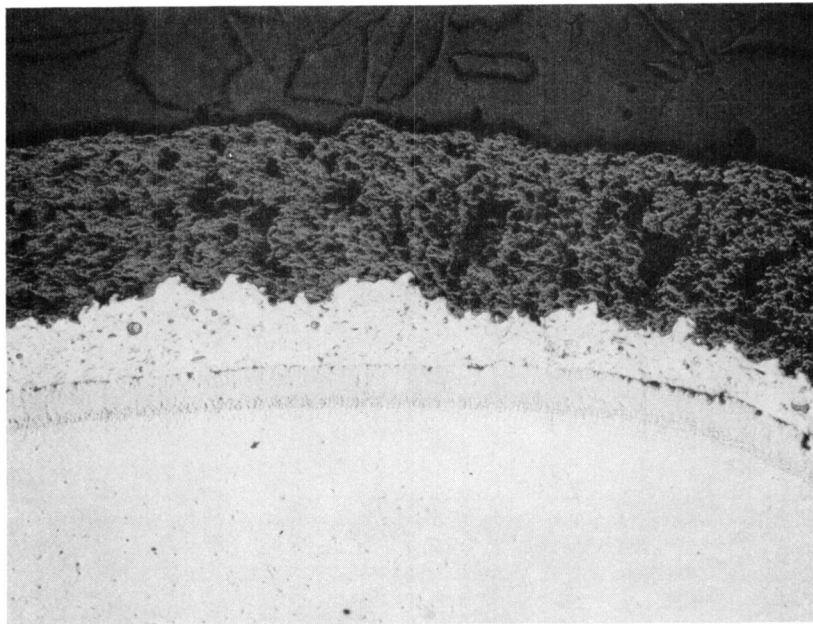


Figure 39. Photomicrograph of Manually Coated JT9D Blade No. "X", Surface "A" at Location 12 (50X).

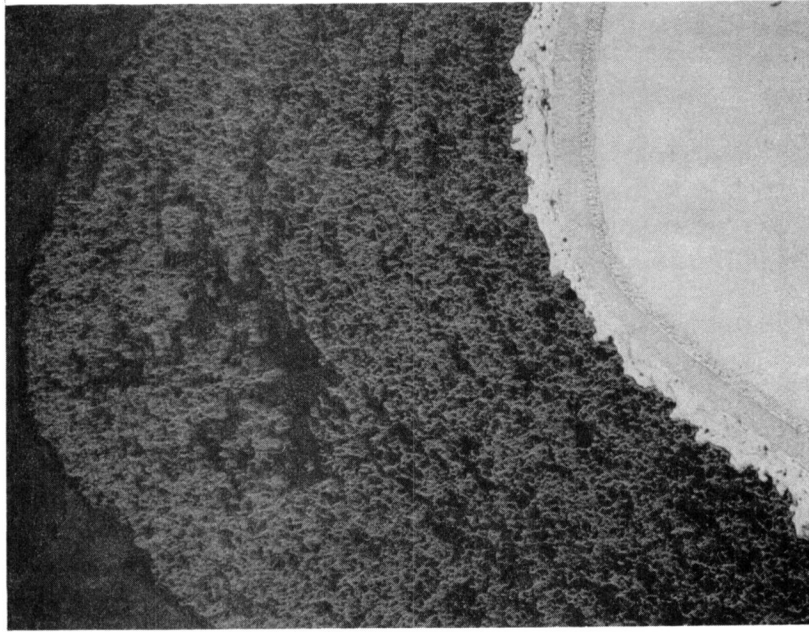


Figure 40. Photomicrograph of Manually Coated JT9D Blade No. "X", Surface "A" at Location 13 (50X).

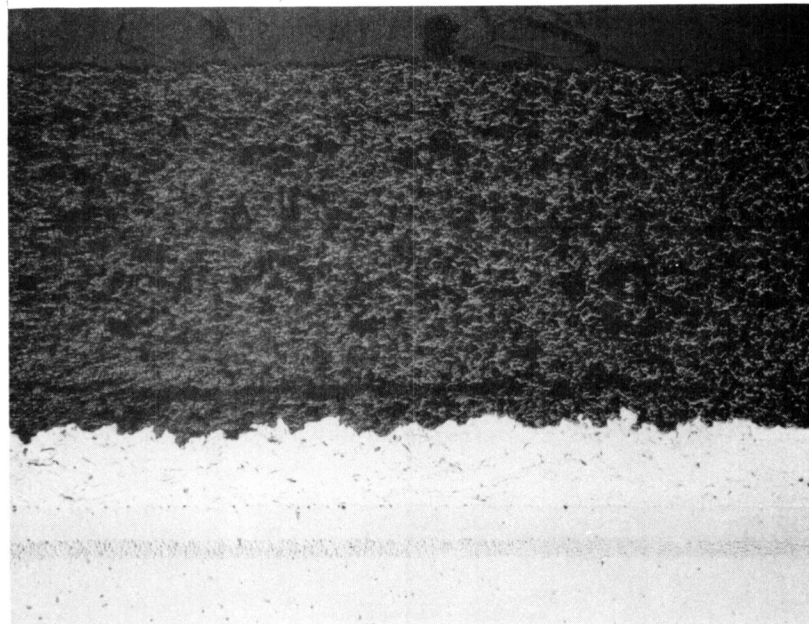


Figure 41. Photomicrograph of Manually Coated JT9D Blade No. "X", Surface "B" at Location 5 (50X).

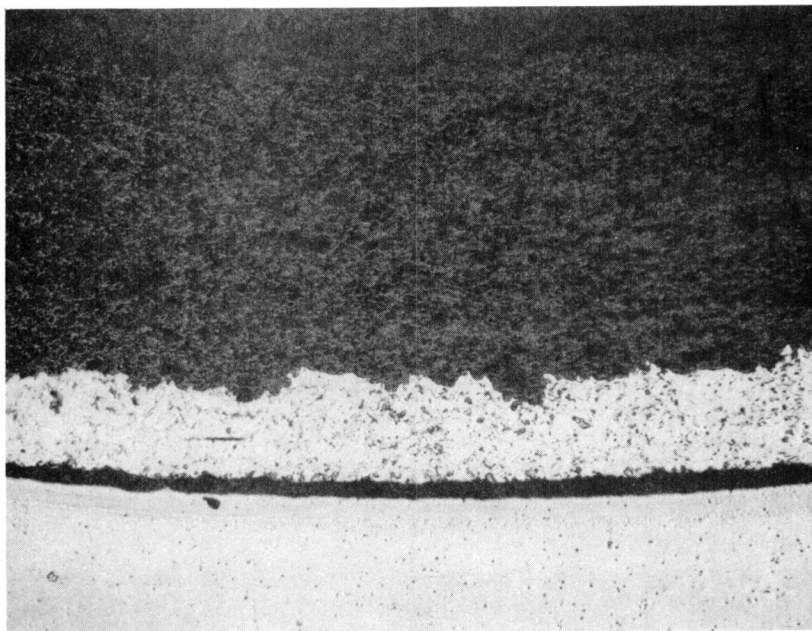


Figure 42. Photomicrograph of Manually Coated JT9D Blade No. "Y", Surface "A" at Location 20 (50X).

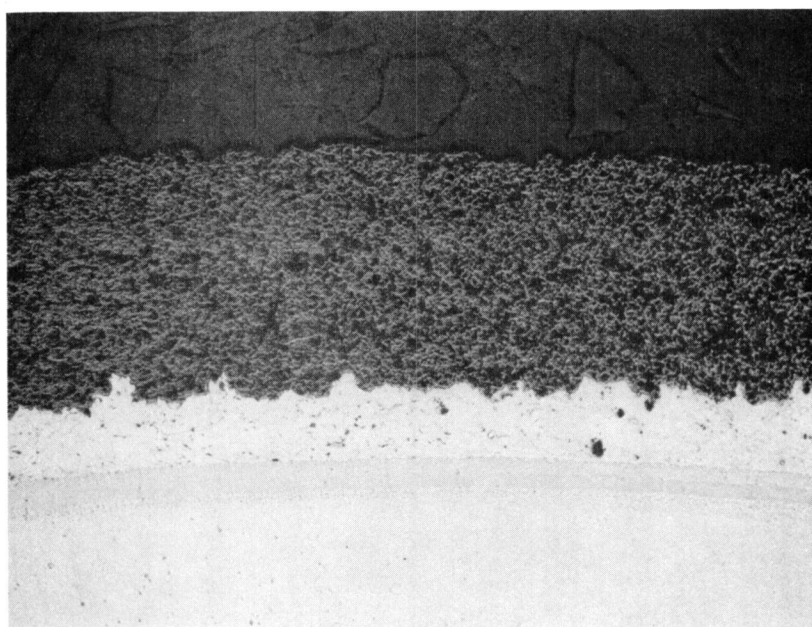


Figure 43. Photomicrograph of Manually Coated JT9D Blade No. "Y", Surface "A" at Location 11 (50X).

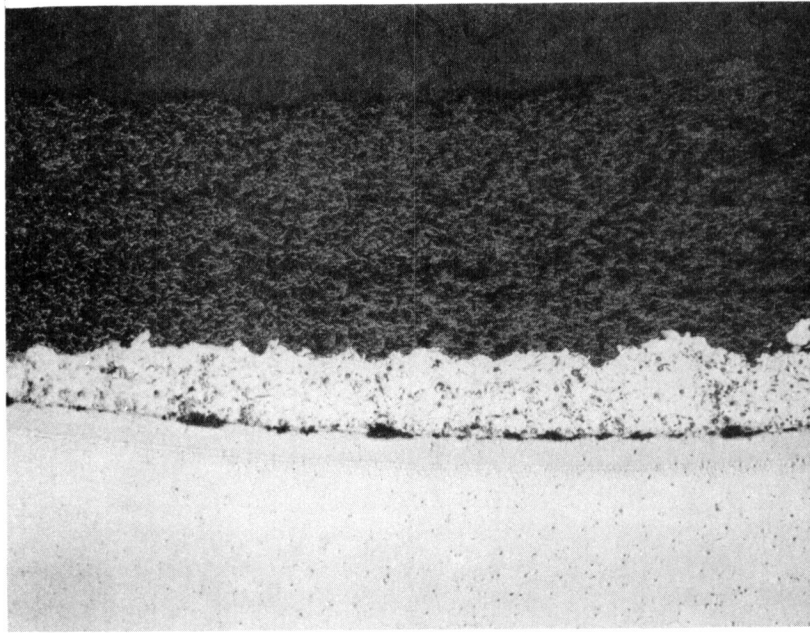


Figure 44. Photomicrograph of Manually Coated JT9D Blade No. "Y", Surface "A" at Location 21 (50X).

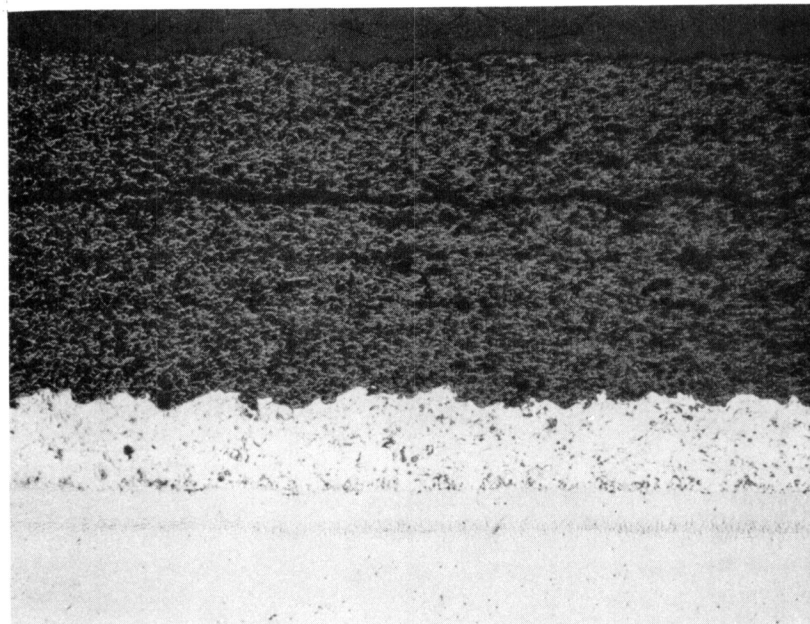


Figure 45. Photomicrograph of Manually Coated JT9D Blade No. "Y", Surface "A" at Location 8 (50X).

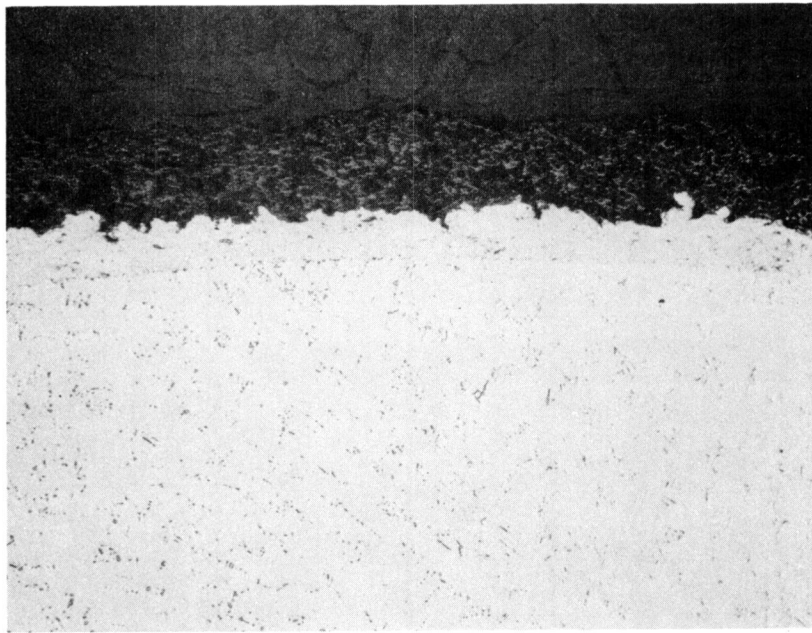


Figure 46. Photomicrograph of the APS System Coated JT9D Blade No. 26, Surface "A" at Location 9 (50X).

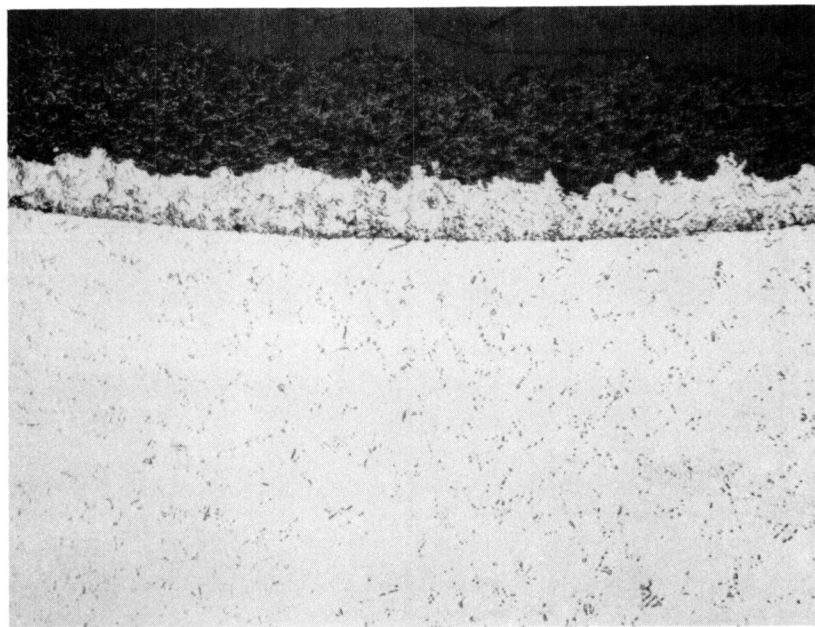


Figure 47. Photomicrograph of the APS System Coated JT9D Blade No. 26, Surface "A" at Location 21 (50X).



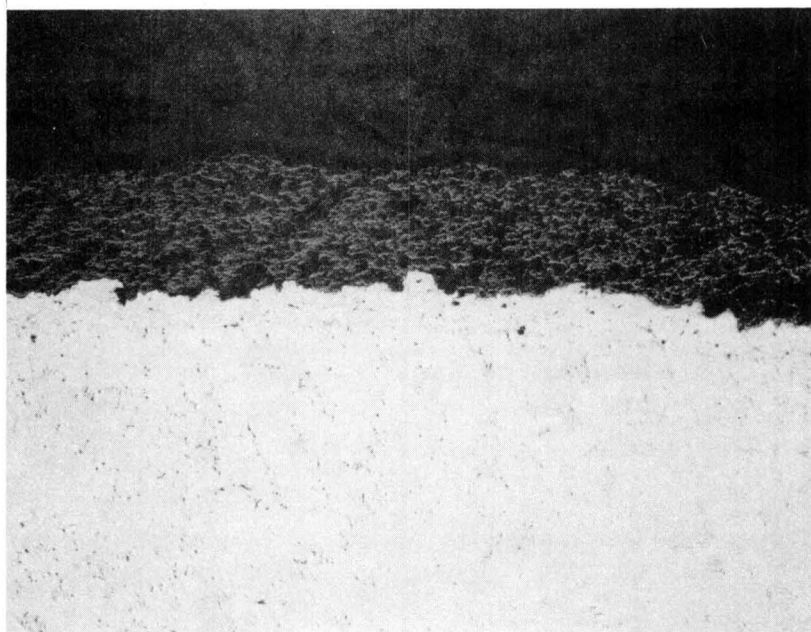


Figure 48. Photomicrograph of the APS System Coated JT9D Blade No. 27, Surface 'A' at Location 10 (50X).

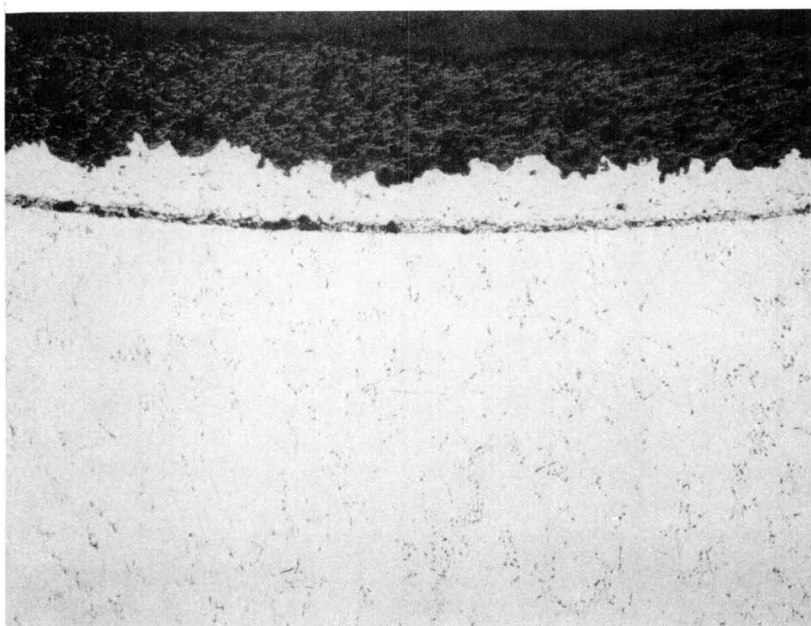


Figure 49. Photomicrograph of the APS System Coated JT9D Blade No. 27, Surface 'A' at Location 20 (50X).

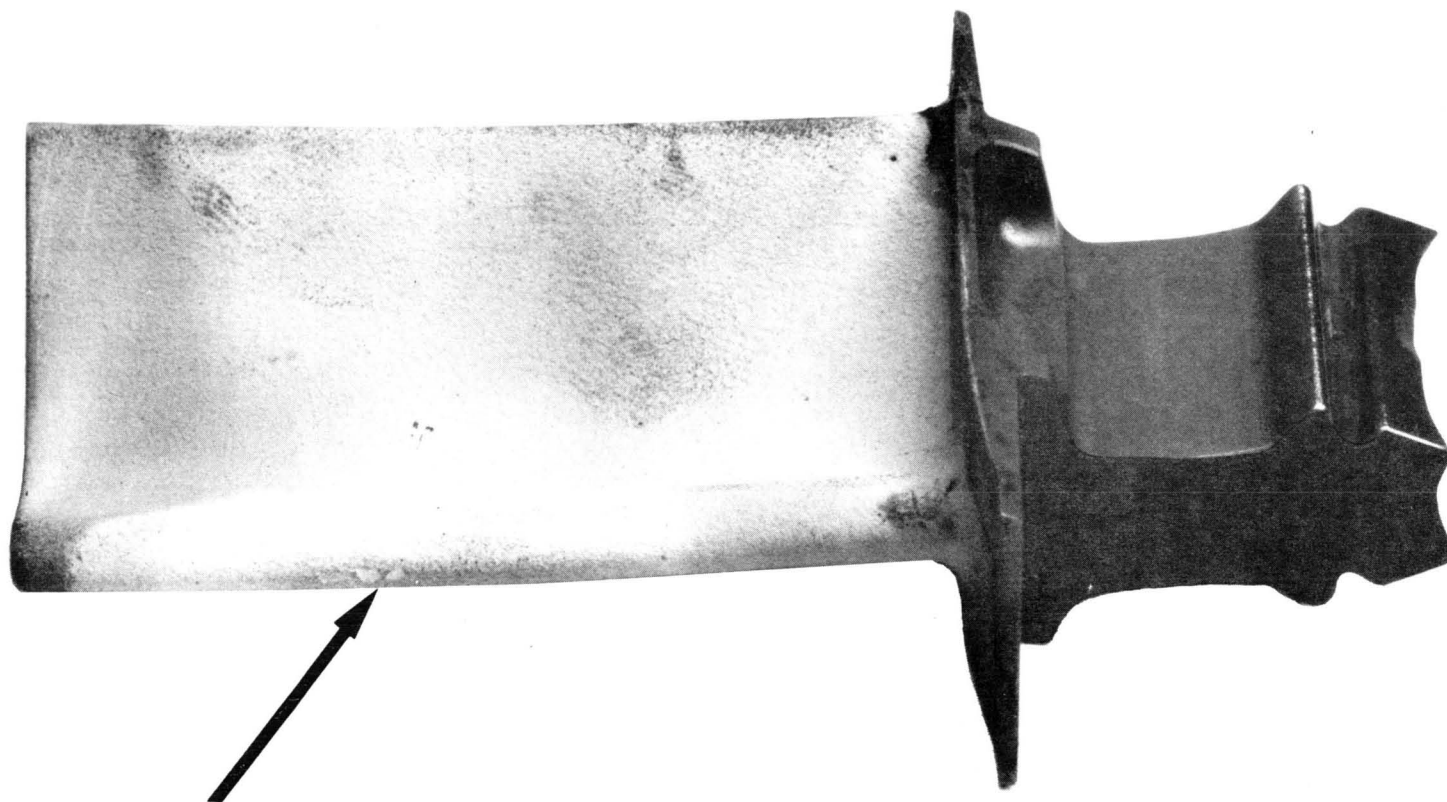
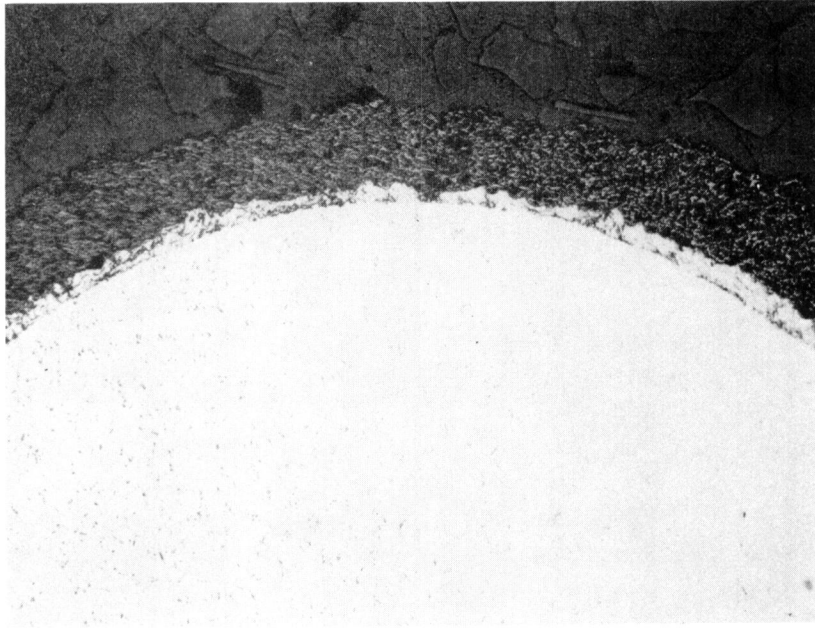
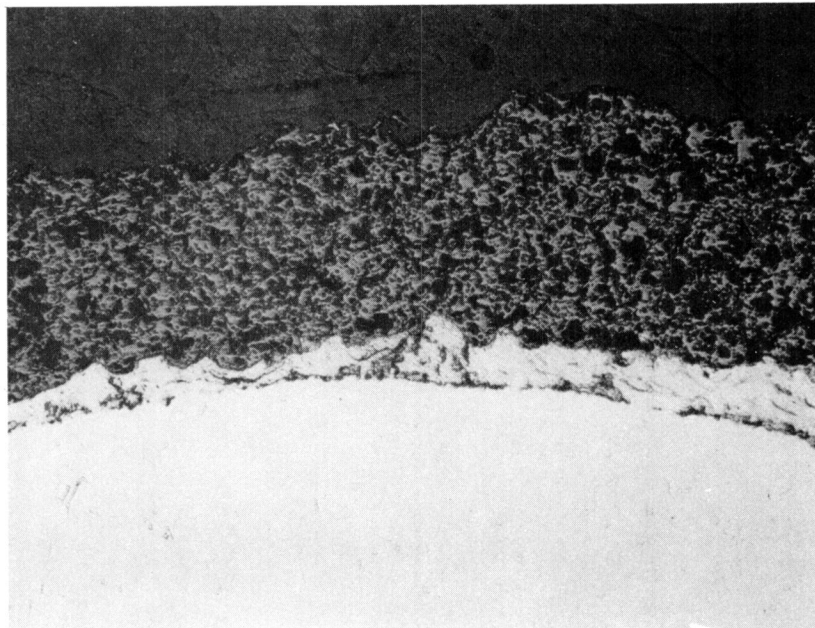


Figure 50. APS Coated, NASA Burner Rig Tested Airfoil No. 26 after 23 Hour Exposure. (Note location of arrow showing some localized thermal barrier coat spalling.)





(40X)



(100X)

Figure 51. Photomicrographs of APS Coated Burner Rig Tested Airfoil No. 26 after 23 Hour Exposure Showing Localized Thermal Barrier Coat Spalling.

<u>NiCrAlY</u> <u>Only</u>		<u>Total</u> <u>Coating</u>		
00	03.0	00	14.0	T.E.
01	03.4	01	16.2	
02	03.8	02	17.0	
03	04.2	03	15.8	
04	04.6	04	15.8	
05	04.4	05	16.0	
06	04.0	06	15.2	Airfoil Convex Surface
07	05.2	07	15.8	
08	04.6	08	16.0	
09	03.6	09	14.8	
10	04.2	10	16.0	
11	03.8	11	18.6	
12	00.6	12	11.8	L.E.
13	01.8	13	14.0	T.E.
14	02.4	14	15.0	
15	03.2	15	14.8	
16	03.4	16	14.8	
17	03.8	17	15.2	
18	03.6	18	14.8	Airfoil Concave Surface
19	04.8	19	15.0	
20	05.2	20	14.4	
21	04.4	21	15.2	
23	02.8	22	13.6	
		23	14.0	L.E.

Note: Location No. 22 data for NiCrAlY thickness is missing on printout due to printer malfunction.

Figure 52. Data Printouts from APS System Showing Actual Deposition Thicknesses (in mils) of NiCrAlY and Zirconium Oxide Coatings on JT9D Specimen No. 26 as Determined by Optical Sensor at Each Gage Point.

## 6.0 CONCLUSIONS AND CONTINUED CONTRACT EFFORT

Feasibility of an automated plasma spray (APS) system to uniformly and reproducibly apply the NASA developed two-layer (NiCrAlY-4 mils and  $\text{ZrO}_2/12\text{Y}_2\text{O}_3$ -12 mils) thermal barrier coatings to aircraft gas turbine blade airfoils has been investigated. In investigating the APS system feasibility, using specially developed and fabricated process hardware, the following conclusions were reached:

1. Feasibility has been demonstrated for an automated process for plasma spraying two-layer thermal barrier coatings on aircraft gas turbine blades. This process incorporates noncoherent optical sensing of actual in-process coating buildup on the blade and provides closed loop control of deposited coating thickness. The process can be programmed to provide a specified, controlled deposited coating thickness over the airfoil surface as well as a uniform thickness.
2. Extrapolation of preliminary data obtained on the APS process on JT9D first stage turbine blades indicates that the desired  $\pm 38 \mu\text{m}$  (1.5 mils) coating thickness uniformity over the airfoil surface is achievable, whereas currently, by manual deposition, the coating uniformity is not less than  $\pm 76 \mu\text{m}$  (3 mils). Closer control of blade temperature during the optical gaging subroutines along with rebuilding of the existing mechanical positioning fixture to eliminate wear and backlash are required to meet the  $\pm 38 \mu\text{m}$  (1.5 mil) objective.
3. The APS process has demonstrated the capability of coating JT9D blade airfoil surfaces with a two-layer thermal barrier coat without masking the blade root section and without masking or plugging the trailing edge cooling ports.
4. The noncoherent optical gaging subsystem developed for the APS process has demonstrated metrology performance capabilities to  $\pm 2 \mu\text{m}$  (.08 mils). Despite the deficiencies in the system mechanical hardware, this subsystem has demonstrated a measurable standard deviation of  $\pm 7.5 \mu\text{m}$  (0.3 mils) on the blades.
5. Additional investigations are required to optimize the APS process control parameters and to statistically verify the process performance capabilities.

The development effort remaining is to statistically demonstrate the system's capability to reproducibly produce coating thickness uniformity of  $\pm 38 \mu\text{m}$  (1.5 mils) on several aircraft gas turbine and electric utility blades. These tasks are also to

obtain data that will indicate that the APS system developed is a viable process for commercial utilization. To accomplish this, a newly designed blade handling subsystem will be built to overcome the mechanical, thermal, and other associated problems with the present system, and will be used to coat 25 aircraft gas turbine and 10 electric utility blades for coating thickness analysis after the system has been fully integrated. The analysis for coating uniformity on the blades will determine the system's capability to maintain  $\pm 38 \mu\text{m}$  (1.5 mils) control of certain thickness. In addition, an economic study will be completed to determine the projected production cost for the APS process. Recommendations for future work and possible application of the technology developed will be included, after which a demonstration of the APS system will be made for industry.

## 7.0 APPENDICES

## 7.1 LIST OF ABBREVIATIONS AND SYMBOLS

<u>Symbol</u>	<u>Quantity</u>	<u>Unit</u>
A	Blade angular rotational axis of motion (around linear motion of X axis)	-
A/D	Analog to digital converter	-
APS	Automated Plasma Spray	-
B	Blade angular rotational axis of motion (around linear motion of Y axis)	-
BHD	Blade handling mechanism	-
C	Blade angular rotational axis of motion (around linear motion of Z axis)	-
CPU	Central processing unit	-
CRT	Cathode raytube	-
CTDM	Coating thickness measurement device	-
EMI	Electromagnetic interference	volt/meter
EPROM	Erasable programmable read only memory	-
FIFO	First-in-first-out	-
g	Mass	gram
g/min	Flow rate	gram/minute
g/s	Flow rate	gram/second
Hz	Frequency	hertz
I/O	Input/output	-
l	Volume	liter
LED	Light emitting diode	-

## 7.1 LIST OF ABBREVIATIONS AND SYMBOLS (cont'd)

<u>Symbol</u>	<u>Quantity</u>	<u>Unit</u>
l/min	Flow rate	liter/minute
l/s	Flow rate	liter/second
min	Time	minute
MPS	Manual plasma spray	-
mt/st	Measurement per step	-
PC	Printed circuit	-
PIA	Peripheral interface adaptor	-
RAM	Random access memory	-
ROM	Read only memory	-
s	Time	second
SGSF	Spray gun scanning fixture	-
TB	Thermal barrier	-
TTL	Transistor-transistor-logic	-
W	Power	watt
Z	Optical detector linear axis of motion	-
ZZ	Plasma gun linear axis of motion	-
X	Blade linear axis of motion (perpendicular to plasma spray direction)	-
Y	Blade linear axis of motion (parallel to plasma spray direction)	-
μP	Microprocessor	-

## 7.2 Prefixes

Decimal multiples and submultiples of the engineering units are formed by means of prefixes. A partial list of the NBS recommended units of prefixes are listed below:

<u>Symbol</u>	<u>Prefix</u>	<u>Factor by Which the Unit is Multiplied</u>
G	giga	$10^9$
M	mega	$10^6$
k	kilo	$10^3$
d	deci	$10^{-1}$
c	centi	$10^{-2}$
m	milli	$10^{-3}$
$\mu$	micro	$10^{-6}$
n	nano	$10^{-9}$
p	pico	$10^{-12}$

## 7.3 APS Mechanism Specification

## 7.4 APS System Circuit Diagrams

## 7.5 APS Process Software Flow Charts and Assembly Listings

The materials of the sections listed above are being published in a separate volume. May be obtained from J. P. Merutka, MS 49-1, NASA/LeRC, 21000 Brookpark Road, Cleveland, Ohio 44135.



## 8.0 REFERENCES

1. Stecura, Stephan: Two-Layer Thermal Barrier Coating for Turbine Airfoils - Furnace and Burner Rig Test Results. NASA TM X-3425, 1976.
2. Gerdeman, D.A. and Hecht, N.L.: Arc Plasma Technology. Materials Science, Springer - Verlag, 1972.
3. Stecura, Stephan, "Effect of Compositional Changes on the Performances of a Thermal Barrier Coating System," NASA Technical Memorandum 78976.

**DO NOT REMOVE SLIP FROM MATERIAL**

[illegible]